Transferrin receptor-mediated gene delivery using functionalised gold nanoparticles

By

Jananee Padayachee

213519464

Submitted in fulfilment of the academic requirements for the degree of Master of Science in the School of Life Sciences, University of KwaZulu-Natal, Durban

Supervisor: Prof M. Singh

Signed: _____   Date: _____

Abstract

Gene therapy strategies have shown their potential in treating numerous central nervous system (CNS) disorders, including highly aggressive brain cancers. Gold nanoparticles (AuNPs) are popular vectors for gene delivery, due to their low toxicity, and ease of synthesis and functionalisation. However, the *in vivo* efficacy of these vectors is dependent on their ability to cross the blood-brain barrier (BBB), a specialised capillary network preventing the movement of compounds into the CNS. Passage across the BBB is often facilitated through targeting of the transferrin (Tf) receptor, leading to uptake by receptor-mediated transcytosis. This study aimed to develop untargeted and Tf-targeted functionalised AuNP (FAuNP) vectors and assess their potential as gene delivery vectors.

AuNPs were prepared through citrate reduction and functionalised with chitosan (CS) and poly(ethylene) glycol 2000 (PEG_{2000}) in two weight ratios [2% and 5% ($^W/_W$)] to produce untargeted FAuNPs. The holo-transferrin protein was conjugated to both PEGylated and unPEGylated FAuNPS to produce the Tf-targeted FAuNPs (TfAuNPs).

The physicochemical characteristics of FAuNPs were evaluated using UV spectroscopy, Fourier-transform infrared spectroscopy (FTIR), transmission electron microscopy (TEM) and nanoparticle tracking analysis (NTA). TEM revealed AuNP to be spherical and relatively monodisperse. FAuNPs displayed hydrodynamic diameters ranging from 94.7 – 196.4 nm with good colloidal stability, as evidenced by NTA. Binding studies viz. band shift and ethidium bromide intercalation assays showed that all FAuNPs were able to fully complex and efficiently condense pCMV-*luc* plasmid DNA, with PEGylated and targeted FAuNPs being capable of partially protecting DNA from nuclease degradation, as determined in nuclease protection assays. *In vitro* studies were conducted in the HEK293, Caco-2, and the Tf receptor-positive HeLa cell lines. Cytotoxicity was assessed using the MTT cytotoxicity assay, which revealed FAuNPs to be relatively non-toxic to HeLa and HEK293 cells. Notably, TfAuNPs displayed low cytotoxicities, and generally exhibited increased cell viabilities compared to the untargeted FAuNPs. The luciferase gene reporter assay was conducted to assess the transfection efficiency of the FAuNPs. Transfection levels were highest in Caco-2 cells, with PEGylated FAuNPs observed to produce reduced transfection compared to the unPEGylated FAuNPs. TfAuNPs displayed

favourable transfection in HeLa cells; with the competition binding assays confirming receptor-mediated uptake for AuCSTf and AuCSTf-5% PEG FAuNPs only, suggesting that a grafting density of the 2% ($^{w}/_{w}$) PEG interfered with receptor binding. These Tf-targeted FAuNPs show the potential to be utilised as vectors for brain delivery; however further optimisation and investigations in an *in vivo* system are required.

Preface

The experimental work described in this dissertation was carried out in the Discipline of Biochemistry, School of Life Sciences, University of KwaZulu-Natal, Durban under the supervision of Prof Moganavelli Singh.

These studies represent original work by the author and have not otherwise been submitted in any form for any degree or diploma to any tertiary institution. Where use has been made of the work of others it is duly acknowledged in the text.

Declaration – Plagiarism

I, Jananee Padayachee, declare that:

1.   The research reported in this dissertation, except where otherwise indicated, is my original research.

2.   This dissertation has not been submitted for any degree or examination at any other university.

3.   This dissertation does not contain other persons' data, pictures, graphs or other information, unless specifically acknowledged as being sourced from other persons.

4.   This dissertation does not contain other persons' writing unless specifically acknowledged as being sourced from other researchers. Where other written sources have been quoted then:

a.   their words have been re-written, but the general information attributed to them has been referenced.

b.   where their exact words have been used, then their writing has been placed in italics and inside quotation marks and referenced.

5.   This dissertation does not contain text, graphics or tables copied and pasted from the Internet, unless specifically acknowledged, and the source being detailed in the dissertation and in the References sections.

Signed:

Date:

Acknowledgements

I would like to express my thanks to the following:

Contents

List of Figures

List of Tables

List of Abbreviations

A431	Human epidermoid carcinoma
A549	Human lung carcinoma
AA	Amino acid
AAV	Adeno-associated viruses
ABC	ATP-binding cassette
ADA-SCID	Adenosine deaminase deficiency
AEE	Apical early endosome
AFM	Atomic force microscopy
AJ	Adherens junction
AMT	Adsorptive-mediated transcytosis
ASO	Antisense oligonucleotides
AuNP	Gold nanoparticles
AuNR	Gold nanorod
BBB	Blood-brain barrier
BBTB	Blood-brain tumour barrier
BCA	Bicinchoninic acid
BCRP	Breast cancer resistance protein
BCSFB	Blood-cerebrospinal fluid barrier
BSA	Bovine serum albumin
Caco-2	Human colorectal adenocarcinoma cell line
CAR	Chimeric antigen receptors
CEC	Cerebral endothelial cells
CED	Convection-enhanced diffusion
CME	Clathrin-mediated endocytosis
CMT	Carrier-mediated transport
CNS	Central nervous system
CRE	Common recycling endosome
CS	Chitosan
CSF	Cerebrospinal fluid
CvME	Caveolae-mediated endocytosis

DAK	2,2-bis(aminoethoxy)propane
DLS	Dynamic light scattering
DMSO	Dimethylsulfoxide
DMT1	Divalent metal transporter 1
DNA	Deoxyribonucleic acid
dsDNA	Double-stranded DNA
EA	Early apoptosis
EB	Ethidium bromide
EB/AO	Ethidium bromide/acridine orange
EDL	Electric double layer
EDTA	Ethylenediaminetetraacetic acid
EPR	Enhanced permeation and retention
FAuNPs	Functionalised gold nanoparticles
FBS	Foetal bovine serum
FCS	Foetal calf serum
FDA	Food and Drug Administration
FGF	Fibroblast growth factor
FTIR	Fourier-transform infrared spectroscopy
FUS	Focused ultrasound
$HAuCl_4$	Hydrogen tetrachloroaurate/chloroauric acid
HBS	Hepes buffered saline
HEK293	Human embryonic kidney 293 cell line
HeLa	Human cervical adenocarcinoma cell line
HEPES	2-[4-(2-hydroxyethyl)piperazin-1-yl]ethanesulfonic acid
HIFU	High-intensity focused ultrasound
HRTEM	High resolution transmission electron microscopy
HSV-1	Herpes simplex virus type 1
HSVTK/GCV	Herpes simplex virus thymidine kinase/ganciclovir
IC	Intra-cerebral
ICV	Intra-cerebroventricular injection
JAM	Junctional adhesion molecules
LA	Late apoptosis

LIP	Labile iron pool
MB	Microbubbles
MHC	Major histocompatibility complex
miRNA	MicroRNA
MPS	Mononuclear phagocytic system
mRNA	Messenger RNA
MTT	3-(4,5-dimethylthiazol-2-yl)-2,5-diphenyltetrazolium bromide
MW	Molecular weight
NCD	Non-communicable disease
NIR	Near infrared
NK	Natural killer cells
NLS	Nuclear localisation signal
NP	Nanoparticle
NPC	Nuclear pore complex
NR	Nanorod
NTA	Nanoparticle tracking analysis
PAMAM	Polyamidoamine
PBS	Phosphate buffered saline
pDMAEMA	poly(2-(dimethylamino)ethyl methacrylate)
pDNA	Plasmid deoxyribonucleic acid
PEG	Poly(ethylene) glycol
PEI	Polyethyleneimine
P-gp	P-glycoprotein
PLGA	Poly(lactic-coglycolic acid)
PLL	Poly(L-lysine)
RES	Reticuloendothelial system
RLU	Relative light units
RME	Receptor-mediated endocytosis
RMT	Receptor-mediated transcytosis
RNA	Ribonucleic acid
ROS	Reactive oxygen species
SDS	Sodium dodecyl sulphate

siRNA	Small interfering ribonucleic acid
SPR	Surface plasmon resonance
ssDNA	Single-stranded DNA
TAA	Tumour-associated antigen
TCR	T-cell receptors
TEM	Transmission electron microscopy
Tf	Transferrin
TfR	Transferrin receptor
TIL	Tumour-infiltrating lymphocytes
TJ	Tight junction
TNF	Tumour necrosis factor
TOAB	Tetraoctylammonium bromide
TSGs	Tumour suppressor genes
UV	Ultraviolet
VEGF	Vascular endothelial growth factor
WHO	World Health Organisation

Chapter 1
Introduction

1.1. Introduction

The mortality rates due to communicable, maternal, neonatal, and nutritional diseases have seen significant decreases in the past few decades, due to improvements in treatments and quality of care in low income countries (Naghavi *et al*., 2017). However, deaths due to non-communicable diseases (NCDs) have risen to become the largest contributors to global mortality, accounting for an estimated 71% of total deaths in 2016 (World Health Organization, 2018). The NCD cancer is the second-leading cause of death worldwide after cardiovascular diseases and is expected to cause approximately 9.6 million deaths in 2018 (Bray *et al*., 2018). Brain and central nervous system (CNS) cancers represent a small proportion of these deaths, but are highly significant, as many are aggressive and resistant to conventional treatment methods.

Conventional cancer treatments include surgery, chemotherapy, and radiation therapy. However, these treatments may be ineffective at preventing recurrence, and often cause potentially debilitating side effects. Chemotherapy utilises cytotoxic drugs; however, they are unable to target cancerous cells alone and are associated with side effects such as nausea, hair loss, and cognitive impairments (Cross and Burmester, 2006; Souho *et al*., 2018). Radiation therapy and surgery target single sites and are unable to kill metastases (Souho *et al*., 2018). The treatment of many brain and CNS cancers using these conventional methods is further complicated by their position in this important organ in the body. Surgery may be risky or impossible, and the non-specific action of chemotherapeutic drugs and radiation therapy may result in adverse effects on brain function. There is, thus, a need to develop alternative treatments that are capable of efficiently eliminating cancers while causing minimal adverse side effects.

At its basis, cancer is a genetic disease, resulting from multiple genetic aberrations that lead to abnormal growth. Thus, the field of gene therapy holds great promise for cancer therapy. Gene therapy involves the use of nucleic acids to exert a therapeutic, diagnostic, or prophylactic effect, and may be used to treat cancers via a variety of different methods, ranging from silencing of overactive genes to boosting the immune response to cancerous

1

cells (Wirth *et al.*, 2013). The success of gene therapy is dependent on the ability of the delivery vector to transport its payload to the target site; however, the development of suitable vectors is a major obstacle hindering the efficiency of gene therapy products *in vivo* (McErlean *et al.*, 2016). Issues such as vector toxicity, lack of specificity, and rapid clearance from the body have driven the need to develop safer and more efficient delivery vehicles (Wang *et al.*, 2016). This has led to the development of nanoparticle (NP) vectors, which have the potential to overcome the problems faced in delivery.

Nanotechnology involves the construction of materials in the nanometre scale, usually ranging from 1-100 nm (Liu *et al.*, 2007). Over the years, these nanomaterials have found application in a wide variety of fields, including electronics, aerospace, and military disciplines (Wong *et al.*, 2017). Nanomedicine can be defined as the use of nanotechnology in the medical setting, and is a field that has gained much attention for the diagnosis and management of diseases (Wong *et al.*, 2012). Cancer in particular is the subject of a large amount of nanomedicine research, as NPs have the potential to improve the diagnosis, imaging, and treatment of cancers (Ranganathan *et al.*, 2012). NPs are highly attractive vectors for gene delivery, due to their small size, versatile synthesis, and easy functionalisation (Chhabra *et al.*, 2015; Wang *et al.*, 2016). Gold nanoparticles (AuNPs) are being extensively researched as delivery vehicles, due to their unique properties, ease of synthesis, and biocompatibility (Mirza and Siddiqui, 2014).

The efficiency of therapies for brain cancer is dependent on their ability to deliver their payload to the relevant site in the brain (Jayant *et al.*, 2016). To do this, they must overcome the blood-brain barrier (BBB), a highly-specialised capillary network that limits the movement of molecules into the brain from the bloodstream. The BBB is the major obstacle hindering the development of therapeutics for CNS disorders, as many pharmaceuticals are unable to cross it and thus cannot enter the brain following systemic administration (Saraiva *et al.*, 2016). While techniques have been developed to disrupt or bypass the BBB, they are often invasive, costly and inefficient, requiring surgery or modification of the drug. A popular non-invasive approach of directing therapeutics across the BBB involves exploiting targeting ligands that bind receptors on the BBB surface, facilitating transport across the BBB by receptor-mediated transcytosis. The iron transport protein transferrin is widely used to target the transferrin receptor, which is expressed on the BBB. The beneficial properties of AuNP, in particular the ease with

which they can be functionalised with targeting molecules, make them ideal vectors for targeted treatment of brain cancers. Transferrin-targeted vectors would have the potential to facilitate efficient therapeutic delivery to the brain, with minimal side effects.

This study focussed on the development of AuNP vectors for gene delivery. The nanoparticles were synthesised using the citrate reduction method and encapsulated with the cationic polymer chitosan. This provided a base for the addition of the steric stabiliser poly(ethylene) glycol and the targeting protein holo-transferrin, and allowed for complexation with negatively-charged plasmid DNA (pDNA). All functionalised AuNP (FAuNPs) were fully characterised using physicochemical methods and investigated for their ability to bind and protect plasmid DNA. The *in vitro* cytotoxicity and transfection efficiencies of the functionalised AuNP were determined.

1.1. Aims and objectives

The aims of the study were to synthesise and characterise AuNP, FAuNPs, and transferrin-targeted FAuNPs, and determine their potential as vectors for gene delivery to cancer cells.

The objectives of the study were to:

- To synthesise AuNP using the citrate reduction method.
- To functionalise AuNP with chitosan, poly(ethylene) glycol in two weight ratios of 2% and 5%, and holo-transferrin.
- To characterise plain AuNP and FAuNPs using UV spectroscopy, FTIR, NTA, and TEM.
- To assess the ability of the FAuNPs to complex and condense plasmid DNA using the band shift and ethidium bromide intercalation assays, respectively, and their ability to protect pDNA from degradation using the nuclease protection assay.
- To assess the cytotoxicity of FAuNPs using the MTT cytotoxicity assay *in vitro* in the HEK293, HeLa, and Caco-2 cell lines.
- To determine the ability of FAuNPs to transfect HEK293, HeLa, and Caco-2 cells *in vitro* using the luciferase gene expression assay.

- To determine the ability of transferrin-targeted FAuNPs to induce uptake via receptor-mediated endocytosis using the competition binding assay in the transferrin receptor-expressing HeLa cell line.

1.2. Outline of dissertation

Chapter 1 provides the background to the research topic and includes the aims, objectives and the outline of the dissertation.

Chapter 2 provides a review of the literature. It highlights the difficulties faced in treating brain cancers, and provides an overview of gene therapy and the nanoparticle vectors that may be utilised. Specific focus is given to AuNP, their synthesis methods, and their potential for gene therapy. Targeting of the transferrin receptor for delivery to brain tumours, as well as possible methods of overcoming barriers faced in gene delivery, are also highlighted.

Chapter 3 provides the materials and methods used in the study. The synthesis and characterisation of AuNP and FAuNPs is described. The procedures of the DNA binding studies viz. the band shift, ethidium bromide intercalation, and nuclease protection assays are outlined. *In vitro* cytotoxicity and gene expression studies in the HEK293, HeLa, and Caco-2 cell lines are described.

Chapter 4 describes the results obtained and provides a critical discussion and interpretation of the data.

Chapter 5 is the conclusion to the study and includes recommendations for future research.

Chapter 2
Literature Review

2.1. Cancer

Cancer is a highly complex and heterogeneous disease, characterised by the uncontrolled proliferation of aberrant cells (Moses *et al*., 2018). Malignant cells display many unique properties that allow them to form tumours, such as replicative immortality, and the abilities to avoid apoptosis and evade the immune system. Hanahan and Weinberg, (2011) first branded these properties as the hallmarks of cancer (Figure 2.1). The attainment of these properties is a multistep process, requiring multiple genetic and/or epigenetic mutations (White and Khalili, 2016). These mutations may arise spontaneously due to errors in replication, or in response to exposure to carcinogenic agents (White and Khalili, 2016; You and Henneberg, 2018). The two major gene groups associated with cancer development are the proto-oncogenes, which promote cell growth and proliferation, and the tumour suppressor genes (TSGs), which control DNA repair and apoptosis. Mutations that knock out TSGs or increase the expression of proto-oncogenes may lead to cancer development.
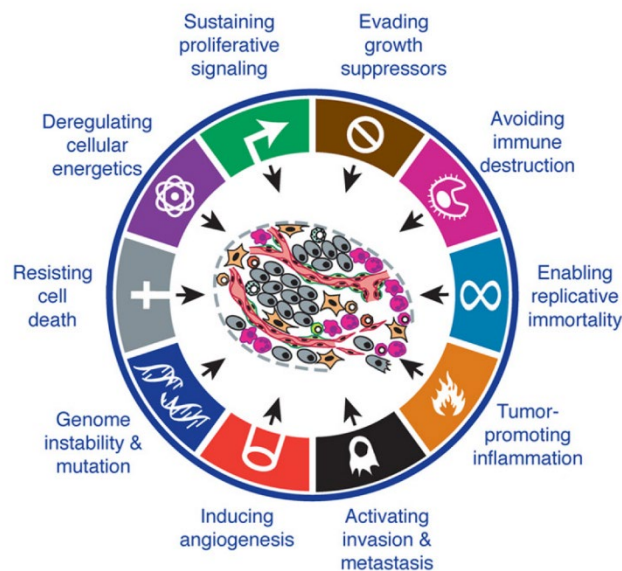
Figure 2.1: The hallmarks of cancer - the properties expressed by malignant cells (Hanahan and Weinberg, 2011).

2.1.1. Cancers of the brain and nervous system

Brain cancers may arise from the brain tissue as primary brain cancers, or secondarily as metastases from other cancers, most often, lung, breast, skin and renal cancers (Lauko *et al*., 2018). They are further classified by the World Health Organisation (WHO) according to the type of cell they arise from, and graded according to their malignancy (Louis *et al*., 2016). The majority of primary brain tumours are gliomas, which arise from glial cells and account for approximately 80% of malignant primary brain tumours (Malhotra *et al*., 2015). Gliomas include astrocytomas arising from astrocytes, oligodendroglias arising from oligodendrocytes, and ependymomas arising from ependymal cells (Malhotra *et al*., 2015). Astrocytomas are the most common glioma, and range from relatively benign grade I tumours to highly aggressive grade IV tumours, such as glioblastoma (Kleihues *et al*., 2014; McNeill, 2016). Glioblastoma, which displays a high rate of recurrence and a 5 year survival rate of only 5%, is the most commonly diagnosed brain tumour (Gallego, 2015). Non-glioma brain cancers include embryonal tumours, meningiomas, and CNS lymphomas (Louis *et al*., 2016). Embryonal tumours are particularly significant, as they occur mostly in children (Steliarova-Foucher and Frazier, 2014).

Brain and CNS cancers are relatively rare, and are expected to account for approximately 1.6% of global incident cancer cases and 2.5% of cancer deaths in 2018 (Bray *et al*., 2018). However, the burden caused by these cancers is disproportionately high, as the years of life lost is behind only lung, breast, liver, stomach, pancreatic, colon and oesophageal cancers (Naghavi *et al*., 2017). Brain and nervous system cancers are the second most common cancers diagnosed in children under 15 years. Despite advances in treatments, many display poor survival rates due to the difficulties experienced using conventional cancer therapies. A major obstacle faced in the treatment of brain cancers is the inability of many drugs to traverse barriers and reach the nervous system.

2.2. Structure and function of the blood-brain barrier

Entry into the CNS is restricted by three barriers: the blood-brain barrier (BBB), the blood-cerebrospinal fluid barrier (BCSFB), and the cerebrospinal fluid-brain barrier. These barriers are composed of extensive capillary networks controlling the movement of molecules into the brain, ensuring that neurons reside in a stable environment

conducive to signalling (Abbott, 2013). However, they also prevent the entry of chemotherapeutic drugs into the brain. The BBB is the largest of the three barriers, with a surface area of 20 m^2, and is thus considered the most important site for substance exchange between the blood and the CNS (Domínguez *et al.*, 2013).

The limited permeability of the BBB is due to the arrangement of cerebral endothelial cells (CEC), astrocytes, pericytes, microglia and neurons into structures called 'neurovascular units' (Figure 2.2) (Bicker *et al.,* 2014; Domínguez *et al.*, 2013). These units facilitate the transfer of nutrients and removal of wastes, and prevent harmful substances from entering the CNS (Abbott, 2013). The CEC display many differences to peripheral endothelial cells and are highly specialised to control substance exchange between the blood and the brain. The CEC membranes are continuous and lack fenestrations, or pores, to limit the uptake of compounds (Chow and Gu, 2015). The polarity of the CEC, in which they have an apical membrane facing the blood and a basolateral membrane facing the brain, further allows for regulation of transporter protein expression on either the apical or basolateral membrane (Banks, 2016; Chow and Gu, 2015). Adjacent CEC are held together by junctional complexes composed of adherens junctions (AJs), tight junctions (TJs), and gap junctions (Stamatovic *et al.*, 2016). These junctions are composed of transmembrane proteins that link with the cytoskeleton and transmembrane proteins of adjacent cells. The TJs are composed of the transmembrane proteins claudin, occludin and junctional adhesion molecules (JAM), which link with cytoplasmic accessory proteins that bind to the cytoskeleton (van Tellingen *et al.*, 2015). They present a barrier to paracellular diffusion between the CEC and prevent the movement of membrane lipids and proteins between the apical and basolateral membranes, allowing for the establishment of membrane polarity (Tietz and Engelhardt, 2015). AJs consist of transmembrane cadherin proteins, anchored in cytoplasmic catenin proteins (Stamatovic *et al.*, 2016). Gap junctions, composed of channel proteins, facilitate cellular communication in the form of ions and other small molecules (Stamatovic *et al.*, 2016). The CEC are surrounded by pericytes and astrocytic end-feet, which regulate the development and maintain the structure of the BBB. Pericytes control the development of blood vessels, and regulation of BBB-specific gene expression in the CEC (Bicker *et al.*, 2014). Astrocytic end-feet help maintain ion and water homeostasis at the BBB and further tighten the TJs (Armulik *et al.*, 2010; Tajes *et al.*, 2014).
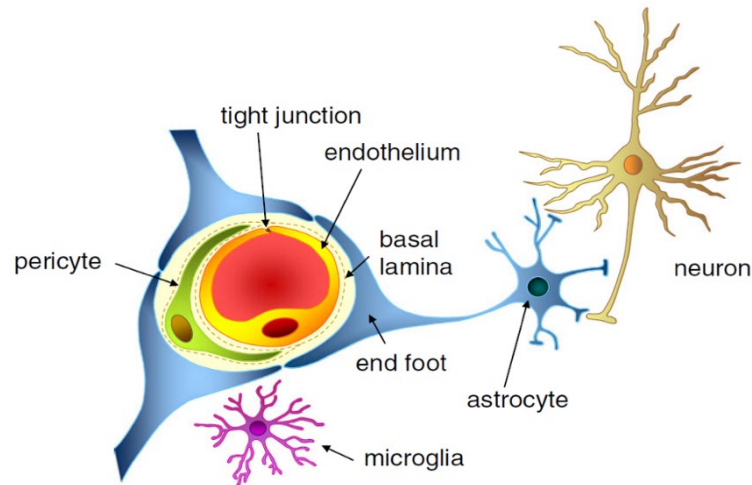
Figure 2.2: The arrangement of CEC, astrocytes, pericytes, neurons and microglia in the neurovascular unit (Abbott, 2013).

2.2.1. Transport across the blood-brain barrier

There are a number of mechanisms by which nutrients and waste material may enter or leave the CNS. The major transport pathways are shown in Figure 2.3, and include diffusion, carrier-mediated transport and transcytosis.
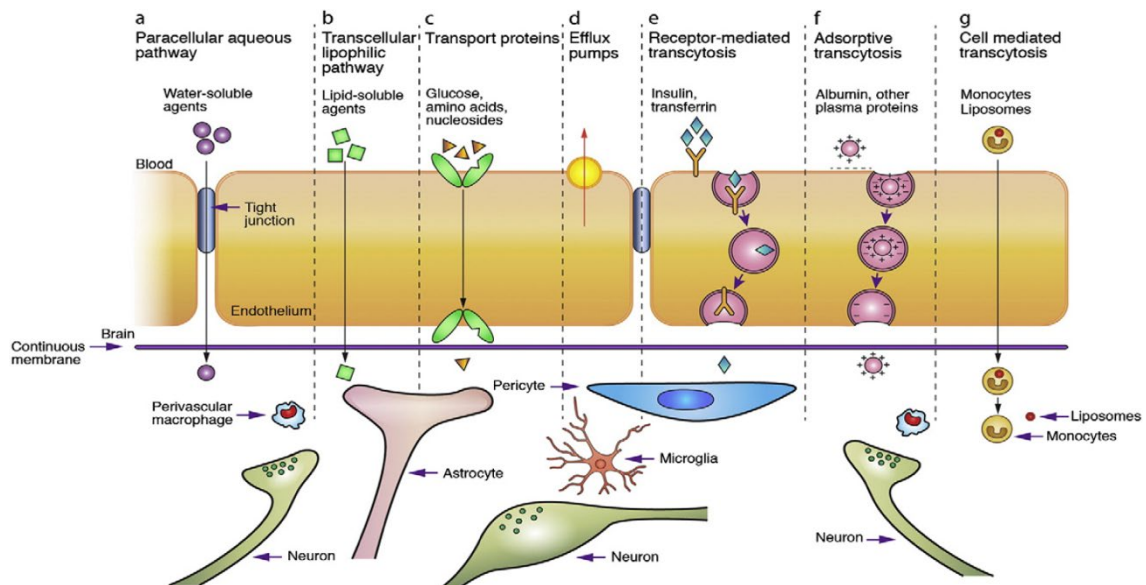
Figure 2.3: Mechanisms of transport across the BBB (Chen and Liu, 2012).

2.2.1.1.   Diffusion

Diffusion involves the passive movement of molecules along a concentration gradient, from an area of high solute concentration to an area of low solute concentration.

Molecules may diffuse across the BBB via transcellular or paracellular pathways (Figure 2.3a-b). Paracellular diffusion involves the movement of small, water-soluble molecules between the TJs (Chen and Liu, 2012). However, it is not a major route of transport due to the tightness of the TJs. Lipid-soluble molecules smaller than 600 kDa and gases diffuse transcellularly across the BBB by dissolving through the phospholipid bilayers of the CEC membranes (Abbott, 2013; Lajoie and Shusta, 2015).

2.2.1.2. Carrier-mediated transport

Carrier-mediated transport (CMT) is mediated by protein transporters that transport small, hydrophilic molecules across the BBB (Ohtsuki and Terasaki, 2007). Influx transporters transport small nutrients along the concentration gradient, from the blood into the brain (Figure 2.3c) (Daneman and Prat, 2015). These carriers are specific to the solute they transport, for example, the GLUT-1 protein transports glucose, while amino acids (AAs) have different transporters based on their physicochemical properties (Tajes *et al.,* 2014). Carrier proteins also mediate the transport of Na^{2+}, K^+, and Cl^- ions into CEC, and the flux of Na^{2+} and K^+ ions across the basolateral membrane (De Bock *et al*., 2016). The BBB also contains efflux proteins, mostly belonging to the ATP-binding cassette (ABC) family of proteins, that remove wastes and toxins from the brain into the bloodstream (Figure 2.3d) (Lai *et al.*, 2013). However, they may also remove drugs before therapeutically active levels can be attained. The P-glycoprotein (P-gp) and breast cancer resistance protein (BCRP) are the most important efflux pumps responsible for the removal of anticancer drugs from the CNS (Lai *et al.*, 2013).

2.2.1.3. Transcytosis

Transcytosis is an active transport mechanism that shuttles macromolecules from the apical membrane to the basolateral membrane, and includes receptor-mediated transcytosis (RMT), adsorptive-mediated transcytosis (AMT) and cell-mediated transcytosis (Figure 2.3e-g) (Lajoie and Shusta, 2015). RMT is an energy-dependent process used for the uptake of hormones, growth factors and high molecular weight (MW) proteins such as insulin and transferrin (Tf) (Tajes *et al.,* 2014). It involves binding of ligands to receptors located on the apical CEC surface, leading to internalisation by endocytosis and transport of the ligand across the CEC (Tajes *et al.,* 2014). AMT is a

nonspecific process based on electrostatic interactions between positively charged solutes and negatively charged membrane components, which triggers endocytic uptake of the substance (Alyautdin *et al.*, 2014). Cell-mediated transcytosis is the mechanism by which immune cells, such as macrophages and monocytes, cross the BBB by moving through the cytoplasm of CEC (Lai *et al.*, 2013).

2.2.2. The blood-brain tumour barrier

The organised structure of the BBB may become disrupted in brain tumours, forming an altered barrier known as the blood-brain tumour barrier (BBTB) (Dong, 2018). Disruption can occur due to the uncontrolled proliferation of tumour cells. Watkins *et al.*, (2014) found that invasive glioma cells can displace the astrocytic end-feet from their position around the CEC, increasing the permeability of the BBTB. Furthermore, the overexpression of pro-angiogenic factors, a common feature of many tumours, promotes the formation of disorganised, leaky blood vessels (Hanahan and Weinberg, 2011). The increased permeability of the BBTB cannot, however, be exploited for the drug delivery, as the extent of BBB disruption varies between different tumour types and grades, and even different positions within the same tumour (van Tellingen *et al.*, 2015). Low-grade gliomas, for example, display minimal BBB disruption compared to high-grade gliomas, while the core of glioblastoma tumours often displays a highly leaky and disrupted BBTB compared to the invasive tumour edges (Kim *et al.*, 2015; van Tellingen *et al.*, 2015).

2.3. Current treatment of brain cancers

First-line therapy for brain cancers usually involves surgery to remove the tumour. However, surgery may not always be possible, or may be insufficient to remove all cancerous cells, and is often followed by chemotherapy or radiation therapy to kill remaining cancer cells (Koo *et al.*, 2006). Both adjuvant therapies are unable to target cancer cells and are often associated with potentially serious side effects. Radiation therapy may cause damage to the white matter of the brain, and has been associated with cognitive decline in adult patients and impairment of brain development in paediatric patients (Koo *et al.*, 2006; Raghubar *et al.*, 2017). Chemotherapeutic options are limited, as most drugs are unable to cross the BBB. Radiation and chemotherapy only lead to

modest increases in the survival times of malignant gliomas such as glioblastoma, and often do not prevent recurrence (Khosla, 2016; Wen and Kesari, 2008).

It is possible to disrupt the BBB by loosening the TJs to allow passage of drugs across the BBB; however this would also leave the CNS open to attack by pathogens or toxic agents (Grabrucker *et al*., 2014). Alternatively, there are three methods of trans-cranial drug delivery: intra-cerebroventricular (ICV) injection, intra-cerebral (IC) implantation, and convection-enhanced diffusion (CED). In ICV, the drug is injected into the cerebrospinal fluid (CSF), which will then carry the drug into the brain (Domínguez *et al.*, 2013). However, the turnover rate of CSF in the brain is faster than the rate at which the drug diffuses into the brain from the CSF (Pardridge, 2007). IC implantation and CED both involve insertion of the drug directly into the brain, but differ in their methods: drugs are directly injected into the brain using a syringe in IC implantation, while CED makes use of a catheter inserted into the brain, through which the drug is continuously pumped (Domínguez *et al.*, 2013).

Given the severity of many brain cancers and the difficulties faced in treating them, there is a need to develop alternative treatment methods, which can efficiently target and kill cancer cells only, without damaging healthy cells. Gene therapy strategies, which can be delivered to cancer cells using nanoparticle vectors, are attractive alternatives, as they have the potential to satisfy these requirements.

2.4. Gene therapy

Gene therapy involves the use of therapeutic nucleic acids to treat or prevent a disease or genetic disorder (Hardee *et al*., 2017). The concept of gene therapy arose in the 1960s, with the first clinical gene therapy trial carried out in 1990 on patients suffering from the monogenetic disorder adenosine deaminase deficiency (ADA-SCID) (Wirth *et al.,* 2013). The first therapeutic trial on cancer using gene therapy was conducted by Rosenberg, (1992), who modified tumour-infiltrating lymphocytes (TILs) *ex vivo* through retroviral gene transfer to express the tumour necrosis factor (TNF). Administration of these modified TILs in conjunction with interleukin-12 to patients with metastatic melanoma resulted in regression of melanoma nodules in one patient. Today, the majority of gene therapy trials are conducted on cancer (Figure 2.4) (Ginn *et al.*, 2018). Despite this extensive research, there are very few gene therapy products approved for cancer

treatment. These include Gendicine, which is licensed for the treatment of head and neck squamous cell cancer in China, and Kymriah™ and Yescarta™, which have recently been approved by the American Food and Drug Administration (FDA) for the treatment of acute lymphoblastic leukaemia and B-cell lymphoma, respectively (Ginn *et al*., 2018; Mullard, 2018).

Cancer diseases 65% (n=1688)
Monogenic diseases 11.1% (n=287)
Infectious diseases 7% (n=182)
Cardiovascular diseases 6.9% (n=180)
Neurological diseases 1.8% (n=47)
Ocular diseases 1.3% (n=34)
Inflammatory diseases 0.6% (n=15)
Other diseases 2.2% (n=58)
Gene marking 1.9% (n=50)
Healthy volunteers 2.2% (n=56)
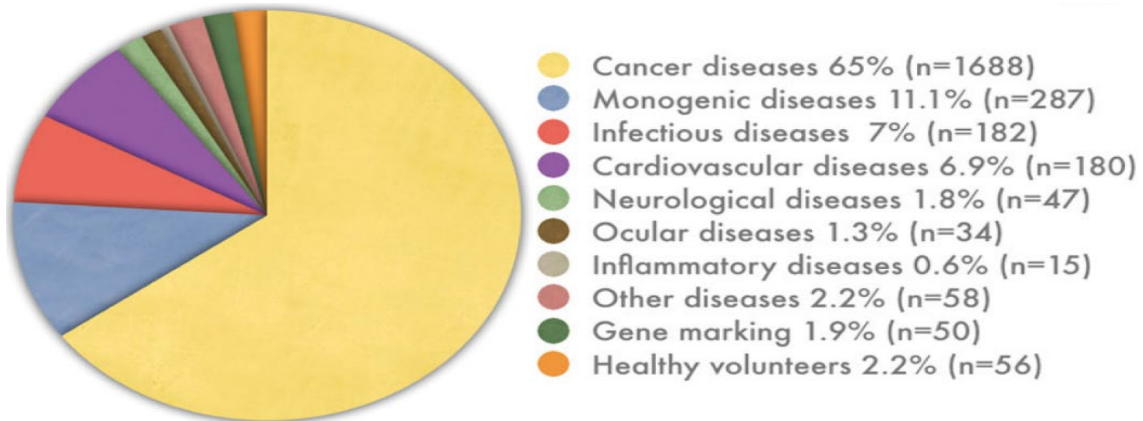
Figure 2.4: Diseases treated by ongoing gene therapy clinical trials until 2017 (Ginn *et al*., 2018).

Traditionally, gene therapy revolved around the introduction of functional copies of defective genes to replace the dysfunctional gene by homologous recombination. This type of gene therapy is well-suited to monogenic disorders, but is less applicable to disorders such as cancer that may arise due to multiple mutations (Kwiatkowska *et al*., 2013). Gene therapy strategies have thus been expanded to include the delivery of other types of genes and nucleic acids (Figure 2.5).
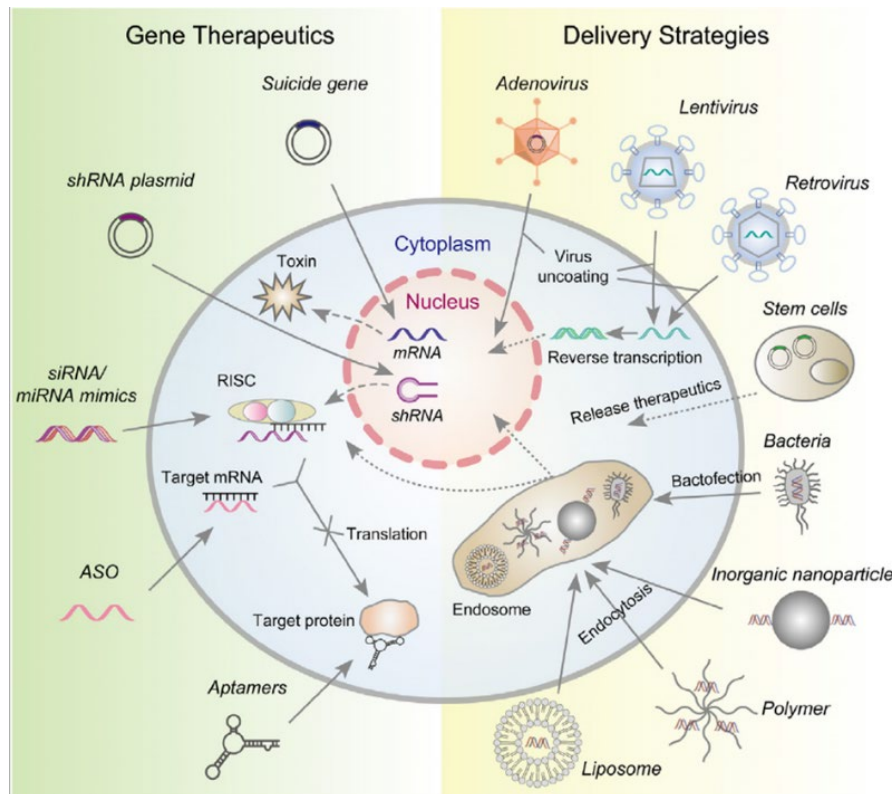
Figure 2.5: The different gene therapy strategies and delivery systems that have been developed for cancer therapy (Wang *et al.*, 2016).

2.4.1. Gene therapy strategies for cancer

Gene therapy strategies can be used to correct mutations that lead to the abnormal expression of oncogenes and TSGs. Overactive oncogenes can be knocked out using antisense technologies, such as siRNA or antisense oligonucleotides (ASO) that bind to and degrade mRNA. The introduction of functional TSGs into cancer cells may lead to the induction of apoptosis, or re-sensitise cells to chemotherapy or immunotherapy (Kwiatkowska *et al.,* 2013). This may also be observed in cancers with intact TSGs, due to overexpression of the TSG product (Asadi-Moghaddam and Chiocca, 2009). The drug Gendicine, comprised of recombinant adenoviral vectors that deliver the TSG p53 to cancer cells, is based on this principle (Zhang *et al.*, 2018).

The immune system plays an important role in the detection and destruction of cancerous cells, through recognition of antigens displayed by major histocompatibility complex (MHC) proteins on the cancer cell surface (Blattman and Greenberg, 2004). However, tumours have developed many mechanisms to evade detection, such as downregulation of immune receptors and secretion of proteins that block the immune response to

cancerous cells (Blattman and Greenberg, 2004). Cancer immunotherapy involves using the host's immune system to fight cancer, by enhancing the immune response to malignant cells. The immune response can be boosted through the delivery of cytokine-encoding genes to the tumour. These genes stimulate the tumour cells to produce cytokines, which recruit T-cells and natural killer (NK) cells (Kwiatkowska *et al*., 2013; Larin *et al*., 2004). An immune response to specific tumour-associated antigens (TAAs) may also be raised using DNA vaccines or through T-cell modification. DNA vaccines are delivered to the skin or muscle, and encode TAAs that, when expressed, raise an immune response against the antigen (Fioretti *et al*., 2010; Wu *et al*., 2017). T-cells may be modified to express T-cell receptors (TCR) that recognise tumour antigens displayed by the MHC; however, downregulation of MHC proteins in tumours limits the efficiency of these modified T-cells (Fesnak *et al*., 2016). Alternatively, T-cells can be modified to express artificial receptors, called chimeric antigen receptors (CAR), that can be synthesised to recognise any surface antigens, not only those displayed by the MHC (Fesnak *et al*., 2016). CAR-T cell therapy has recently shown great promise in treating glioblastoma tumours (Brown *et al*., 2016). Kymriah™ and Yescarta™ are CAR-T cell therapies, which utilise T-cells engineered to target the CD19 antigen expressed on B-cells (Mullard, 2018).

Other therapeutic approaches include modification of the tumour microenvironment or delivery of suicide genes. Solid tumours are characterised by disorganised and leaky vasculature, which is not only incapable of adequately supplying tumour cells with blood and oxygen, but also limits the delivery of chemotherapeutic agents (Ramjiawan *et al*., 2017). The distorted vasculature arises in response to the overexpression of pro-angiogenic factors, such as vascular endothelial growth factor (VEGF) and the fibroblast growth factors (FGF), which are upregulated by overactive oncogenes or hypoxic conditions (Hanahan and Weinberg, 2011). Gene knockout strategies, such as siRNA, can be used to silence overexpressed angiogenic genes, to limit the spread of tumours or normalise blood vessels to improve treatment delivery (Ramjiawan *et al*., 2017). Suicide gene therapy, or gene directed enzyme prodrug therapy, involves the delivery of suicide genes encoding enzymes that convert non-toxic prodrugs into cytotoxic drugs (Karjoo *et al*., 2016). The herpes simplex virus thymidine kinase/ganciclovir (HSVTK/GCV) system, in which the prodrug ganciclovir is converted into a nucleoside analogue that interferes

14

with DNA replication, is the most commonly used suicide gene system (Karjoo *et al*., 2016).

2.5. Vectors for gene therapy

Successful gene therapy depends on the therapeutic gene entering the nucleus of the target cell with minimal biodegradation. However, the negative charge on nucleic acids prevents them from interacting with the anionic cell membrane, and free nucleic acids are susceptible to attack by nucleases (Ibraheem *et al*., 2014). For this reason, a variety of viral and non-viral delivery systems have been developed. The ideal vector should be capable of carrying large genes, allow for prolonged expression of the transgene at levels that are appropriate for effective treatment, and should be cheap and easy to produce in large quantities, and at an appropriate purity for therapeutic applications (Lentz *et al*., 2012; Ibraheem *et al*., 2014). Further challenges faced in *in vivo* gene delivery include a number of extra- and intracellular barriers that must be overcome, and avoidance of adverse host reactions by the vector not triggering an immune response or destroying healthy cells.

2.5.1. Viral vectors

Viruses have evolved many mechanisms of infecting host cells and hijacking the cell machinery to produce viral copies; and this ability to efficiently deliver and drive expression of their genes makes them obvious candidates for gene delivery. They are highly efficient at transfecting cells, display modifiable tissue tropisms, and can lead to stable and long-term expression of transgenes in dividing and non-dividing cells, depending on the virus used (Lentz *et al*., 2012). Viral vectors are thus currently the most commonly used vectors in gene therapy trials (Ginn *et al*., 2018). Apart from gene delivery, viruses can also be used in oncolytic therapy. This type of therapy utilises viruses that selectively infect and proliferate in tumour cells, lysing them or stimulating an immune response against them (Hulou *et al*., 2016).

Adenoviruses, adeno-associated viruses (AAV), retroviruses, and Herpes simplex virus type 1 (HSV-1) are commonly used for gene delivery to the CNS (Lentz *et al*., 2012). Adenoviruses are double-stranded DNA (dsDNA) viruses with a 34 - 43 kbp genome (Kotterman *et al*., 2015). They are the most commonly used vectors in gene therapy

clinical trials, due to their relatively large packaging capacity and ability to be produced in high titres (Choudhury *et al*., 2017; Ginn *et al*., 2018). However, they may induce strong host immune responses, with the first death in a gene therapy trial occurring in response to a high dose of adenoviral vectors (Wirth *et al.,* 2013). AAVs are non-pathogenic, single-stranded DNA (ssDNA) viruses that require the presence of a helper virus for replication (Ojala *et al*., 2015). They display low immunogenicity and can be synthesised at high titres (Choudhury *et al*., 2017). However, the use of AAVs is limited by their small packaging size, as their genome is only 4.7 kbp in length (Ojala *et al*., 2015). Retroviruses are ssRNA viruses that integrate into the host genome during their replication cycle. Complex retroviruses, in particular lentiviruses, are popular for CNS delivery, as they are capable of transfecting non-dividing cells (Escors and Breckpot, 2010). The integration of retroviral vectors into the genome allows for long-term expression of the transgene; however it may also lead to insertional mutagenesis, as was observed in a retroviral gene therapy trial treating X-linked severe combined immunodeficiency (Hacein-Bey-Abina *et al*., 2003). HSV-1 is an attractive vector for CNS therapy due to its natural neurotropism (Artusi *et al*., 2018). Furthermore, they display a large packaging capacity of up to 150 kbp and do not integrate into the genome, eliminating risks of insertional mutagenesis (Artusi *et al*., 2018).

2.5.2. Non-viral delivery

While adenoviruses and retroviruses remain the most commonly used vectors in clinical trials, their usage has seen a decrease due to safety concerns (Ginn *et al*., 2018). Several non-viral vectors are being explored as safer alternatives for gene delivery. While they are less effective than viral vectors at transfecting cells, non-viral vectors have gained interest due to their lower immunogenicity, relative ease of synthesis, and ability to carry larger transgenes (Chira *et al*., 2015; Riley II and Vermerris, 2017).

Non-viral delivery may involve physical administration of the gene, using physical force to weaken the cell membrane, or delivery via a vector. Physical methods include electroporation, sonoporation, and biolistic transfer. Nanoparticles (NPs) that range from 1-100 nm in length have gained much attention as non-viral vectors for gene delivery. They display many characteristics that make them useful vectors, such as their small size allowing entry into cells, and large surface area-to-volume ratio allowing for

functionalisation with therapeutic or targeting compounds (Mendes *et al.,* 2017). NPs composed of both inorganic and organic materials have shown promise in cancer treatment.

2.5.2.1. Physical methods of non-viral gene delivery

2.5.2.1.1. Electroporation

Electroporation is a highly versatile technique that can be used for the *in vivo, in ovo* or *in utero* delivery of proteins, DNA or RNA (De Vry *et al.*, 2010b). It involves the application of electric pulses to cells, creating pores in the plasma membranes (Bonakdar *et al.*, 2016). Therapeutic compounds can then enter cells through diffusion, or migrate along the electric current through the pores and into cells (De Vry *et al.*, 2010a). The pores are able to close, trapping exogenous compounds inside the cell (Cwetsch *et al.*, 2018). However, if the current is too strong, or the cells are exposed to the field for an extended duration of time, the pores may be too large to reseal, leading to cell death (Yarmush *et al.*, 2014). Optimisation of electroporation parameters is thus highly important in order to maximise transfection efficiency while minimising tissue damage (De Vry *et al.*, 2010b). Electroporation has been used to deliver DNA to organs such as the liver, brain and skin (De Vry *et al.*, 2010a), and has also been shown to increase the permeability of the BBB, allowing for uptake of compounds via transcellular diffusion (Bonakdar *et al.*, 2016).

2.5.2.1.2. The biolistic method

The biolistic method uses a gene gun to fire DNA-coated particles into target tissues, by propelling them at high speeds using helium gas or a high voltage electric discharge (Pahle and Walther, 2016). Microparticles $1 - 1.5$ μm in diameter and composed of non-toxic and non-reactive metals, such as gold, are often used (Mehier-Humbert and Guy, 2005). Transfection efficiency is influenced by the number of particles delivered, the particle size, and the amount of DNA loaded onto the particles (Mehier-Humbert and Guy, 2005). The gene gun is a fast and simple method of transfecting cells; however, its use for treating tumours is limited by its inability to penetrate deep tissues without surgery (Alsaggar and Liu, 2015). Moreover, it is often associated with cell damage due to the pressure released by the gun and the large size of the microparticles used (O'Brien and

Lummis, 2011; Sato *et al*., 2000). The gene gun is a popular technique for the delivery of DNA vaccines, as it can efficiently deliver a small amount of DNA into skin and muscle cells to elicit an immune response (Lee *et al*., 2018; Pahle and Walther, 2016).

2.5.2.1.3.　　Focused ultrasound

Focused ultrasound (FUS), or sonoporation, represents a non-invasive method of treating cancers. High-intensity focused ultrasound (HIFU) functions by focusing ultrasound beams on tumour cells, leading to a lethal increase in temperature in the area where the beams converge (van den Bijgaart *et al*., 2017). FUS may also be used in combination with microbubbles (MB) to create temporary pores in cell membranes for gene delivery. The application of FUS in the target region leads to the oscillation of MBs, creating shear stress and leading to the expansion and subsequent collapse of MBs, releasing a micro shockwave that temporarily disrupts cell membranes (Mellott *et al*., 2013; Shin *et al.*, 2018). The MB oscillations are also capable of transiently loosening the TJs to allow therapeutic agents into the brain, and have been shown to improve doxorubicin delivery to glioblastoma tumours in rats (Aryal *et al.*, 2013; Liu *et al.,* 2010; Treat *et al.,* 2007).

2.5.2.2.　　Liposomes

Liposomes are composed of one or more phospholipid bilayers surrounding an aqueous core (Posadas *et al*., 2016; Vieira and Gamarra, 2016). Since their discovery in the 1960s, they have become popular vectors due to their biocompatibility, low immunogenicity, and ability to carry genes, as well as hydrophobic, hydrophilic and lipophilic drugs. Hydrophobic and lipophilic drugs interact with the phospholipid tails, while hydrophilic drugs are trapped in the aqueous core, or interact with the hydrophilic phospholipid heads (Vieira and Gamarra, 2016).

Liposomes are often categorised into four groups according to their lipid composition: conventional, stealth, targeted and cationic liposomes (Figure 2.6). Conventional liposomes, composed of neutral or anionic phospholipids, are characterised by short circulation times due to aggregation with serum proteins and clearance by the reticuloendothelial system (RES) (Storm and Crommelin, 1998). Furthermore, they are unable to electrostatically bind nucleic acids and instead encapsulate them, which is an inefficient process (Semple *et al*., 2001). Long-circulating, or stealth, liposomes are

surface-modified through the addition of glycolipids and hydrophilic polymers, such as poly(ethylene) glycol (PEG) (Immordino *et al*., 2006). These compounds reduce liposomal interactions with serum components, thus preventing clearance and extending circulation times (Immordino *et al*., 2006). Cationic liposomes bear a net positive charge, allowing them to easily complex nucleic acids into lipoplexes, and promote interactions with cell membranes. Joshi *et al*., (2014) showed that cationic liposomes are capable of efficiently crossing the BBB following intra-arterial delivery, possibly by AMT. The addition of polymers such as PEG can be used to increase circulation time and the likelihood of cerebral uptake (Tam *et al*., 2016). Targeted liposomes are functionalised with ligands, such as proteins or antibodies, which recognise receptors on specific cells, allowing for targeted delivery of therapeutics. Receptors such as the Tf receptors expressed on the BBB have been exploited for liposomal delivery to the brain.
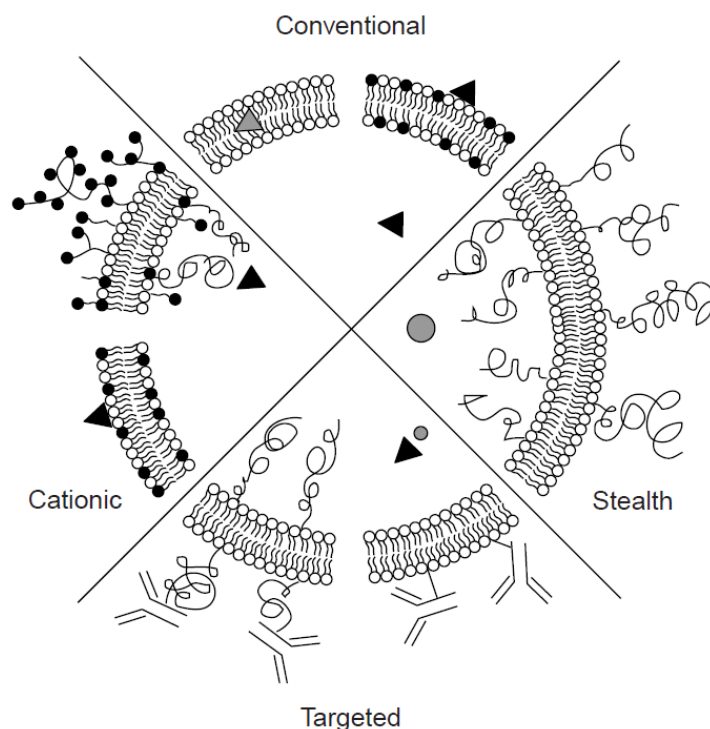
Figure 2.6: The four categories of liposomal vectors (Storm and Crommelin, 1998).

2.5.2.3.   Polymeric nanoparticles

Both naturally-occurring and synthetic cationic polymers have been used for gene delivery. These polymers are positive due to the presence of amine groups and carry multiple functional groups allowing for conjugation with targeting, and other, ligands

(Posadas *et al*., 2016). Their ability to efficiently bind and condense nucleic acids into polyplexes, which are generally more stable and smaller in size than lipoplexes, has made them attractive vectors for gene delivery (Ibraheem *et al*., 2014; Mao *et al*., 2001). However, the cytotoxicity and immunogenicity displayed by some cationic polymers has hampered their use *in vivo*.

The synthetic polypeptide poly(L-lysine) (PLL) was the first cationic polymer developed for delivery, but its use has been limited by its cytotoxicity and low transfection efficiency (Posadas *et al*., 2016). PLL-conjugates with peptides and PEG have since been developed, which show reduced toxicity and increased transfection efficiency (Nayerossadat *et al*., 2012). Other polymers have also been investigated, the most popular of which are chitosan and polyethyleneimine.

2.5.2.3.1. Polyethyleneimine

The second-generation synthetic polymer polyethyleneimine (PEI) bears a strong positive charge that promotes nucleic acid condensation and cellular uptake, and has a buffering capacity that promotes endosomal escape via the proton sponge effect (Rafael *et al*., 2015). For these reasons, PEI is considered as the gold standard for transfection (Joshi *et al*., 2018). The characteristics of PEI must be carefully controlled when designing vectors, as branched and/or high MW forms display significant cytotoxicity, while low MW forms display low transfection efficiencies (Posadas *et al*., 2016). Kafil and Omidi, (2011) observed increased cytotoxicity in human epidermoid carcinoma (A431) cells treated with branched PEI compared to linear PEI, and Zhong *et al*., (2013) observed that higher MW branched and linear PEI induced aggregation of red blood cells at lower concentrations than lower MW PEI. Cytotoxicity may be reduced through optimisation of chain length and conjugation with PEG (Rafael *et al*., 2015).

2.5.2.3.2. Chitosan

Chitosan (CS) is a biocompatible and biodegradable natural polysaccharide composed of repeating β(1,4)-linked D-glucosamine and N-acetyl-D-glucosamine units (Mao *et al*., 2001). CS compounds differ in their degree of deacetylation and MW, and, as with PEI, these features must be optimised to enhance transfection efficiency. A high degree of deacetylation promotes interactions with nucleic acids (Rafael *et al*., 2015), and uptake

by cells (Huang *et al*., 2004). However, Huang *et al*., (2004) found that CSNPs with high degrees of deacetylation displayed high toxicities that were not associated with increased uptake. CSNPS are nevertheless promising vectors for delivery to the brain, as they have been shown to be capable of efficiently entering human BBB cerebral microvessel endothelial cells by macropinocytosis (Sahin *et al*., 2017). They have further been shown to enter and accumulate around the nuclei of neuronal cells (Malatesta *et al*., 2012).

2.5.2.4. Inorganic nanoparticles

Inorganic NPs have more recently been investigated as vectors, as they display several advantages over traditional organic vectors. These include their small size, high stability, good biocompatibility, and ease of synthesis and functionalisation (Xu *et al*., 2006). The sizes, shapes and chemical compositions of inorganic NPs can be easily tailored during synthesis, and they often display unique optical, magnetic and electrical properties, making them highly versatile vectors for both therapeutic delivery and imaging (Wang *et al*., 2016). A variety of widely-available inorganic compounds have shown potential for CNS delivery, including metals, magnetic compounds and silica. The noble metals, particularly gold, have received a significant amount of research (Mendes *et al*., 2017), and are used in this study.

2.6. Gold nanoparticles

Colloidal gold solutions have been used medicinally for thousands of years, to treat a variety of diseases ranging from dysentery in the Middle Ages, to alcoholism in the early 20th century (Dykman and Khlebtsov, 2011). Faulk and Taylor (1971) were the first to use gold nanoparticles (AuNPs) in a field outside medicine, when they labelled AuNP with antibodies, allowing for visualisation of the antibodies with an electron microscope. Nowadays, AuNP are extensively studied in many different fields, and have a wide range of applications, including disease diagnosis, imaging, nanoelectronics, and the therapeutic delivery of drugs and genes (Perala and Kumar, 2013).

2.6.1. Properties of gold nanoparticles

AuNPs display many unique and useful optical and physicochemical properties that facilitate their use in different fields of science. They display good biocompatibility, large surface-to-volume ratio, and ease of surface modification, as gold easily forms strong covalent bonds with sulphur, allowing for functionalisation with thiols (Mendes *et al.*, 2017). They are also highly tunable and can be easily synthesised in a variety of shapes and sizes, each displaying its own unique size- and shape-dependent optical properties (Figure 2.7).

Figure 2.7: The colour of colloidal solutions of gold (a) nanorods, (b) nanoshells, and (c) nanocages changes in response to their different physical properties (Dreaden *et al.*, 2012).

Colloidal AuNP solutions ranging from 10 - 20 nm in diameter display a characteristic wine-red colour, while larger AuNP solutions are purple. This occurs due to the surface plasmon resonance (SPR), a phenomenon describing the oscillation of free electrons in response to light (Figure 2.8). Upon exposure to light, the free electrons in the AuNP, also called the conduction band of electrons, collectively shift in response to the electromagnetic field. The resulting dipole, in combination with the electromagnetic field,

causes the free electrons to oscillate (Huang and El-Sayed, 2010). The energy required to move the electrons is absorbed as light, with the 10–20 nm AuNP absorbing light at approximately 520 nm in the green part of the visible spectrum, and scattering red light, giving the colloidal solution its characteristic red colour (Huang and El-Sayed, 2010). SPR is influenced by many factors, such as the shape, size, and charge of the NP, the presence of surface modifications, and particle aggregation (Yeh *et al*., 2012). The SPR property of AuNP makes them valuable components of detection and imaging systems, for example, tumour-targeted AuNP that absorb maximally at near-infrared (NIR) wavelengths can be used to image tumours (Singh *et al*., 2018).
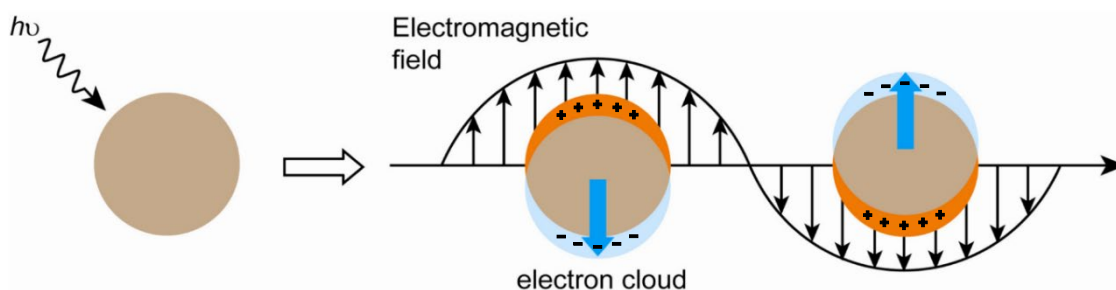
Figure 2.8: Representation of surface plasmon resonance, the oscillation of free electrons in response to light (Adapted from Yeh *et al*., (2012)).

2.6.2. Synthesis of gold nanoparticles

2.6.2.1. Chemical methods

The first scientific report on the chemical synthesis of AuNP was published in 1857 by Michael Faraday, who described a two-phase system in which phosphorous in carbon disulphide (CS_2) reduced hydrogen tetrachloroaurate, or chloroauric acid, ($HAuCl_4$) (Daniel and Astruc, 2004; Dreaden *et al*., 2012). Chemical methods involve the reduction of the Au^{3+} ions in $HAuCl_4$ to metallic gold (Luty-Błocho *et al*., 2017). Chemicals that act as stabilising and capping agents are often added during synthesis. Stabilising agents attach to the NP surface and prevent aggregation, while capping agents control the size of the NP by adsorbing to the surface to form a highly thermodynamically stable capped NP (Polte, 2015).

2.6.2.1.1. The citrate reduction method

The citrate reduction method was first described by Turkevich *et al*., (1951), and remains the most popular synthesis method due to its simplicity and ability to produce stable AuNP of varying sizes (Elahi *et al*., 2018). It involves the addition of trisodium citrate to a boiling HAuCl$_4$ solution in water (Figure 2.9). Trisodium citrate further functions as both the capping agent and the stabilising agent (Mpourmpakis and Vlachos, 2009). The resulting citrate-capped AuNP bear a strong negative charge, and are usually spherical and 10 - 20 nm in diameter (Yeh *et al*., 2012). Frens, (1973) modified the procedure to synthesise AuNP ranging from 15 - 150 nm in diameter by varying the ratio of gold to citrate, with lower citrate concentrations producing larger NPs. This size variation was shown to be dependent on the pH of the solution, which is influenced by the citrate concentration (Ji *et al*., 2007). Different mechanisms have been proposed for AuNP formation in the citrate reduction method. Following X-ray scattering and absorption studies, Polte *et al*., (2010) proposed a synthesis model involving four phases. Initially, approximately 20% of the Au^{3+} is reduced to form 2 nm AuNP, which merge to form larger NPs. In the third and fourth phases, the AuNP increase in size by diffusion of gold atoms in solution onto the nanoparticles, and through reduction of the remaining Au^{3+}. In contrast, Pong *et al*., (2007) proposed that AuNP synthesis occurs via the formation of gold nanowire intermediates. They observed the formation of 5 nm nanoclusters which assemble into nanowires. As the nanowires increase in diameter, they destabilise and fragment into smaller particles that develop into spherical AuNP (Pong *et al*., 2007).
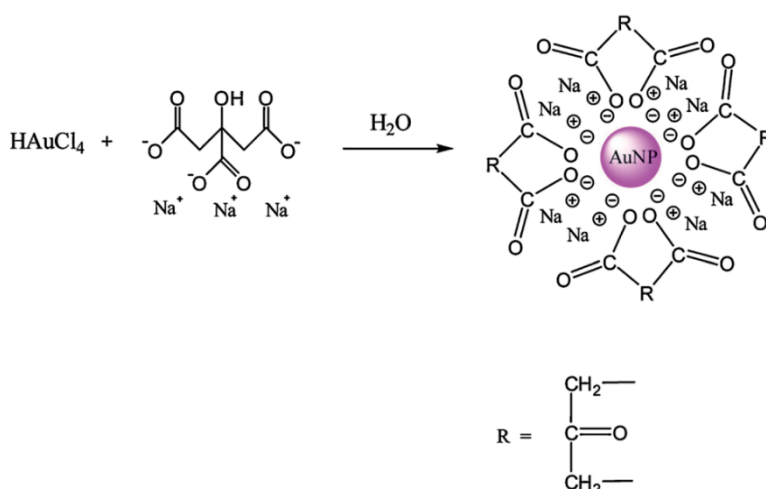
Figure 2.9: Synthesis of AuNP via the citrate reduction method. HAuCl$_4$ is reacted with trisodium citrate to form citrate-capped AuNP (Herizchi *et al*., 2016).

2.6.2.1.2. The Brust-Schiffrin method

This method, developed by Brust *et al*., (1994), synthesises AuNP in a two-phase system, composed of an aqueous solution of HAuCl$_4$ and an organic phase containing toluene. Tetraoctylammonium bromide (TOAB) is added as a phase-transfer agent, transporting AuCl^{4-} ions from the aqueous phase to toluene, where sodium borohydride (NaBH$_4$) reduces the gold to form AuNP (Perala and Kumar, 2013). Alkanethiols, such as dodecanethiol, are often used as the stabilising agent, as, upon addition to the toluene layer, they form strong gold-thiol interactions that result in highly stable AuNP (Figure 2.10) (Yeh *et al*., 2012). AuNP range from 1.5 – 5 nm in diameter depending on factors such as the reaction temperature and gold-to-thiol ratio, and can be recovered by precipitation and re-suspended in non-polar solvents to produce stable colloidal solutions (Brust *et al*., 1994; Yeh *et al*., 2012).
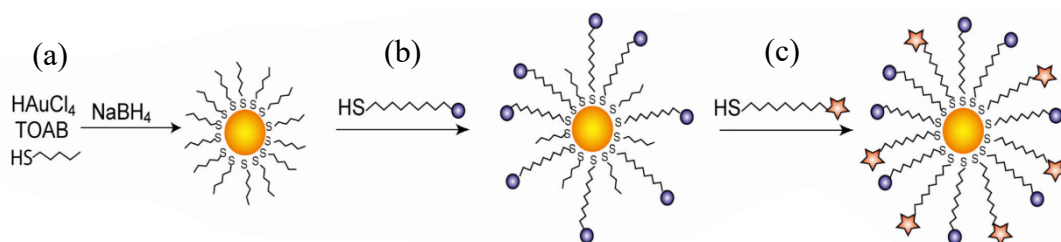
Figure 2.10: The Brust-Schiffrin method producing thiol-stabilised AuNP. Different kinds of functionalised thiols can be conjugated to AuNP via place exchange reactions ((b) and (c)) (Yeh *et al*., (2012).

2.6.2.2. Biological methods

Chemical methods of NP synthesis tend to use toxic and expensive reducing reagents, which may limit upscaling production and be harmful to the environment (Menon *et al*., 2017). Thus, a number of eco-friendlier biological methods have been developed, which utilise microorganisms or plant extracts to synthesise AuNP. Gold ions are toxic to microbes, and thus many bacteria, fungi, and algae produce intra- or extracellular enzymes that convert the toxic ions to non-toxic nanoparticles (Li *et al*., 2016; Menon *et al*., 2017). Bacteria such as *Escherichia coli* and *Deinococcus radiodurans* are capable of synthesising AuNP (Li *et al*., 2016). Fungi often display high tolerance for toxic metals and secrete large amounts of extracellular enzymes, making them attractive for large-

scale production of AuNP (Kitching *et al*., 2015). It may, however, be difficult to isolate pure solutions of microbially-synthesised NPs that are not contaminated by cellular components (Kitching *et al*., 2015). Plant extracts from *Aloe vera* and onions have been used to synthesise AuNP. These extracts are cheap, easily available, eco-friendly, and act as both reducing and stabilising agents, allowing for a one-step synthesis (Herizchi *et al*., 2016).

2.6.2.3.   Characterisation of gold nanoparticles

Determination of the physiochemical characteristics of NPs is vital to understanding their behaviour *in vivo* (Bhattacharjee, 2016). The size and morphology of synthesised AuNP can be analysed through transmission electron microscopy (TEM). The zeta potential, or electrokinetic potential, of the NP is another important characteristic that provides information about NP interactions with cellular surfaces, as well as with other NPs. When in solution, NPs are surrounded by the electric double layer (EDL), composed of the stern and the diffuse layers (Figure 2.11) (Bhattacharjee, 2016; Forest and Pourchez, 2017). The stern layer is formed by ions in the solution that bind directly to the surface of the NP, while the diffuse layer is composed of both anionic and cationic ions that form around the stern layer (Bhattacharjee, 2016). The zeta potential is the potential of the shear, or slipping plane, the boundary between the ions of the diffuse layer and the free ions in the solution (Forest and Pourchez, 2017). It is commonly used as an indication of the stability of the colloidal solution, as NPs with high zeta potentials will tend to repel each other, while those with weak potentials will be unable to repel each other and aggregate (Table 2.1) (Bhattacharjee, 2016).

Table 2.1: The relationship between zeta potential and the stability of colloidal solutions (adapted from Bhattacharjee, (2016)).

Zeta potential range (mV)	Stability of colloidal solution
$\pm$ 0 – 10	Unstable
$\pm$ 10 – 20	Relatively stable
$\pm$ 20 – 30	Moderately stable
> $\pm$ 30	Highly stable
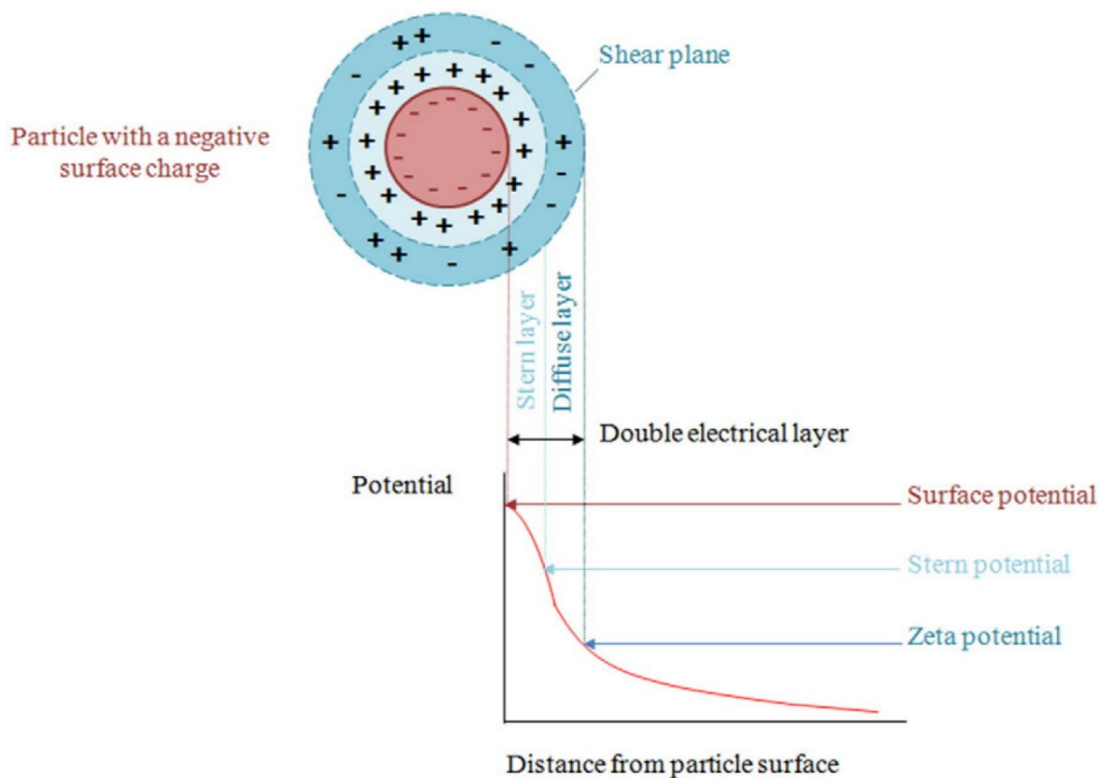
Figure 2.11: The electrical double layer that forms around NPs in solution (Forest and Pourchez, 2017).

2.6.3. Gold nanoparticles for gene delivery

Newly-synthesised citrate-capped AuNP bear a net negative charge and are therefore unable to directly bind anionic nucleic acids for delivery. Instead, they may be bound to AuNP via covalent thiol linkages, or via electrostatic interactions with cationic ligands. Mirkin *et al*., (1996) were the first to take advantage of the strong gold-sulphur bond to attach thiolated nucleic acids to AuNP. This method is commonly used for functionalising AuNP with short oligonucleotides, such as siRNA, microRNA (miRNA), or DNA aptamers, which are able to retain their activity after being modified to carry a thiol group (Ding *et al*., 2014a). Oligonucleotides may be anchored via a simple sulfhydral group (SH) at the 3' or 5' end of the sequence, or via more complex alkanethiols, or disulfides (Li *et al*., 2013a). Alternatively, non-modified nucleic acids can be electrostatically bound to AuNP coated with cationic polymers or AAs that can complex and condense nucleic acids. Early studies by Han *et al*., (2006) indicated that anionic phosphate backbone of DNA wraps around cationic AuNP in a similar manner to how DNA wraps around proteins such as histones, providing protection from degradation by nucleases or free

27

radicals. AuNP coated with the cationic polymer PEI have been shown to effectively bind siRNA and facilitate knockdown of the eukaryotic elongation factor 2 kinase (*eEF-2K*) gene in triple negative breast cancer cells (Shahbazi *et al*., 2017); and complex pDNA for the treatment of melanoma (Niu *et al*., 2017).

2.6.4. Biodistribution of gold nanoparticles

Multiple groups have observed the accumulation of AuNP in many different organs, such as the liver, spleen, kidneys, and intestines, following intravenous injection (De Jong *et al*., 2008; Lopez-Chaves *et al*., 2018; Sonavane *et al*., 2008; Takeuchi *et al*., 2017). Larger AuNP tend to accumulate in the liver and spleen, while smaller AuNP tend to accumulate in the kidneys – as Lopez-Chaves *et al*., (2018) noted, NPs small enough to make the renal cut-off will be cleared by the kidneys, while larger NPs will instead be cleared by the RES and accumulate in the liver and spleen.

The AuNP studied by these groups were also detected in the brain tissue, suggesting they are able to cross the BBB without the need for functionalisation with targeting ligands. De Jong *et al*., (2008) and Takeuchi *et al*., (2017) observed that AuNP smaller than 20 nm were present in rat brains following intravenous injection, while Sonavane *et al*., (2008) detected AuNP up to 100 nm in diameter in mice brains following intravenous injection. Hillyer and Albrecht, (2001), who analysed the distribution of AuNP after oral delivery, also observed the presence of AuNP in the brain. This ability of AuNP to enter the rat brain was investigated by Sela *et al.*, (2015), who hypothesised that 1.3 nm AuNP may cross the BBB via ion channels. Li *et al*., (2015) studied the interactions between 40 nm AuNP and the TJs of the BBB. They observed that the AuNP increased BBB permeability by downregulating TJ proteins, potentially providing a means for uncoated AuNP to cross the BBB. These data also suggest that the route of administration may not be an important factor influencing the delivery of AuNP to the brain (Masserini, 2013).

2.6.5. Cytotoxicity of gold nanoparticles

While AuNP are often described as being highly biocompatible and non-toxic, several studies have found that they display cytotoxicity dependent on characteristics such as their size, shape and composition. Size-dependent cytotoxicity was shown by Pan *et al*., (2007), who found that 1.4 nm AuNP displayed higher toxicities than 0.8, 1.2, and 15 nm

AuNP. These results were corroborated by Tsoli *et al*., (2005), who found 1.4 nm AuNP to be toxic to both cancerous and normal cells. This size-specific cytotoxicity was found to be due to the 1.4 nm AuNP' ability to bind to the major groove of DNA, possibly interfering with important cellular functions (Pan *et al*., 2007; Tsoli *et al*., 2005). Pernodet *et al*., (2006) found that 14 nm citrate-capped AuNP displayed dose-dependent cytotoxicity to fibroblast cells, with higher concentrations causing more damage to actin filaments in cells. Often, contradictory results are obtained in cytotoxicity studies: Chen *et al*., (2009) observed low toxicity for 3, 5, 50, and 100 nm AuNP in mice; however, mice injected with AuNP between 8 – 37 nm displayed severe abnormalities in liver, lung and spleen tissue. In contrast, Fan *et al*., (2009) observed higher toxicities for 5 nm AuNP, compared to 15 and 30 nm AuNP, in human bone marrow stem cells and hepatocarcinoma (HuH-7) cells. These conflicting results led Khlebtsov and Dykman, (2011) to suggest that observed cytotoxicities for AuNP larger than 3 nm may be due to the number of particles per ml, rather than directly due to AuNP size, and also that cell type may be an important factor influencing AuNP cytotoxicity.

2.7. Targeting the brain

Ensuring that intravenously-administered therapeutic cancer agents selectively accumulate in cancer cells is a major hurdle for treatment development, and this problem is exacerbated for brain cancer treatments that must first overcome the BBB. To achieve this, NPs may either be passively or actively targeted towards the BBB. Passive targeting relies on the enhanced permeation and retention (EPR) effect, the process by which systemically-administered NPs passively accumulate in tumours due to their leaky vasculature and reduced lymphatic drainage (Kim *et al*., 2015; Pinto *et al*., 2017). The EPR effect is observed in most solid tumours, making it a popular targeting method (Danhier *et al*., 2010). However, it is an unreliable and inefficient method of treating brain tumours, due to the inconsistent nature of the BBTB and BBB disruption (Kim *et al*., 2015). Active targeting involves functionalisation of NPs with targeting ligands, such as proteins, peptides and antibodies, which bind to receptors expressed on target cells. The BBB contains many receptors that can be exploited for delivery via CMT, such as GLUT1, or RMT, such as insulin and Tf. It is, however, difficult for NPs to exploit the CMT pathway as it is composed of highly substrate-specific proteins that transport small

molecules across the BBB, making them more suited to uptake via RMT (Furtado *et al.*, 2018). Tf is a popular targeting ligand due to its presence on the BBB and cancer cells, facilitating passage into the brain via RMT and cellular uptake via receptor-mediated endocytosis.

2.7.1. Receptor-mediated endocytosis

Endocytosis is an important process facilitating the uptake of nutrients, and regulation of surface receptor expression and membrane lipid composition (Canton and Battaglia, 2012; Fullstone *et al.*, 2016). Receptor-mediated endocytosis (RME) is initiated by ligand binding to its receptor on the cell surface, followed by invagination of the membrane and budding off as vesicles (Tashima, 2018). Uptake of the receptor-ligand complex occurs by caveolae-mediated (CvME) or clathrin-mediated endocytosis (CME). CvME internalises complexes in caveolae, which are flask-shaped invaginations in the cell membrane containing caveolin membrane proteins. Following budding off, the caveolae fuse with early endosomes, and commonly transport their cargo to the Golgi bodies or transcytose them (Zaki and Tirelli, 2010).

CME, however, is the major endocytic uptake mechanism, and is utilised for uptake of Tf, insulin, and low density lipoprotein (LDL) (Barar *et al.*, 2016; Bitsikas *et al.*, 2014). It involves the uptake of complexes in invaginations called clathrin-coated pits. These pits are coated with many cytosolic proteins, including the protein clathrin, which promotes membrane bending, leading to invagination (Kaksonen and Roux, 2018). Following uptake, the clathrin coat is broken down by ATP-dependent uncoating enzymes, and the vesicle fuses with the early endosome (Tortorella and Karagiannis, 2014). The early endosome experiences a drop in pH to an acidic 6.5, through the action of membrane-bound ATPases that pump protons into the endosome from the cytoplasm (Tashima, 2018). Some receptors, such as the LDL receptor, release their ligand under these acidic conditions; however, some ligands, such as the epidermal growth factor, remain bound to their receptor (Elkin *et al.*, 2016).

There are multiple sorting routes that the early endosome may undergo, and the receptor-ligand complex may be directed to the lysosome or be recycled back to the cell membrane (Grant and Donaldson, 2009). Degradation involves the maturation of the early endosome into a late endosome with an acidic pH of approximately 5.5. The late endosome then

fuses with lysosomes containing hydrolytic proteins, leading to the degradation of the endosomal contents (Barar *et al*., 2016). The receptors may be degraded along with the ligand; alternatively, they may bud off from the endosome and recycle to the cell membrane (Otero *et al*., 2006). Recycling of the receptor-ligand complex may occur through a fast recycling pathway, in which the early endosome is recycled directly back to the membrane, or via recycling endosomes (Welling and Weisz, 2010). Receptors may also be transported to the Golgi apparatus via retrograde transport. The Golgi apparatus is responsible for the synthesis of certain proteins involved in endocytosis, such as acid hydrolase precursors involved in degradation (Bonifacino and Rojas, 2006). These proteins bind to sorting receptors in the Golgi apparatus, which transport them to endosomes (Johannes and Popoff, 2008). These receptors dissociate from their cargo in the acidic early endosome, and are sent back to the Golgi apparatus (Johannes and Popoff, 2008).

The Rab family of GTPases play vital roles in endosomal sorting. They are small membrane proteins that localise to specific organelles, for example, Rab7 is expressed on late endosomes, and Rab4 and Rab5 associate with early endosomes (Lakadamyali *et al*., 2006; Smith and Gumbleton, 2006). Lakadamyali *et al*., (2006) used this property of Rab proteins to identify two populations of early endosomes: dynamic endosomes and static endosomes. Dynamic endosomes were found to acquire Rab7 within 30 seconds of internalisation, and thus matured quickly into late endosomes. In contrast, static endosomes did not acquire Rab7 for more than 100 seconds after internalisation, and matured slowly.

2.7.2. Receptor-mediated transcytosis

The process of RMT transports molecules across cells, and involves three major steps: endocytosis of the receptor-ligand complex, intracellular trafficking, and exocytosis (Fullstone *et al*., 2016). For transport from the bloodstream to the brain, a circulating ligand must bind to its corresponding transmembrane receptor on the apical membrane (Lajoie and Shusta, 2015). Receptor-ligand complexes are internalised via CME or CvME to form apical early endosomes (AEE), which undergo sorting.

For successful transcytosis, the receptor-ligand complex, or the dissociated ligand, must cross the cell for release from the basolateral membrane via exocytosis (Jones and Shusta,

2007). This may occur via direct transfer of the AEE to the basolateral membrane, or via transfer of the receptor's cargo to other vesicles that are specific for exocytosis from the basolateral membrane (Thuenauer *et al.*, 2017). The latter, indirect, form of transcytosis may be important in polarised cells, to maintain the different membrane compositions of the apical and basolateral membranes (Thuenauer *et al.*, 2017). In indirect transcytosis, the AEE is transported to the common recycling endosome (CRE), which sorts the cargo either back to the apical membrane or across to the basolateral membrane (Welling and Weisz, 2010). Alternatively, the early endosome may develop into a late endosome and fuse with lysosomes, leading to degradation of the endosomal contents (Barar *et al.*, 2016).

2.7.3. Transferrin

Iron is an essential nutrient and important cofactor, however, free iron is highly toxic due to its ability to catalyse the formation of free radicals (Choudhury *et al.*, 2018). The transport of iron is mediated by the protein Tf, which reversibly binds two Fe^{3+} ions and transports them into cells following binding with its cognate receptor, the transferrin receptor (TfR) (Tortorella and Karagiannis, 2014). The human Tf protein is an 80 kDa glycoprotein mainly produced by the liver and secreted into the bloodstream (Lambert, 2012). Tf is also produced by choroid plexus cells and oligodendrocytes in the brain; however, the oligodendrocytes do not secrete Tf (Leitner and Connor, 2012). Apart from iron, Tf is also capable of binding many other metals, such as aluminium, uranium, cobalt, gallium and bismuth (El Hage Chahine *et al.*, 2012).

The Tf protein consists of two domains: a C-lobe, which contains the C-terminal sequence, and the N-lobe, which contains the N-terminal sequence (Macedo and de Sousa, 2008). Each lobe is further divided into two sub-domains, denoted N1, N2, C1 and C2 (Cheng *et al.*, 2004). Fe^{3+} binding occurs within a cleft formed between the two sub-domains, which contains four highly conserved iron-binding residues: two tyrosine AAs, an aspartic acid, and a histidine (Lambert *et al.*, 2005). The sub-domains are linked by two β polypeptide chains that act as a hinge, allowing the sub-domains to open and close (Luck and Mason, 2012). Iron-free apo-transferrin (apoTf) initially assumes an open conformation, in which the sub-domains are separated from each other and Fe^{3+} can access the iron-binding site (Choudhury *et al.*, 2018). However, during binding, a series of conformational changes take place as the iron-binding residues bind Fe^{3+}, leading to

the domain assuming a closed conformation with Fe^{3+} enclosed in the cleft (El Hage Chahine *et al.*, 2012). The resulting holo-transferrin (holoTf) can then bind to TfR. Iron binding first requires binding of an anion, most often a carbonate, to a conserved arginine residue in each lobe; this is thought to bring the separate AAs involved in binding closer together to promote interactions with the Fe^{3+} (Luck and Mason, 2012). Binding strength is further increased by AAs termed "second-shell" residues that form hydrogen bonds with iron-binding residues (Luck and Mason, 2012).

During endocytosis of holoTf, the drop in pH experienced in the early endosome stimulates the release of Fe^{3+} ions from the Tf, creating apoTf. Iron release from the N-lobe has been suggested to occur due to protonation of two hydrogen-bonded second-shell lysine residues, leading to repulsion and opening the sub-domain (Luck and Mason, 2012). Protonation of the his349 residue of the C-lobe has been implicated in playing a major role in Fe^{3+} release from the C-lobe (Steere *et al.*, 2010). Protonation of the anion may also lead to repulsion and contribute to iron release (Lambert *et al.*, 2005).

2.7.3.1. The transferrin receptor

The TfR family contains two proteins: the TfR1 receptor, also called CD71, and the TfR2 protein (Daniels *et al.*, 2012). The *TfR2* gene was first sequenced by Kawabata *et al.*, (1999), and produces two isoforms of the TfR2 protein: an α and β form. TfR2α is expressed on liver, erythroid, and duodenal cells, and is implicated in the regulation of body iron levels rather than iron transport, as *TfR2* mutations are associated with haemochromatosis, a disorder characterised by iron build-up in the liver (Kawabata *et al.*, 2004). The TfR2β protein is expressed at low levels in tissues, such as brain, spleen, and heart, and is a cytosolic protein of unknown function (Kawabata, 2018). In contrast, the TfR1 protein is expressed on most tissues in the human body and is the primary receptor for iron uptake, displaying a stronger binding affinity for Tf thanTfR2 (Kleven *et al.*, 2018; West *et al.*, 2000).

The presence of TfR1 on non-malignant cells is low; however, it is overexpressed on the BBB, to transport iron into the brain, and on tumour cells, due to their increased iron demands (Choudhury *et al.*, 2018; Sharma *et al.*, 2016). The presence of TfR on the BBB was first shown by Jefferies *et al.*, (1984), with subsequent studies providing differing receptor densities. Raub and Newton, (1991) estimated that 10 000–15 000 TfRs are

expressed on the BBB cell surface, while Descamps *et al*., (1996) estimated this amount to be approximately 35 000. The overexpression of TfR1 has been observed in multiple cancers, and, in some cases, is associated with the aggressiveness and prognosis of the cancer. TfR1 overexpression has been observed on oesophageal squamous cell carcinoma (Chan *et al*., 2014); glioblastoma, where increased TfR expression has been linked with higher tumour grade (Recht *et al*., 1990; Rosager *et al*., 2017; Schonberg *et al*., 2015); hepatocellular carcinoma (Kindrat *et al*., 2016); and breast cancer, where TfR overexpression was associated with increased proliferation and tumour size (Habashy *et al*., 2010).

TfR1 is a homodimer, composed of two 90 kDa monomers linked by two disulphide bonds between cysteine residues at positions 89 and 98 (Qian *et al*., 2002). Each monomer consists of a cytoplasmic domain, a transmembrane domain, and an extracellular domain capable of binding one Tf protein, allowing TfR to internalise two Tf proteins simultaneously (Lambert, 2012; Macedo and de Sousa, 2008). Binding is influenced by the iron content of the Tf and the pH. TfR1 binds diferric holoTf (carrying two Fe^{3+} ions) with a 10 - 30 fold stronger binding affinity than for monoferric Tf (carrying one Fe^{3+} ion), and a 1000 fold stronger affinity than apoTf (Gammella *et al*., 2017). Eckenroth *et al*., (2011) identified 30 AAs on the N1, N2 and C1 sub-domains that may mediate Tf binding, through hydrogen bonds, van der Waals forces, hydrophobic interactions, and salt bridges formed between AA side chains, and between side chains and AA backbones. Under acidic conditions, TfR binds apoTf with a higher affinity than holoTf, allowing Tf to remain bound to the TfR during endocytosis.

2.7.3.2. Receptor-mediated endocytosis of holo-transferrin

Cellular uptake of holoTf occurs via CME (Figure 2.12) (Johnsen and Moos, 2016). At physiological pH, circulating holoTf proteins bind to the TfR, and are internalised in clathrin-coated pits that lose their clathrin coat to form early endosomes. Studies by Lakadamyali *et al*., (2006), observed that the majority of TfR-Tf early endosomes do not acquire Rab7 within 100 s of internalisation, placing them in the static population that mature slowly into late endosomes. At the acidic pH of the early endosome, Fe^{3+} is released from holoTf and reduced to Fe^{2+} by an endosomal ferri-reductase enzyme (Lane *et al*., 2015). Fe^{2+} is then transported across the endosomal membrane via the divalent

metal transporter 1 (DMT1) protein into the cytosolic labile iron pool (LIP), from where they can be stored as ferritin, utilised by the cell, or released from the cell (Daniels *et al.*, 2012; Lane *et al.*, 2015). ApoTf remains bound to the TfR at the low endosomal pH (Tortorella and Karagiannis, 2014). The endosome may further mature into a late endosome and fuse with lysosomes, degrading the TfR and apoTf, or recycle the receptor. The vast majority of TfRs - approximately 85 – 95% - are recycled back to the plasma membrane with the apoTf (Johnsen and Moos, 2016). Upon return to physiological pH, TfR loses its affinity for apoTf and releases it back into circulation (Cheng *et al.*, 2004). Early studies showed that the entire process, from endocytosis to TfR recycling, takes approximately 10-20 minutes (Hopkins and Trowbridge, 1983; Bleil and Bretscher, 1982).
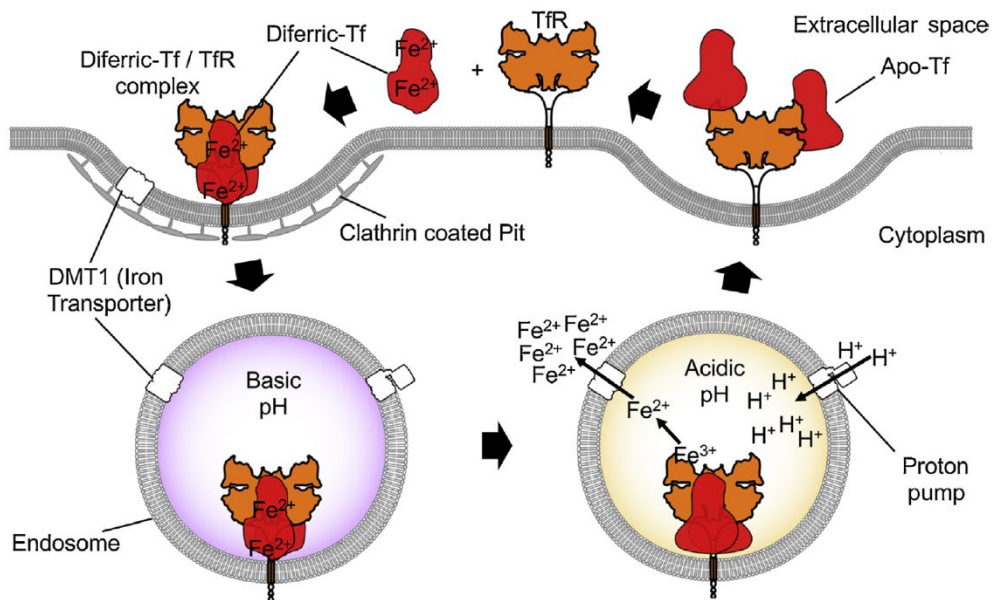
Figure 2.12: Endocytosis of holoTf proteins via clathrin-coated pits. Acidification of the early endosome leads to release of Fe^{3+} ions, which are transported into the cytosol by DMT1. The apoTf is then recycled to the membrane (Luria-Pérez *et al.*, 2016).

2.7.3.3. Receptor-mediated transcytosis of holo-transferrin

The RMT process of TfR1 is responsible for transporting iron across the BBB into the brain parenchyma, for uptake by CNS cells. However, the process is not entirely understood, which presents a major obstacle to efficient therapeutic delivery. At physiological pH, circulating holoTf binds to TfR1 on the blood side of the CEC, triggering uptake via clathrin-coated pits that develop into early endosomes. The

established theory is that the holoTf is able to avoid endosomal sorting pathways and is instead transcytosed across the CEC into the brain (Johnsen and Moos, 2016). Early studies by Descamps *et al.*, (1996) observed no lysosomal degradation of holoTf in a co-culture of bovine brain capillary endothelial cells and astrocytes, suggesting that this pathway is bypassed during RMT at the BBB. Moreover, very few (approximately 10%) holoTf molecules are recycled back to the apical membrane, indicating that most holoTf molecules cross the BBB (Descamps *et al.*, 1996). However, there are weaknesses to this theory, as it does not explain how iron levels in the brain are regulated or how holoTf is released from TfR into the brain parenchyma (Simpson *et al.*, 2015).

Other studies suggest that iron transfer into the brain may involve endocytic mechanisms rather than direct transcytosis across the CEC. Burdo *et al.*, (2003) observed the movement of both Tf-bound iron and free iron across cells in an *in vitro* BBB model. In contrast to these results, and those of Descamps *et al.*, (1996), Roberts *et al.*, (1993) observed no direct transcytosis of transferrin across the BBB in morphological studies using rats. Recently, Duck *et al.*, (2017) and Simpson *et al.*, (2015) proposed a model in which Fe^{3+} ions are released from holoTf in the endosome during RMT, and apoTf is recycled to either the apical or basolateral membrane. The Fe^{3+} is reduced to Fe^{2+} and may be used by the CEC or stored for use when required. When iron levels are low in the brain, Fe^{2+} is released from the stores in the CEC, oxidised to Fe^{3+}, and bound by apoTf in the brain (Simpson *et al.*, 2015). The reaction kinetics of the Tf RMT process was recently modelled by Khan *et al.*, (2018), and their results suggest that both mechanisms of iron uptake occur at the BBB. HoloTf is constantly transcytosed across the BBB to fulfil the iron requirements of the brain, while the release of free iron is regulated in response to the iron status of the CEC (Khan *et al.*, 2018). Despite the lack of certainty of the exact mechanisms of Tf transcytosis, it remains a highly relevant method of targeting the brain (Johnsen and Moos, 2016).

2.7.4. Factors influencing targeting efficiency

The avidity of targeted NPs and receptor binding strength is influenced by the affinity of the targeting ligand for its cognate receptor, the ligand density on the NP, and steric hindrance. The targeting ligand should ideally display a high affinity for its receptor.

However, several groups have observed lower uptake of high affinity antibodies compared to that of low affinity antibodies. Yu *et al*., (2011) observed lower brain uptake of high affinity anti-TfR antibodies in mice. Immunohistochemical staining of mice brains revealed that the majority of high affinity antibodies remained bound to the blood vessels, while lower affinity antibodies were released from the receptor into the brain parenchyma (Yu *et al*., 2011). Johnsen *et al*., (2018) obtained similar results in an *in vitro* BBB model. Studies by Bien-Ly *et al*., (2014) showed that antibodies with high affinities for the TfR were likely to lead to lysosomal degradation, ultimately reducing the number of TfRs on the BBB and impacting uptake of a subsequent dose of low affinity anti-TfR antibodies. It has been suggested that the presence of high affinity antibodies on the TfR may interfere with the conformational changes that TfR-Tf complexes undergo during endosomal uptake, leading to redirection of the endosome to the lysosome (Clark and Davis, 2015).

The affinity of a ligand for its receptor may also be reduced when it is conjugated to an NP (Saraiva *et al*., 2016); thus, to increase both the avidity and selectivity of targeting NPs, multiple targeting ligands may be conjugated to them (Wiley *et al*., 2013). The ligand density is dependent on the size and surface area of the NP, and must be balanced to optimise targeting. Wiley *et al*., (2013) analysed the brain uptake of AuNP conjugated with varying amounts of Tf, ranging from 3 to 200 Tf molecules per AuNP. They found that AuNP conjugated with too many Tf molecules were not released from TfR into the brain parenchyma, while those bound to too few Tf molecules displayed low avidity, which they suggested was due to competition with endogenous Tf. Work by Colombo *et al*., (2016) showed that AuNP conjugated with two antibodies displayed lower targeting efficiencies than AuNP bound to only one antibody, leading them to suggest that the size difference may have interfered with diffusion to the target site. Receptor binding may also be sterically hindered due to the presence of too many targeting ligands, or the presence of other ligands such as PEG (Colombo *et al*., 2016; Furtado *et al*., 2018).

2.7.5. Targeting gold nanoparticles to the transferrin receptor

AuNPs have been functionalised with Tf proteins, as well as polypeptides and antibodies targeting the TfR to facilitate uptake by RME. Yang *et al*., (2005) covalently bound Tf molecules to 20 nm AuNP via a mercaptoacetic acid linker. Using atomic force

microscopy (AFM), they visualised the uptake of Tf-conjugated AuNP into cells by endocytosis, with competition binding experiments verifying RME. Targeting was further shown to significantly increase uptake in human nasopharyngeal carcinoma cells compared to untargeted AuNP.

Tf-targeted peptides have been investigated for brain-targeted delivery. These peptides display high specificity and can be easily conjugated to vectors without losing their binding efficiencies (Dixit *et al*., 2015). Lee *et al*., (2001) identified two peptide sequences, composed of seven and twelve AAs, capable of binding to TfR. Brain uptake of AuNP has been shown to be enhanced following targeting using both seven AA (Dixit *et al*., 2015) and twelve AA (Prades *et al*., 2012) peptide sequences. Dixit *et al*., (2015) further observed increased uptake by glioma cells compared to untargeted AuNP.

Following the observations by Wiley *et al*., (2013) that high avidity TfR-targeted AuNP show reduced uptake, Clark and Davis, (2015) developed TfR-targeted AuNP designed to cleave from their targeting ligands during transcytosis. AuNP were bound to Tf molecules via the acid-labile linker 2,2-bis(aminoethoxy)propane (DAK), with the expectation that the acidic conditions of the endosome would cleave the DAK linker, separating the AuNP from the Tf molecules and allowing for release of the AuNP into the brain parenchyma (Clark and Davis, 2015). These AuNP were shown to display an enhanced ability to cross an *in vitro* BBB model, and displayed increased accumulation in the brain parenchyma of mice following systemic injection when compared to AuNP conjugated to Tf via a non-cleavable linker. They further found that AuNP bound to anti-TfR antibodies exhibited a reduced ability to cross the BBB *in vivo*, compared to all Tf-bound AuNP, with Tf-DAK-AuNPs displaying significantly higher accumulations in the brain.

2.8. Overcoming barriers to transfection

Following systemic administration, vectors must overcome a number of extra- and intra-cellular barriers to delivery (Figure 2.13). In the bloodstream, vectors must avoid clearance from circulation, and protect the therapeutic gene from degradation by circulating serum endonucleases (Yin *et al.*, 2014). To enter cells, the vector must first escape the bloodstream into the target tissue, then mediate cell entry and endosomal escape (Yin *et al.*, 2014). DNA must be further transported through the cytoplasm to the nucleus, and released from the vector to allow for transcription (Schaffer *et al.*, 2000). Viruses, being infectious agents, have evolved many mechanisms for overcoming these barriers, and thus transfect cells at higher rates than non-viral vectors. However, non-viral vectors may be synthesised to display certain characteristics or conjugated to compounds that allow them to circumvent these barriers to gene delivery.
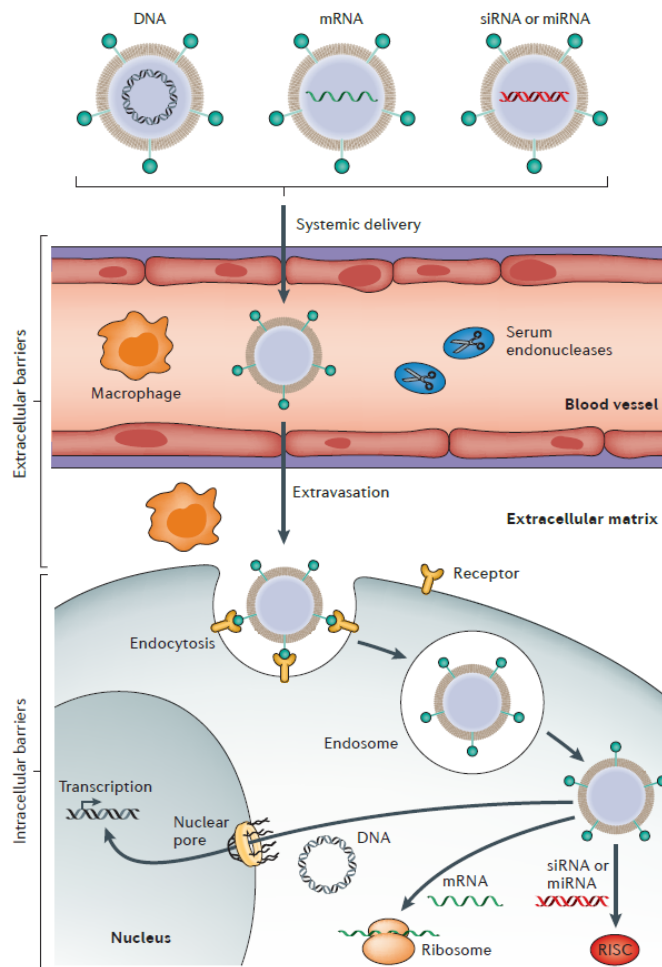
Figure 2.13: The many extra- and intra-cellular barriers to gene delivery faced by non-viral vectors during systemic delivery (Yin *et al.*, 2014).

2.8.1. Evading the immune system

One of the major challenges faced in systemic delivery is avoiding clearance of the vector from circulation by the RES, or mononuclear phagocytic system (MPS), an important part of the immune system responsible for the removal of foreign materials from the bloodstream. Upon intravenous administration, proteins and other biomolecules adsorb to the NP surface, forming a layer called the corona (Chandran *et al.*, 2017). Clearance occurs due to adsorption of plasma proteins called opsonins. This process, called opsonisation, allows vectors to be recognised and phagocytosed by cells of the MPS (Suk *et al.*, 2016). Opsonisation is influenced by factors such as the vector size, surface charge and composition, and hydrophobicity, with larger, cationic NPs being most susceptible to clearance (Blanco *et al.*, 2015; Furtado *et al.*, 2018). The binding of opsonins has also been shown to impede receptor-mediated uptake of targeted NPs by preventing receptor binding and by promoting non-specific uptake by cells (Suk *et al.*, 2016).

Various methods have been utilised to avoid opsonisation. Some more recently developed methods include functionalisation of vectors with erythrocyte or leukocyte cell membranes, allowing NPs to avoid opsonisation by mimicking endogenous cells, or conjugation of peptides expressed by components of the MHC, causing macrophages to recognise NPs as 'self' and avoid phagocytosis (Blanco *et al.*, 2015). However, the traditional method of functionalising NPs with hydrophilic polymers such as PEG remains most popular.

2.8.1.1. PEGylation of nanoparticles

The ability of PEG to increase the systemic circulation times and prevent degradation of administered proteins was first shown by Abuchowski *et al.*, (1977). Since then, it has become the most widely used polymer to stabilise inorganic and organic NPs due to its biocompatibility, and low toxicity and immunogenicity (van Vlerken *et al.*, 2007). PEG is theorised to inhibit opsonisation through a variety of mechanisms. Firstly, the PEG molecules may sterically hinder opsonin proteins from binding to the NP and reduce the surface area available for binding (Karakoti *et al.*, 2011). The cationic surface charges of NPs, which promote interactions with plasma components, are shielded also by PEG (Karakoti *et al.*, 2011). Furthermore, the oxygen molecules in the repeat ether units of the PEG backbone are able to bind water molecules through hydrogen bonds, leading to the

formation of a hydration layer around NPs that inhibits opsonin binding (van Vlerken *et al*., 2007). In preventing opsonisation, PEGylation ultimately reduces uptake by the MPS during circulation (Figure 2.14). This principle was demonstrated by Niidome *et al*., (2006), who observed increased circulation times and reduced uptake by the liver for PEGylated Au nanorods (NR) compared to unPEGylated AuNRs.
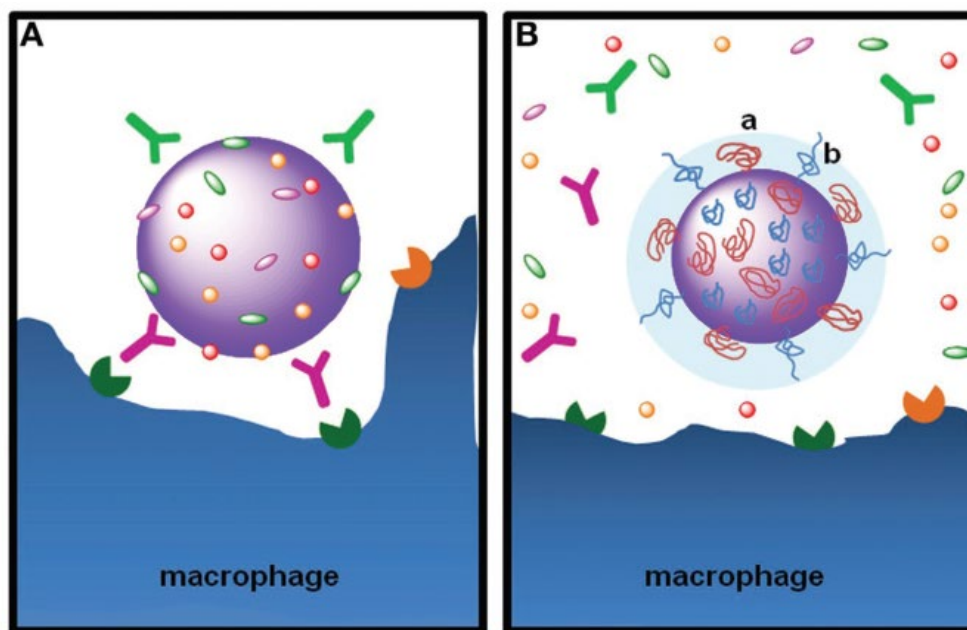
Figure 2.14: (A) unPEGylated NPs are able to interact with plasma proteins, ultimately leading to opsonisation and clearance by the MPS. (B) Functionalisation with PEG, however, inhibits these non-specific interactions, reducing MPS clearance and increasing circulation time (Furtado *et al*., 2018).

Upon binding to the NP surface, PEG may assume different conformations depending on the length and density of PEG molecules (Figure 2.15). At lower densities, the PEG is able to coil and acquires the 'mushroom' conformation (Rahme *et al*., 2013). At higher densities, the PEG chains are unable to coil, as they overlap, and instead acquire a 'brush' conformation in which PEG chains extend outwards from the NP surface (Jokerst *et al*., 2011). As a result, NPs carrying the brush conformation of PEG tend to display larger hydrodynamic diameters than those carrying PEG in the mushroom configuration (Figure 2.16). These different conformations display varying abilities to prevent MPS clearance. The brush conformation generally leads to reduced clearance compared to the mushroom conformation, as the increased density of PEG inhibits opsonisation more effectively (Jokerst *et al*., 2011). The mushroom conformation of PEG may also interfere with

receptor binding to a greater extent than the brush conformation, as the active site of the targeting ligand may become embedded within the PEG coils (Jokerst *et al.*, 2011).
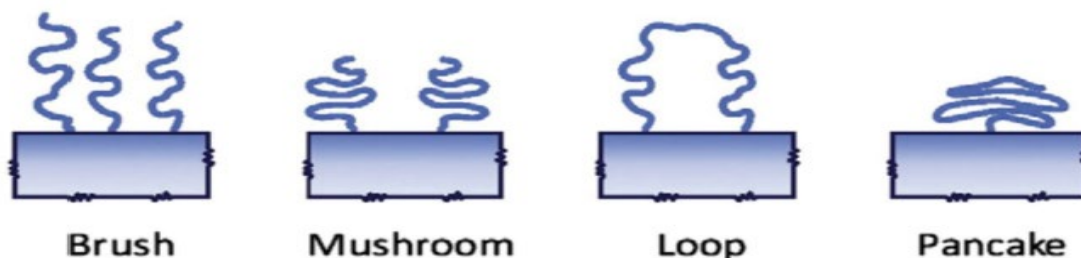
Figure 2.15: The different conformations PEG may assume upon binding to the NP surface (Furtado *et al.*, 2018).
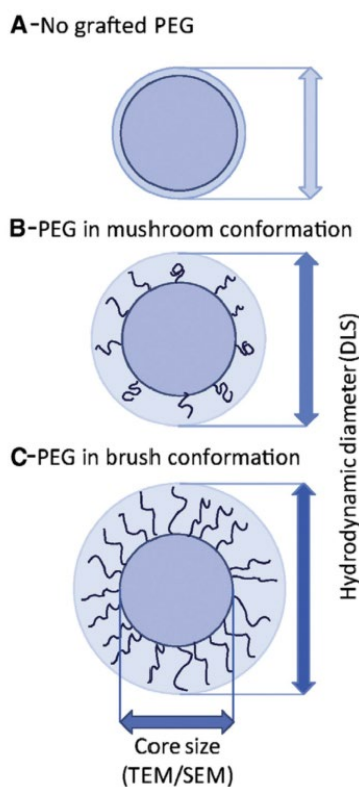
Figure 2.16: The different conformations of PEG influence the hydrodynamic diameter of NPs. (A) an uncoated NP, (B) NPs with the mushroom conformation display intermediate sizes, (C) the brush conformation displays increased sizes compared to the mushroom conformation (Furtado *et al.*, 2018).

Despite PEG's ability to increase the circulation life of NPs, it has also been associated with reduced transfection efficiencies, a phenomenon known as the PEG dilemma. Many of the properties of PEGylation that prevent opsonisation can hamper cell uptake and

endosomal escape – for example, shielding of the cationic charge from opsonins also inhibits electrostatic interactions with the anionic cell surface (Hatakeyama *et al*., 2013). Endosomal escape may also be hindered by PEG molecules preventing interactions between the NP and the endosomal membrane (Hatakeyama *et al*., 2013; Li *et al*., 2013b). To overcome the PEG dilemma, cleavable PEGylation strategies have been developed. These PEG molecules are released from the NP core in response to a change in the environment (Fang *et al*., 2017). Acid-labile PEG molecules that cleave in response to the drop in endosomal pH are attractive options (Fang *et al*., 2017).

2.8.2. Cell binding

The surface charge and surface modifications of NPs influence their interactions with cell membranes, ultimately influencing cellular internalisation by endocytosis. The cell membrane is composed of phospholipids and membrane proteins, covered by a negatively-charged carbohydrate coat called the glycocalyx (Forest and Pourchez, 2017). NPs with cationic surface charges have thus been shown to be more effective at entering cells than anionic or neutral NPs, as they are can form electrostatic interactions with the cell membrane and induce uptake by endocytosis (Forest and Pourchez, 2017). Anionic and neutral NPs may exploit the receptor-mediated endocytosis pathway for uptake or may be functionalised with cationic polymers to promote interactions with the cell membrane. AuNP capped with the cationic polymer chitosan, for example, showed enhanced cellular uptake compared to anionic citrate-capped AuNP (Boyles *et al*., 2015). The protein corona that forms around NPs also greatly influences cellular interactions, although conflicting results have been found regarding whether it enhances or inhibits uptake (Forest and Pourchez, 2017). Yallapu *et al*., (2015), for example, observed higher uptake of serum-coated magnetic NPs compared to uncoated NPs.

2.8.3. Endosomal escape

Following binding to the cell surface, NPs are internalised via endocytosis. Endocytic pathways include phagocytosis, macropinocytosis, CME, and CvME. All these pathways lead to the formation of early endosomes, which may develop into late endosomes, and lysosomes, leading to degradation of the therapeutic cargo. It is thus important that the vector escapes from the endosome before it is degraded; however, unlike viral vectors,

most non-viral vectors are unable to escape the endosomes, making endosomal release is a major limiting step for non-viral gene delivery (Varkouhi *et al*., 2011). Many strategies have thus been explored to facilitate endosomal escape; some of which disrupt the endosome and others the lysosome. These methods are especially important for negatively-charged citrate-capped AuNP, as they are unable to interact with the anionic endosomal membrane and disrupt it themselves (Ma, 2014).

2.8.3.1.   The proton sponge effect

The proton sponge hypothesis was first proposed by Behr, (1997), who suggested that the relatively high transfection efficiencies of polycations with high buffering capacities, such as PEI and lipopolyamines, is due to their ability to lyse the endosomal compartment, allowing for escape of the nanocomplex. These polycations often carry secondary or tertiary amine groups that can be protonated, allowing them to sequester the protons pumped into endosomes during maturation (Figure 2.17a) (Parodi *et al*., 2015). The influx of protons is followed by diffusion of chloride ions (Cl^-) into the endosome and, in turn, the osmosis of water molecules, eventually causing the swelling and rupture of the endosome (Figure 2.17b) (Behr, 1997; Liang and Lam, 2012). Protonation also leads to swelling of the polycation due to repulsion of the protonated groups, further contributing to endosomal rupture (Behr, 1997). Many cationic polymers are thought to act as proton sponges and can be used to coat inorganic NPs (Ma, 2014). AuNP have been functionalised with polymers such as PEI (Cebrián *et al*., 2011), and poly(propyleneimine) dendrimers (Daniel *et al*., 2011) to facilitate endosomal escape. CS has often been regarded as having a weak buffering capacity at endosomal pH; however, Richard *et al*., (2013) showed that the buffering capacity of CS is greater than that of PEI at equal charge concentrations, suggesting that it can induce endosomal escape via the proton sponge effect.
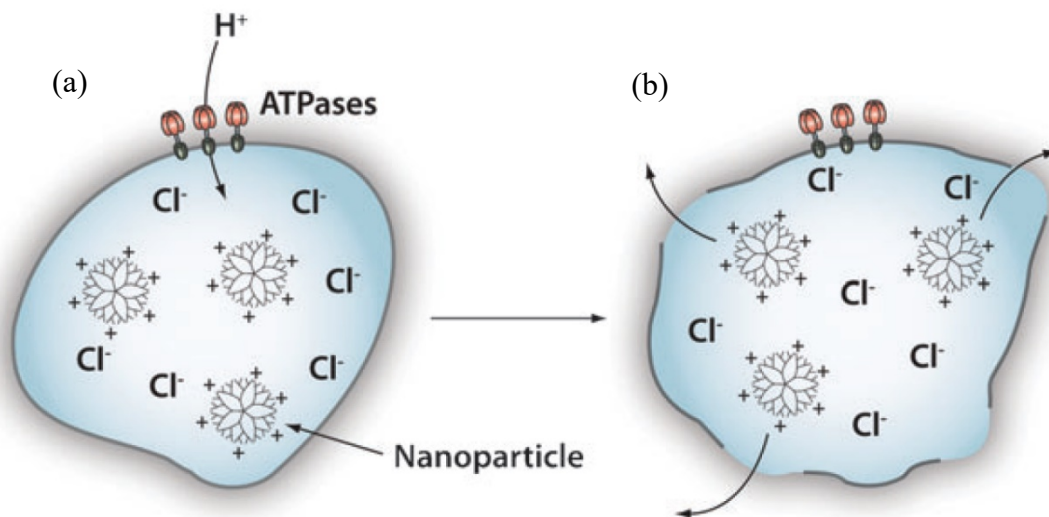
Figure 2.17: Endosomal escape as proposed by the proton sponge hypothesis. Endosomal membrane-bound ATPases pump protons into the endosome; this is followed by the influx of Cl⁻ ions and water molecules (a), causing the endosome to burst and the nanoparticle to be released (b) (Chou *et al*., 2011).

Despite its popularity as an endosomal escape method, the proton sponge effect remains contentious. Sonawane *et al*., (2003) provided evidence for the hypothesis using PEI and polyamidoamine (PAMAM) polyplexes, when they observed increases in endosomal Cl⁻ concentration, volume, and pH. These are expected due to the influx of ions and water into the endosome, as predicted by the proton sponge hypothesis. Benjaminsen *et al*., (2013) and Forrest and Pack, (2002), however, observed no increase in endosomal pH for PEI and PLL vectors. Different cell types may also display different endosomal sizes, with different degrees of membrane leakiness, which will ultimately influence whether polymers can induce osmotic rupture (Vermeulen *et al*., 2018).

2.8.4. Nuclear targeting

Successful gene therapy requires the gene to be delivered to the nucleus, where transcription can take place. However, vectors must first overcome the nuclear membrane, a phospholipid bilayer regulating the entry of molecules into the nucleus. The nuclear membrane contains nucleoporin protein-lined pores, called nuclear pore complexes (NPC), that facilitate the transport of molecules across the membrane (Pan *et al*., 2018). Passive diffusion through the pore is limited to molecules smaller than 40 kDa, with larger molecules requiring active transport by the nucleoporins (Parodi *et al*., 2015). Active

transport across the nuclear membrane can be achieved through functionalisation with nuclear localisation signals (NLS), peptide sequences that bind to nucleoporins and induce translocation across the membrane (Parodi *et al*., 2015). NP vectors are also capable of passively entering the nucleus if they are small enough, as was shown by Tsoli *et al*., (2005) and Pan *et al*., (2007) with 1.4 nm AuNP. However, this size limitation may be removed for cancerous cells, as the nuclear membranes of malignant cells often overexpress transporter proteins, or are disrupted during mitosis, allowing for the entry of larger NPs (Kodiha *et al*., 2015).

Chapter 3
Methods and Materials

3.1. Materials

Tris (hydroxymethyl)-aminomethane, acetic acid, sodium dihydrogen phosphate (NaH_2PO_4), ethylenediaminetetraacetic acid (EDTA) disodium salt, dimethylsulfoxide (DMSO), poly(ethylene) glycol 2000 (PEG_{2000}), 3-[4,5-dimethylthiazol-2-yl]-2.5-siphenyltetrazolium bromide (MTT), sodium citrate, 2-[4-(2-hydroxyethyl)piperazin-1-yl]ethanesulfonic acid (HEPES) and phosphate buffered saline (PBS) tablets were purchased from Merck, Darmstadt, Germany. Chitosan (>75% deacetylated), holo-transferrin, gold chloride ($HAuCl_4$), bicinchoninic acid (BCA), and 12 kDa dialysis tubing were obtained from Sigma-Aldrich, St. Louis, USA. The pCMV-*luc* pDNA was supplied by Plasmid Factory, Bielefield, Germany. Ultrapure grade agarose was obtained from Bio-Rad Laboratories, Inc., Hercules, USA. Eagles Minimum Essential Medium (EMEM), L-glutamine, trypsin-versene and penicillin/streptomycin were purchased from Lonza BioWhittaker, Walkersville, USA. Foetal bovine serum (FBS) was obtained from Gibco Invitrogen, Karlsruhe, Germany. All sterile cell culture plasticware was purchased from Nest Biotechnologies, Wuxi, China, and Corning Incorporated, New York, USA. The luciferase assay reagent (20 mM tricinek; 1.1 mM magnesium carbonate hydroxide, pentahydrate; 2.7 mM magnesium sulphate; 0.1 mM EDTA; 33.3 mM dithiothreitol; 270 µM coenzyme A; 470 µM luciferin; 350 µM ATP) and 5X cell lysis (25 mM Tris-phosphate, pH 7.8; 2 mM dithiothreitol; 2 mM 1,2-diaminocyclohexane-N-N-N′-N′-tetra-acetic acid; 10 % (v/v) glycerol; 1 % (v/v) Triton X-100) reagents were purchased from Promega Corporation, Madison, USA. The NucleoBond Xtra Maxi Plus DNA, RNA, and protein purification kit was purchased from Macherey-Nagel, Düren, Germany. All other reagents were of analytical grade and ultrapure 18 Mohm was used in all experiments.

3.2. Synthesis and functionalisation of gold nanoparticles

3.2.1. Synthesis of gold nanoparticles

A 0.375×10^{-3} M solution of AuNP was synthesised according to the citrate reduction method. Briefly, approximately 30 ml of 18 Mohm water was heated to 85-90 °C with

stirring. Thereafter, 375 µl HAuCl$_4$ was added into the vortex; followed immediately by the addition of 1 ml of 1% sodium citrate. The solution rapidly changed to a purple colour, finally turning to a deep red, indicating the formation of citrate-capped AuNP in the 10 – 20 nm diameter range. The solution was boiled for a further 10 minutes following the development of the red colour, before being removed from the heat and allowed to cool to room temperature.

3.2.2. Functionalisation of gold nanoparticles

A stock CS solution (1 mg/ml) was prepared in 1% acetic acid and added to AuNP in a 1:1 volume ratio in a dropwise manner with mixing. The resulting AuCS nanoparticles were dialysed overnight (MWCO 12 kDa) to remove unbound reactants. The PEG$_{2000}$ was added to AuCS in two weight ratios of 2% and 5%, to produce AuCS-2% PEG and AuCS-5% PEG nanoparticles. Approximately 10.44 and 26.09 µl of a 1 mg/ml stock PEG$_{2000}$ solution was added to AuCS with stirring for two hours to produce the AuCS-2% PEG and AuCS-5% PEG, respectively, and dialysed overnight as above. Holo-transferrin (Tf) was then added according to a method modified from Yang *et al*., (2005). Briefly, 0.1 mg/ml Tf stock solution (in 18 Mohm water), was added in a 1% weight ratio to AuCS, AuCS-2% PEG and AuCS-5% PEG NPs while stirring. The resulting AuCSTf, AuCSTf-2% PEG and AuCSTf-5% PEG NPs were incubated at 4 °C overnight, and thereafter stored at 4 °C. Figure 3.1 provides a scheme for the synthesis of all nanoparticles.
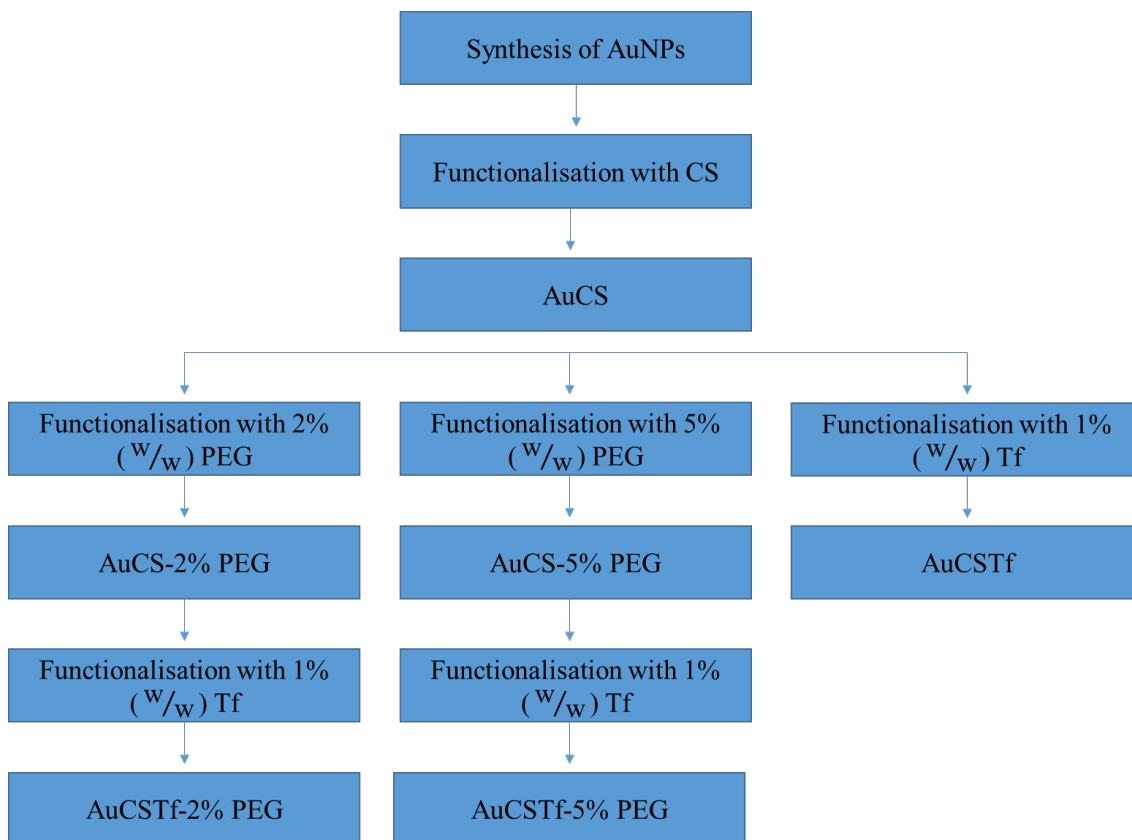
Figure 3.1: Scheme showing synthesis of FAuNPs.

3.2.3. Preparation of nanocomplexes

Plasmid pCMV-*luc* DNA (pDNA) was amplified in *Escherichia coli* JM109 according to standard protocol, and isolated and purified using the NucleoBond Xtra Maxi Plus DNA, RNA, and protein purification kit. Nanocomplexes were formed by adding a constant volume of pCMV-*luc* pDNA (0.25 μg/μl) to varying amounts of the FAuNPs. The FAuNP/pDNA suspensions were made up to a final volume of 10 μl with HEPES buffered saline (HBS) (20 mM HEPES, 150 mM NaCl, pH 7.4), centrifuged briefly, and incubated at room temperature for one hour to allow for binding. The resulting nanocomplexes were used further in binding studies (section 3.4) and *in vitro* studies (section 3.5).

3.3. Characterisation of nanoparticles and nanocomplexes

UV-vis spectrophotometry was used to determine the absorbance spectrum of the synthesised AuNP, and to confirm functionalisation with CS, PEG and Tf as evidenced by red or blue shifts in the peaks of FAuNPs. Analysis was carried out using a Jasco V-

49

730 Bio Spectrophotometer (JascoInc, Japan). The size and morphology of AuNP and FAuNPs was assessed using transmission electron microscopy (TEM). Briefly, a drop of the NP solution was placed on a 400 mesh copper grid (Ted Pella Inc. Redding, USA), allowed to air-dry at room temperature, and viewed in a Jeol T1010 TEM (Microscopy and Microanalysis Unit, UKZN). The images were analysed using the analySIS LS Research software (Olympus Soft Imaging Solutions). The average diameter of the NPs was calculated by measuring the diameters of individual AuNP and FAuNPs. Nanoparticle tracking analysis (NTA) was used to determine the hydrodynamic diameters and zeta potentials of AuNP, FAuNPs, and nanocomplexes. NPs were diluted 1:1000 and analysed using the Nanosight NS500 (Malvern Instruments, Worcestershire, UK). Nanocomplexes were prepared for NTA as described in section 3.2.3, according to their optimum ratios determined in the band shift assay (section 3.4.1). The volume of FAuNP and pDNA was doubled, and nanocomplexes diluted as for the NPs. Fourier-transform infrared spectroscopy (FTIR) was used to determine the presence of CS, PEG, and Tf, through identification of peaks corresponding to specific bonds in the ligands. FTIR analysis was conducted using a Perkin Elmer Spectrum 100 FT-IR spectrometer fitted with a universal ATR sampling accessory.

3.4. Binding studies

3.4.1. Band shift assay

The band shift assay was conducted to determine the ability of the FAuNPs to bind pDNA. Nanocomplexes were prepared as described in section 3.2.3, with the mass of pDNA constant at 0.25 μg/μl, while the mass of FAuNPs were varied, to produce different FAuNP:pDNA mass ratios. Following incubation, gel loading buffer (40% sucrose, 0.25% bromophenol blue) was added to bring the samples up to a constant volume of 10 μl. The samples were then loaded into a 1% agarose gel [0.28 g agarose, 25.2 mL 18 Mohm water, 2.8 mL 10x TBE electrophoresis buffer (0.36M Tris-HCl; 0.3M Na_2HPO_4 and 0.1 M EDTA in 1 L 18 Mohm water, pH 7.5], containing 1.5 μl ethidium bromide (EB) (10 mg/ml). Electrophoresis was conducted in 1x TBE electrophoresis buffer in a Mini-Sub® electrophoretic apparatus (BioRad Laboratories, Richmond, USA) at 50 V for 90 minutes, and images were viewed and captured in a Vacutec Syngene G: Box BioImaging system (Syngene, Cambridge, UK). The ratio at which all pDNA was bound

(the optimal ratio), as well as the ratio above (supra-optimal) and the ratio below (sub-optimal), were used for the nuclease protection assay (section 3.4.3) and all *in vitro* cell based studies (section 3.5).

3.4.2. Ethidium bromide intercalation assay

Approximately 100 µl of HBS and 2 µl of EB (100 µg/ml) was added to a well in a 96-well FluorTrac flat-bottom black plate. The fluorescence value at excitation and emission wavelengths of 520 nm and 600 nm, respectively, was measured in a GloMax®-Multi Detection System (Promega BioSystems, Sunnyvale, USA), to establish a baseline fluorescence of 0%. Thereafter, 1.2 µg of pDNA (0.25 µg/µl) was added to the well and incubated at room temperature for 10 minutes, to allow the EB to fully intercalate with the pDNA. The fluorescence value obtained was used as the 100% fluorescence. The FAuNPs were then added to the well in 1 µl aliquots, and the fluorescence read, until a plateau was reached. The sample was mixed following each addition to ensure that the EB-pDNA and FAuNPs were dispersed evenly. The relative fluorescence (F_r) was calculated using the equation:

$$\% \, F_r = \frac{F_i - F_0}{F_{max} - F_0} \; x \; 100$$

F_i represents the fluorescence of the sample following addition of a given concentration of FAuNPs; F_0 represents the fluorescence of the EB in the absence of pDNA; and F_{max} represents the fluorescence of the EB in the presence of pDNA. The % F_r was then plotted against the FAuNP:pDNA ($^W/_W$) ratios.

3.4.3. Nuclease protection assay

Nanocomplexes were made up according to the optimal, sub-optimal and supra-optimal ratios obtained from the band shift assay. Two controls were set up: a positive control (C1) containing naked pDNA with no added FBS; and a negative control (C2), containing naked pDNA treated with FBS. Complexes were prepared as previously (section 3.4.1). All complexes, excluding C1, were then treated with FBS to a final concentration of 10% ($^V/_V$) (1 µl), and incubated at 37 °C for 4 hours, followed by the addition of EDTA to a final concentration of 100 mM (1.1 µl) to inhibit the nuclease action. Complexes were then treated with 1.33 µl of 5% SDS ($^W/_V$) and incubated at 55 °C for 20 minutes, to

allow for the release of the pDNA from the FAuNPs. Samples were then subjected to agarose gel electrophoresis and gels visualised as described in section 3.4.1.

3.5. *In vitro* cell culture and transfection studies

3.5.1. Growth and maintenance of cells

In vitro studies were conducted in 3 human cell lines: the non-cancerous embryonic kidney (HEK293), the cervical adenocarcinoma (HeLa), and the colorectal adenocarcinoma (Caco-2). The cells were grown in EMEM supplemented with 10% ($^V/_V$) FBS and 1% ($^V/_V$) penicillin/streptomycin. Cells were maintained in 25 cm^2 flasks in a Steri-cult CO$_2$ incubator (Thermo-Electron Corporation, Waltham, Massachusetts, USA) at 37 °C under 5% CO$_2$.

3.5.2. Reconstitution of frozen cells

Cryovials were removed from the biofreezer and thawed to 37 °C. The cell suspension was then transferred to a microcentrifuge tube and centrifuged at 1400 x g for 1 minute to pellet the cells. The supernatant was discarded, and cells were resuspended in 1 ml of fresh medium. Cells were transferred to a flask containing 5 ml medium and incubated overnight to allow for attachment. Thereafter, the medium was replaced to ensure complete removal of DMSO. Cells were trypsinised and split 1:3 every 3 days, or as required for assays.

3.5.3. Trypsinisation

Briefly, medium was decanted from the flasks, and cells were washed with 4 ml PBS (150 mM sodium chloride, 2.7 mM potassium chloride, 1 mM potassium dihydrogen phosphate, 6 mM disodium hydrogen phosphate, pH 7.5). Approximately 1 ml of trypsin-versene was then added to the cells, to facilitate detachment of the cells from the flask. Cells were allowed to stand for 1 – 5 minutes at room temperature depending on the cell line and viewed under an inverted microscope to observe rounding off. Cells were dislodged by tapping the flask against the palm of the hand, and 2 ml of medium containing FBS was added to inhibit the activity of the trypsin. Cells were split 1:3 into new flasks containing 5 ml medium, or plated for the cytotoxicity and transfection assays.

3.5.4. Cryopreservation

Cells were trypsinised as outlined in section 3.5.3 and centrifuged at 3000 rpm for 1 minute. The medium was then removed, and cells were resuspended with mixing in 0.9 ml EMEM and 0.1 ml DMSO (10%). The cell suspension was thereafter transferred to 2 ml cryovials and frozen at a rate of -1 °C per minute in a Nalgene^{TM} Cryo 1 °C Freezing Container containing isopropanol. Cells were then stored at -80 °C in a biofreezer (Nuaire, Lasec Laboratory and Scientific Equipment) for short term storage.

3.5.5. MTT cytotoxicity assay

Cells were seeded into 96-well plates at densities of 1–1.5 x 10^4 cells per well and incubated at 37 °C for 24 hours to allow for attachment. The medium was then replaced and nanocomplexes, prepared in triplicate, were added to wells. A positive cell control was set up, to which no nanocomplexes were added. The cells were incubated for a further 48 hours at 37 °C, after which the medium was replaced and fresh medium (100 µl) containing 10 µl of MTT reagent (5 mg/ml in PBS) added to each well. Cells were incubated for 4 hours at 37 °C. Thereafter, the medium containing MTT was removed and 100 µl DMSO added to each well to dissolve the formazan crystals. Cells were incubated for approximately 20 minutes at 37 °C to allow for colour development, and absorbance at 570 nm was read in a Mindray MR-96A microplate reader (Vacutec, Hamburg, Germany). Cell survival was assumed to be 100% for the control.

3.5.6. Apoptosis assay

Apoptosis was assessed using ethidium bromide/acridine orange (EB/AO) dual staining. Cells were seeded at densities of 6 x 10^5 cells per well in a 24-well plate and incubated for 24 hours at 37 °C. The medium was then replaced and nanocomplexes were added to cells, followed by incubation for a further 24 hours at 37 °C. Thereafter, the medium was removed, and cells were washed twice with PBS. Cells were then stained with EB/AO dual stain (100 µg/ml AO, 100 µg/ml EB in PBS) for 5 minutes at 25 °C, and viewed under an Olympus inverted fluorescent microscope fitted with a CC12 fluorescent camera. Images were captured using the analySIS LS Research software version 2.6. The apoptotic index was calculated using the following formula:

$$\text{Apoptotic index} = \frac{\text{number of apoptotic cells}}{\text{total number cells counted}}$$

The total number of apoptotic cells included cells in both early and late apoptosis.

3.5.7. Transfection analysis

3.5.7.1. Luciferase assay

Cells were seeded and treated as described in section 3.5.5, with the addition of a naked pDNA-only control not containing nanoparticles. Following the 48-hour incubation, the medium was removed, and cells were washed twice with PBS. Approximately 100 μl 1X cell lysis reagent was added to each well and the plate was rocked at 30 rpm for 15 minutes. The cells were then scraped from the wells, and the suspensions were transferred to micro-centrifuge tubes and centrifuged at 12000 xg for 5 seconds. Approximately 20 μl of the cell-free supernatants were added to wells in a white 96-well plate and luminescence was measured using the GloMax®-Multi Detection System (Promega BioSystems, Sunnyvale, USA), via automatic injection of 50 μl of luciferase assay reagent to each well. The relative light units (RLU) were normalised against the protein content of the cell lysates, determined using the standard BCA assay. Results were expressed as relative light units per milligram of total protein (RLU/mg protein).

3.5.7.2. The bicinchoninic acid assay

The bicinchoninic acid (BCA) assay was used to determine the protein content of the cell lysates obtained from section 3.5.7.1. Briefly, the triplicates for each ratio were pooled, and mixed with freshly-prepared BCA working reagent [1 part $CuSO_4$:50 parts BCA ($^V/_V$)] in a ratio of 1 part lysate:20 parts working reagent ($^V/_V$). The solution was incubated at 37 °C for 30 minutes, and the absorbance at 526 nm was read using the Mindray MR-96A microplate reader (Vacutec, Hamburg, Germany). A standard curve was constructed using standard BSA solutions and used to determine the protein content of the cell lysates.

3.5.7.3.　　　　Competition binding assay

This assay was conducted only in the Tf receptor-expressing HeLa cells, to determine the efficiency of receptor-mediated uptake by Tf-targeted FAuNPs. Cells were seeded as described in section 3.5.5 and incubated for 24 hours. Following incubation, the medium was replaced, and free holo-transferrin (0.8 mg/ml) was added to wells 20 minutes prior to addition of the Tf-targeted FAuNPs. Cells were then incubated at 37 °C for 48 hours and subject to the luciferase assay (section 3.5.7.1) to assess gene expression.

3.6. Statistical analysis

All cytotoxicity and luciferase assay results are presented as means ± SD (n=3). Groups were analysed using two-way analysis of variance (ANOVA) followed by Tukey's multiple comparisons test. P-values < 0.05* and p-values < 0.01** were considered statistically significant. GraphPad Prism version 6.01 was used to conduct all statistical analysis and draw all graphs.

Chapter 4
Results and Discussion

4.1. Preparation of functionalised gold nanoparticles

The FAuNPs comprised AuNP functionalised with CS, PEG_{2000}, and holoTf. Different studies have shown that AuNP ranging from 40 – 50 nm in diameter show optimal transfection compared to larger and smaller AuNP (Chithrani *et al.*, 2006; Liu *et al.*, 2013; Yue *et al.*, 2017). However, smaller NPs are generally seen as advantageous for functionalisation, as they display larger surface areas compared to larger NPs. This allows for functionalisation with high densities of ligands and optimises interactions with nucleic acids. Cebrián *et al.*, (2011) observed that AuNP smaller than 10 nm bound almost three times more PEI than larger AuNP up to 100 nm in diameter, and a smaller amount of the <10 nm AuPEI NPs were required to fully complex pDNA. Functionalisation is a requirement if the citrate-capped AuNP produced using the Turkevich method are to be used for gene delivery. Plain AuNP can aggregate in response to the salt levels in the blood, and their negative charge prevents nucleic acid binding (Hansen *et al.*, 2015). To facilitate their use as effective gene delivery vectors, the AuNP were functionalised with CS and PEG_{2000}.

The cationic polymer CS was used to coat the AuNP, providing a base for the attachment of PEG, Tf, and pDNA. CS bears positive charges at weakly acidic and neutral pH due to the presence of protonated amine groups (Figure 4.1) (Min *et al.*, 2014; Ritthidej, 2011). These positive groups allow CS to easily adsorb onto the surface of anionic AuNP, and facilitate electrostatic interactions with the pDNA payload.
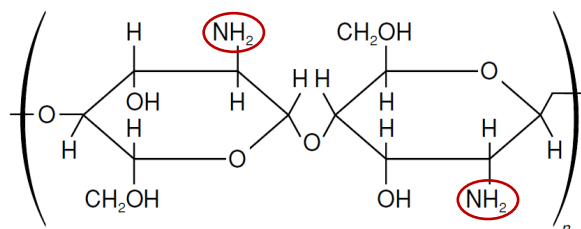
Figure 4.1: The structure of repeating D-glucosamine and N-acetyl-D-glucosamine units in CS. The amine groups (circled) become protonated in weakly acidic and neutral solutions, facilitating interactions with anionic substances (Jiang and Han, 1998).

PEG was conjugated to CS to confer steric stability to the nanoparticles (Figure 4.2A). It has been suggested that PEG binds CS through the formation of intermolecular hydrogen bonds between the hydroxyl groups of PEG and CS (Figure 4.2B) (Halabalová and Šimek, 2006; Jiang and Han, 1998). The oxygen molecule of the PEG hydroxyl or ether may also interact with the nitrogen of the amide or amine in CS (Halabalová and Šimek, 2006). Two important parameters influencing the success of PEG coatings are the PEG grafting densities and MWs. Generally, increasing MWs, and thus increasing PEG chain lengths, are associated with increased blood circulation times (Suk *et al.*, 2016). PEG with a MW of 2000 kDa (PEG$_{2000}$) was used in this study. PEG$_{2000}$ has been shown to increase the circulation time and reduce the liver uptake of liposomes compared to PEG$_{350}$ (Managit *et al.*, 2003). While PEG$_{5000}$ and PEG$_{10000}$ have been shown to lead to longer circulation times of AuNP (Perrault *et al.*, 2009) and AuNRs (Niidome *et al.*, 2009), it is important to optimise chain length in the context of targeting, as long chains may interfere with receptor binding.
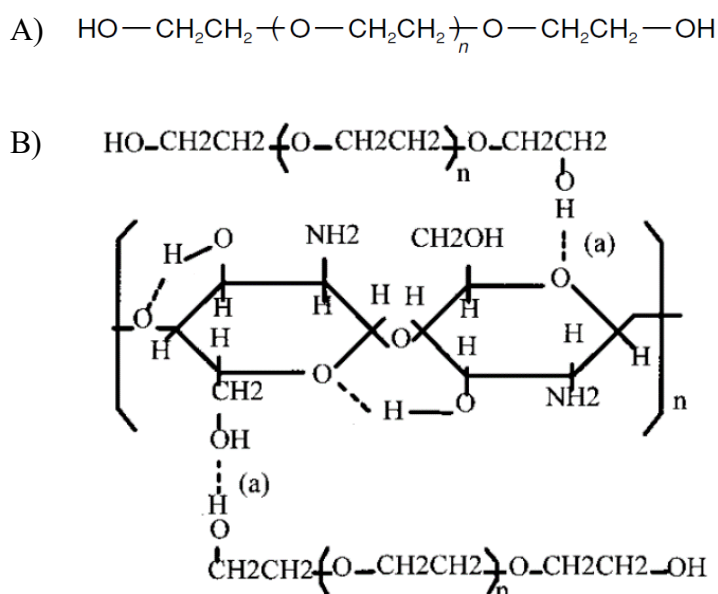
Figure 4.2: 1) The structure of PEG. n refers to the number of repeating ethylene units. 2) Possible interactions between CS and PEG through the formation of (a) intermolecular hydrogen bonds (adapted from Jiang and Han, 1998).

The optimal PEG grafting density should confer stability and reduce non-specific interactions while also allowing uptake. PEG grafting density is also especially important when developing vectors using active targeting, as the different grafting densities and

conformations of PEG may influence the efficiency of RME. Increasing PEG densities have been observed to lead to increased circulation and tumour uptake (Akiyama *et al.*, 2009). A study by Gref *et al.*, (2000) observed that conjugation of PEG_{2000} to polymeric NPs in a weight ratio of 2% reduced protein binding by approximately 50%. However, 5% ($^W/_W$) PEG significantly reduced protein binding compared to 2% ($^W/_W$), with no significant decreases observed at higher PEG grafting densities. In this study, the effects of 2% and 5% ($^W/_W$) PEG on FAuNPs' characteristics and transfection were compared to determine which ratio would be optimal for gene delivery.

Targeting was facilitated by the holoTf protein, targeting the TfR. The Tf protein is negatively charged glycoprotein, due to the presence of anionic sialic acid groups (Helander and Beck, 2008). These negative groups may facilitate interactions with the positive groups of CS, allowing for Tf bonding.

4.2. Physicochemical characterisation of nanoparticles and nanocomplexes

4.2.1. UV-vis spectrophotometry

The presence of AuNP can be determined through detection of the SPR using UV-vis spectrophotometry (Mirza and Siddiqui, 2014). UV-vis spectrophotometry can also be used to determine the success of functionalisation, as changes in the physical and chemical characteristics of the NP following functionalisation may lead to changes in the observed peak.

The results for the UV-vis analysis are shown in Figure 4.3. The plain AuNP showed a single, narrow peak with a maximum wavelength (λ_{max}) of 528 nm. This value is characteristic of AuNP in solution, and it has been reported that AuNP generally produce a single peak with a λ_{max} between 510 and 550 nm (Verma *et al.*, 2014). The presence of a single peak corresponding to the AuNP indicates that there was no contamination by citrate or other by-products from the synthesis reaction. Red shifts compared to the plain AuNP were observed following the addition of CS (531 nm), 2% PEG (534 nm), and 5% PEG (534 nm). The AuCSTf and AuCSTf -2% PEG NPs showed red shifts following functionalisation with Tf, with λ_{max} values of 534 nm and 540 nm, respectively. However, AuCSTf -5% PEG displayed a blue shift, with λ_{max} decreasing to 522 nm. The Tf-targeted FAuNPs displayed higher peak intensities compared to their corresponding FAuNP. A

similar observation was reported when comparing Tf-PEG-AuNPs to untargeted PEG-AuNPs and uncoated AuNP (Parab *et al.*, 2011).
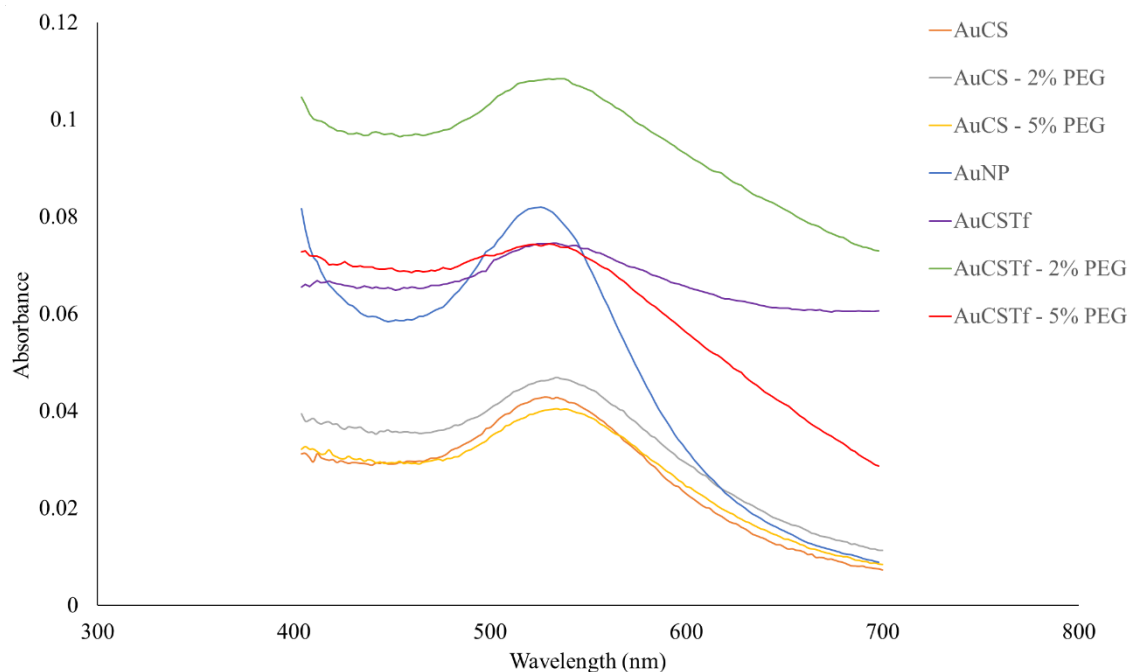
Figure 4.3: UV-vis spectrum of AuNP and FAuNPs.

Successful functionalisation can be inferred from the UV-vis spectra in two ways: by observing shifts in the λ_{max}, and by observing changes in the peak shape. All FAuNPs displayed maximum wavelengths that differed from that of the plain AuNP, suggesting successful functionalisation. Oh *et al.*, (2008) similarly observed a red shift in the absorption spectrum of AuCS NPs compared to plain AuNP. In a study of AuNP conjugated to thiolated PEG (PEG-SH), Manson *et al.*, (2011) observed that higher grafting densities of PEG resulted in greater red shifts in the absorption spectrum compared to the citrate-capped AuNP. However, the shifts were relatively small: a red shift of 0.2 nm was observed when the PEG concentration was increased from 3.6 μg PEG/ml AuNP solution to 8.4 μg/ml. A maximum shift of 0.7 nm was observed at a PEG concentration of 25.2 μg/ml. This may account for the observations in this study, where both the AuCS-2% PEG and AuCS-5% PEG NPs peaked at the same wavelength.

The observed shifts may correlate with the variations in NP size that occurred following functionalisation, as determined by NTA and described in section 4.2.4. It is known that blue shifts can occur due to decreases in particle size (Lazarus *et al.*, 2014); thus the blue

shift of AuCSTf-5% PEG corresponds with its smaller size compared to AuCS-5% PEG. Conversely, red shifts occur due to increases in particle size (Link and El-Sayed, 1999). Thus the red shifts observed may correlate with the increases in particle size that occurred following functionalisation for all FAuNPs except AuCSTf -5% PEG.

In addition to the shifts in λ_{max}, FAuNPs were observed to display slightly broader peaks compared to that of the colloidal AuNP. Parab *et al*., (2011) noted a widening of the peak of sodium hexametaphosphate (HMP) - capped AuNP following conjugation with PEG-SH and Tf, indicating that the SPR peak of the AuNP is being influenced by the ligands. This further implies that the AuNP were successfully functionsalised. The Tf-targeted FAuNPs displayed broader peaks compared to the untargeted FAuNPs, as has been observed in literature (McDonagh *et al*., 2015).

4.2.2. Fourier-transform infrared spectroscopy analysis

FTIR was also used to confirm binding of the ligands. The FTIR spectra are provided in Appendix A. The peaks observed following functionalisation with CS, as well as the functional groups they correspond to, are shown in Table 4.1. Peaks were assigned according to that reported in literature.

Table 4.1: Major peaks observed in the FTIR spectra of FAuNPs containing CS and the functional groups corresponding to them (adapted from Queiroz *et al*., (2014))

Peak wavenumber (cm^{-1})	Functional group
3252.03	N-H stretching
	O-H stretching
	CS intramolecular hydrogen bonds
2917.86	C-H stretching
1556.10	N-H bending of amide II bond
1406.43	CH$_2$ bending
1150.54	C-O-C stretching
1019.00	C-O stretching

Following the addition of PEG, an increase in the peak intensity at 2916.87 and 2918.24 cm^{-1}, for AuCS-2% PEG and AuCS-5% PEG respectively, and at 1036.28 and 1030.92 cm^{-1}, for AuCS-2% PEG and AuCS-5% PEG respectively, was observed. This is due to

CH$_2$ stretching and C-O-C stretching on the PEG chains, and indicate that PEGylation was successful (Luo *et al*., 2016). Following functionalisation with Tf, a peak at 1700 - 1600 cm^{-1} was expected, as this peak corresponds to the amide I bond in the protein backbone (Cai *et al*., 2018). However, this peak was not observed, possibly due to masking by residual water, or by the PEG chains.

4.2.3. Transmission electron microscopy analysis

TEM allows for visualisation of the shape, size, and surface morphology of NPs, and can be used to determine the average diameter and size distribution (Bhatia, 2016). From the TEM images (Figure 4.4), it can be seen that the AuNP were successfully synthesised, producing uniform spherical shapes, and were relatively monodisperse, displaying little aggregation. AuNP were found to have an average diameter of 12.17 nm, which was similar to that observed by Ivanov *et al*., (2009), who synthesised citrate-capped AuNP with an average diameter of 13.3 ± 0.6 nm. The FAuNPs also displayed uniform sizes, with average diameters between 12 and 13 nm, as shown in Table 4.2.

Table 4.2: Average diameter of AuNP and FAuNPs determined using TEM

Nanoparticle	Average diameter (nm ± SD)
AuNP	12.17 ± 1.15
AuCS	12.70 ± 1.29
AuCS-2% PEG	12.59 ± 1.51
AuCS-5% PEG	12.46 ± 1.36
AuCSTf	12.58 ± 1.04
AuCSTf-2% PEG	12.71 ± 1.09
AuCSTf-5% PEG	12.97 ± 1.21

No significant changes in the morphology or size of FAuNPs following functionalisation can be observed from the TEM images. Zhang *et al*., (2012) were able to observe the CS coating on AuCS NPs using high resolution TEM (HRTEM); however, no layer around the FAuNPs indicating the presence of CS could be observed in this study with TEM. Manson *et al*., (2011) and Ding *et al*., (2014b) reported no differences in the size and shape of PEGylated AuNP compared to unPEGylated AuNP when viewed using TEM.

This is expected as TEM is often unable to view biological compounds without staining, as they do not adequately deflect the electron beam to produce an image (Hall *et al*., 2007). Narayanan and Sivakumar, (2014) noted that it may be difficult to observe CS on TEM for this reason. The sizes obtained from TEM may thus only reflect the size of the electron-dense AuNP core, rather than the size of the FAuNP including the ligands. Furthermore, TEM gives the dry size of the NP, as the solution is air-dried before analysis. The NP size in liquid may be more important given that the NP will be in liquid when in the body. A more accurate estimation of particle size may be obtained using NTA, which measures the hydrodynamic diameter of NPs.
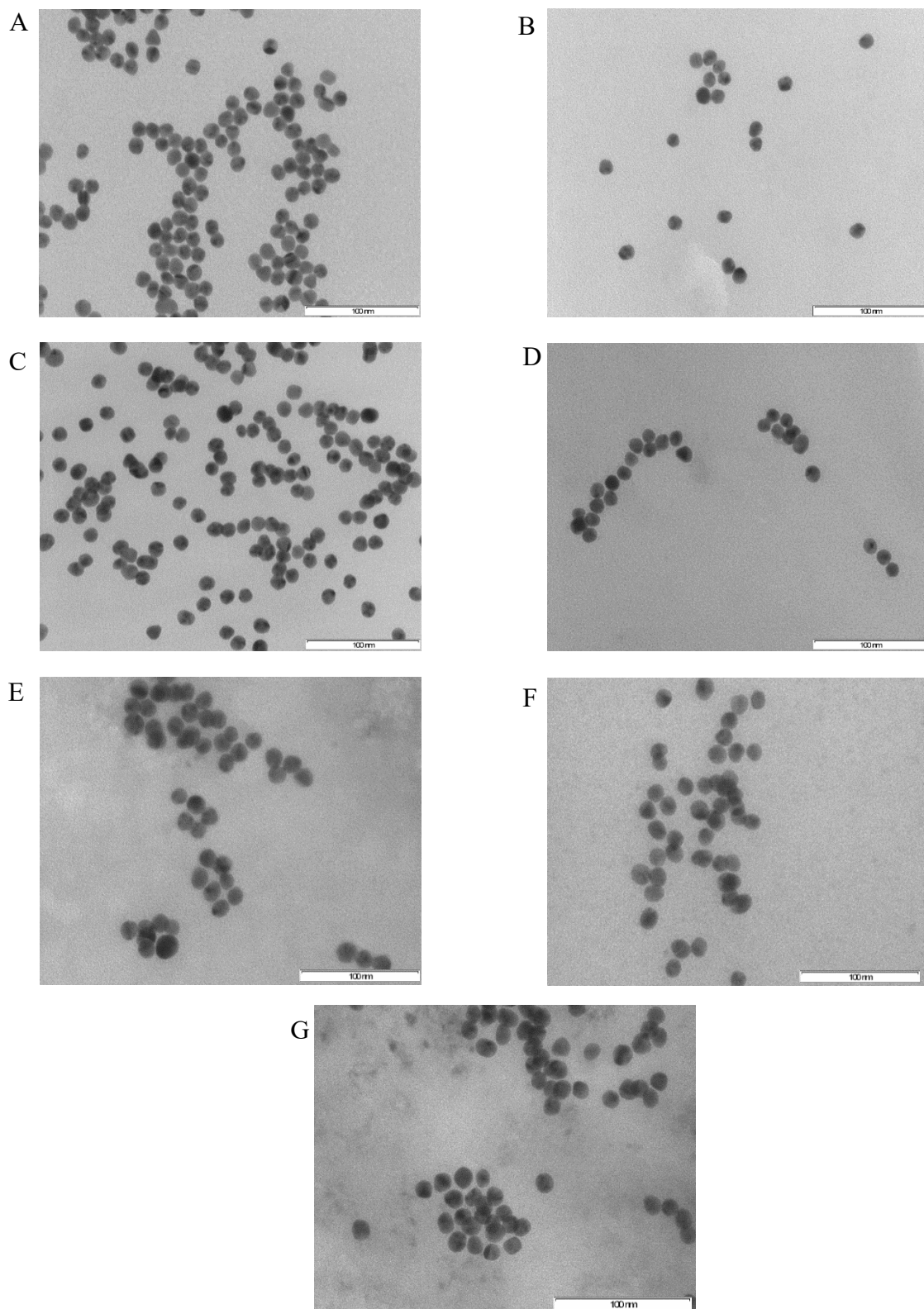
Figure 4.4: TEM images of (A) AuNP, (B) AuCS, (C) AuCS-2% PEG, (D) AuCS-5% PEG, (E) AuCSTf, (F) AuCSTf-2% PEG, and (G) AuCSTf-5% PEG at 400 000x. Scale bar represents 100nm.

4.2.4. Nanoparticle tracking analysis: Size and zeta potential

When in solution, a hydrodynamic shell forms around NPs, composed of particles in the solvent. The size of this shell is dependent on many characteristics of the NP, such as its shape, size, composition, and surface roughness (Pabisch *et al.*, 2012). The hydrodynamic diameter determined by NTA takes the hydrodynamic shell into account, and can be defined as the diameter of a theoretical sphere that diffuses in fluid in the same manner as the NP (Stetefeld *et al.*, 2016). This size may be more relevant than TEM size when analysing the *in vitro* or *in vivo* behaviour of the NPs, since it is an indication of the NP size in fluid. Zeta potential is a useful indication of the stability and surface charge of NPs. The sizes and zeta potentials of AuNP, FAuNPs, and nanocomplexes are shown in Table 4.3.

Table 4.3: Hydrodynamic diameters and zeta potential of FAuNPs measured using NTA

Nanoparticle	Hydrodynamic diameter (nm ± SD)	Zeta potential (mV ± SD)
AuNP	64.8 ± 19.5	-25.1 ± 0.9
AuCS	94.7 ± 2.7	37.8 ± 0.4
AuCS/pDNA	150.2 ± 4.8	-17.4 ± 0.8
AuCS-2% PEG	111.2 ± 14.2	30.5 ± 0.3
AuCS-2% PEG/pDNA	268.3 ± 10.1	-38.7 ± 0.2
AuCS-5% PEG	196.4 ± 140.1	22.3 ± 1.4
AuCS-5% PEG/pDNA	139.8 ± 97.5	-37.6 ± 0.9
AuCSTf	174.9 ± 70.6	27.9 ± 0.5
AuCSTf/pDNA	154.4 ± 51.9	-39.2 ± 0.2
AuCSTf-2% PEG	155.7 ± 30.6	27.5 ± 1.0
AuCSTf-2% PEG/pDNA	118.4 ± 54.5	-41.0 ± 0.8
AuCSTf-5% PEG	94.2 ± 19.8	18.8 ± 0.3
AuCSTf-5% PEG/pDNA	104.0 ± 7.0	-17.8 ± 0.8

The plain AuNP were found to have a hydrodynamic diameter of 64.8 nm, much larger than the size determined by TEM. Farkas *et al.*, (2010) also observed that larger sizes were reported by NTA (30 - 50 nm) for citrate-capped AuNP than TEM (5 – 10 nm). This is due to the formation of a hydrodynamic shell around the AuNP. The zeta potential of

plain AuNP was determined to be -25.1 mV, due to the presence of anionic citrate ions capping the particles. All FAuNPs showed increased sizes compared to the plain AuNP. This is expected since NTA takes into account the presence of ligands, and indicates that functionalisation was successful. Following conjugation with CS, the zeta potential and size increased to +37.8 mV and 94.7 nm, respectively, indicating that the AuNP had successfully become encapsulated by the CS to form highly stable AuCS NPs.

Functionalisation with PEG further increased the size of the FAuNPs, with AuCS-5% PEG displaying a larger size than AuCS-2% PEG. It was also reported using dynamic light scattering (DLS) that the hydrodynamic diameter of PEGylated AuNP increased with increasing PEG grafting density (Uz *et al.*, 2016). In a study using PEGylated linoleic acid and poly(b-malic acid)-functionalised CSNPs, it was observed that a low density of PEG did not significantly increase the size compared to the unPEGylated NPs; however, higher grafting densities resulted in a significant size increase, similar to what was observed with the AuCS-5% PEG NPs (Zhang *et al.*, 2015). It was further suggested that this was due to the changes in the conformation of the PEG layer as the grafting densities increased.

The zeta potentials decreased upon conjugation with PEG, to +30.5 mV for AuCS-2% PEG and +22.3 mV for AuCS-5% PEG. This is possibly partly due to PEG interacting with the amine groups of CS. However, decreased zeta potentials upon PEGylation are expected due to the shielding effect conferred by PEG. The shielding effect has also been reported to increase with increasing PEG densities. It has been reported that increasing grafting densities decreased the surface charge of liposomes (Kumar *et al.*, 2014). This was also observed in this study, as the AuCS-5% PEG NPs had a lower zeta potential than AuCS-2% PEG. Nevertheless, both PEGylated FAuNPs displayed adequately strong positive charges that would facilitate binding of pDNA. The zeta potentials suggest that AuCS-2% PEG NPs are highly stable, while AuCS-5% PEG NPs are only moderately stable. However, in the case of PEGylated NPs, zeta potential may not be an accurate indication of stability, as PEG shields the surface charge and confers steric stability.

The hydrodynamic diameters of the Tf-targeted FAuNPs were found to be: 174.9 nm (AuCSTf), 155.7 nm (AuCSTf-2% PEG), and 94.2 nm (AuCSTf-5% PEG). The increases in size relative to the untargeted FAuNPs for AuCSTf and AuCSTf-2% PEG are an

indication that Tf was successfully bound (James and Driskell, 2013). AuCSTf-2% PEG displayed a smaller increase in size compared to AuCSTf, which may have been due to embedding of the Tf in the PEG layer. A similar observation was made using AFM to analyse the binding of bovine serum albumin (BSA) to PEGylated and unPEGylated silica wafers, which showed that the root mean squares of the PEGylated wafers exposed to BSA were smaller than those of unPEGylated wafers, indicating that the surface was "smoother" (Natte *et al.*, 2013). This smoothness was attributed to the embedding of BSA proteins within the PEG chains. It is also possible that the Tf proteins assumed a different orientation when they adsorbed onto the PEGylated FAuNPs. When proteins bind to a NP, they may stick out perpendicularly from the NP surface, lie flat on the NP, or lie at an angle (James and Driskell, 2013). In contrast to the other Tf-targeted FAuNPs, AuCSTf -5% PEG decreased in size compared to AuCS-5% PEG. Cai *et al.*, (2018) also reported that thiol PEG$_{2000}$-coated AuNP displayed a decrease in size upon conjugation with Tf, as determined by DLS. They suggested that this decrease occurred due to the Tf embedding in the PEG layer. In further studies, they analysed the influence of increasing Tf concentration on the size of PEGylated AuNP, and observed that higher Tf concentrations resulted in reduced sizes. They suggested that the Tf proteins are able to displace PEG chains and form a protein patch, leading to a decrease in the average NP diameter measured by DLS. It is possible that this occurred with the AuCS-5% PEG NPs, where the higher PEG density may have led to displacement of some PEG chains upon Tf conjugation.

The zeta potential of all FAuNPs decreased upon conjugation with Tf, to +27.9 mV (AuCSTf), +27.5 mV (AuCSTf-2% PEG), and +18.8 mV (AuCSTF-5% PEG). These decreases may be due to a combination of factors. The Tf protein bears a net negative charge and binds to the positive groups on CS, thus reducing the positive charge. Parab *et al.*, (2011) also observed that the conjugation of Tf to Au-HMP-PEG NPs resulted in a small decrease in the zeta potential, which they attributed to the presence of amide bonds in the Tf. Furthermore, the Tf may shield the positive charges on CS in a similar manner to PEG (Ogris *et al.*, 1999).

Upon complexation with pDNA, the zeta potentials decreased for all FAuNPs, from positive to strongly negative values. Cebrián *et al.*, (2011) also reported that the positive zeta potential of AuPEI NPs became negative following complexation with pDNA, which

they suggested indicated that the pDNA had successfully electrostatically bound to the NPs. All nanocomplexes, except AuCS/pDNA and AuCSTf-5% PEG/pDNA, displayed zeta potentials below -30 mV, indicating that they are highly stable. Size increases were observed for AuCS/pDNA, AuCS-2% PEG/pDNA, and AuCSTf -5% PEG/pDNA, which displayed sizes of 150.2, 268.3, and 104 nm, respectively. The relatively small sizes of the Tf-targeted nanocomplexes may correlate with their increased ability to condense pDNA, as shown in the EB intercalation assay (section 4.3.2). This may have led to the formation of smaller nanocomplexes.

4.3. DNA binding studies

4.3.1. Band shift assay

The NP vector must be able to efficiently bind DNA for gene delivery. Thus, the band shift assay was conducted to determine the amount of FAuNPs required to complex a specific amount of pDNA. Increasing FAuNP:pDNA weight ratios were formed by incubating a constant amount of pDNA (0.25 µg) with increasing amounts of FAuNPs. pDNA that has been completely bound by FAuNPs will form electroneutral nanocomplexes, in which the negative charge of the pDNA has been completely neutralised by the positive groups on the FAuNP. These nanocomplexes will not migrate during gel electrophoresis and will instead remain in the well. The optimum, supra-optimum, and sub-optimum ratios obtained (Table 4.4) were used further in nuclease protection and *in vitro* cell based studies. The agarose gel images are shown in Figure 4.5.

Table 4.4: Optimal, sub-optimal, and supra-optimal FAuNP:pDNA ($^W/_W$) ratios determined in the band shift assay

	Sub-optimal	Optimal	Supra-optimal
AuCS	2:1	2.4:1	2.8:1
AuCSTf	4:1	4.4:1	4.8:1
AuCS-2% PEG	3.2:1	3.6:1	4:1
AuCSTf-2% PEG	2.8:1	3.2:1	3.6:1
AuCS-5% PEG	3.6:1	4:1	4.4:1
AuCSTf-5% PEG	5.6:1	6:1	6.4:1
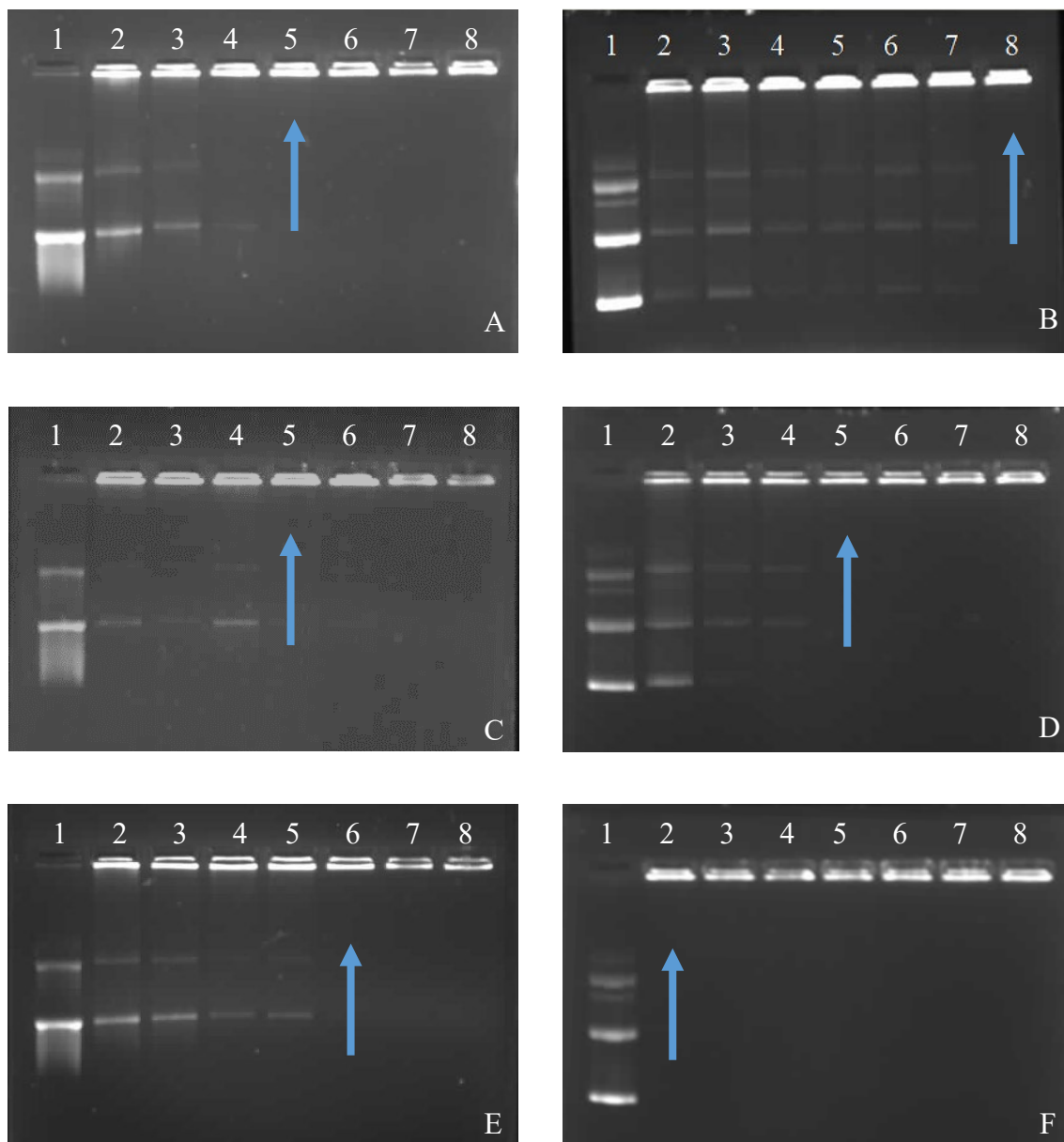
Figure 4.5: Band shift assays for A) AuCS B) AuCSTf C) AuCS-2% PEG D) AuCSTf-2% PEG E) AuCS-5% PEG F) AuCSTf-5% PEG. Lane 1 contains pDNA only; lanes 2-8 contain increasing FAuNP:pDNA weight ratios. Endpoints are indicated by arrows. Endpoint ratios are given in Table 4.4.

All FAuNPs were able to completely bind pDNA, at FAuNP:pDNA ratios (optimum) ranging from 2.4:1 to 6:1 (Table 4.4). The control in lane 1, which contains pDNA in the absence of FAuNPs, shows the circular, linear, and supercoiled conformations (Figures 4.3 B, D, F) of pDNA. Retardation of pDNA movement through the gel can be seen by the decrease in the fluorescent intensity and, in some cases, the disappearance of bands as the weight ratios increase. Endpoints can be seen where there is no further migration

of pDNA into the gel. AuCS displayed the lowest binding ratio of 2.4:1. The addition of PEG onto the NP resulted in an increase of binding ratios to 3.6:1 and 4:1 for AuCS-2% PEG and AuCS-5% PEG, respectively. Both the AuCSTf and AuCSTf-5% PEG NPs displayed binding ratios higher than their untargeted counterparts, with optimum binding ratios of 4.4:1 and 6:1, respectively. However, the AuCSTf-2% PEG NPs bound one ratio lower than the AuCS-2% PEG NPs, at 3.2:1.

The binding ratios generally correlate with the zeta potentials obtained for the FAuNPs. The zeta potentials of the FAuNPs decreased as ligands were conjugated, as both the PEG and Tf interacted with the amine groups of CS. This would have decreased the number of positive groups available for pDNA binding, and thus larger amounts of FAuNPs were required to fully complex the pDNA payload.

The PEGylated FAuNPs displayed discrete endpoints, indicating complete complexation of the pDNA (Figures 4.3 C, D, E, F). In addition to potential interactions with the amine groups of CS, PEGylation may reduce the binding affinity of CS for DNA by forming an inert layer over the CS that inhibits interactions with DNA (Kawano *et al*., 2006). Multiple groups have observed that the addition of PEG to NPs results in weakened DNA binding abilities. Kawano *et al*., (2006) observed that positively-charged 2-amino ethanethiol-coated AuNP displayed a stronger DNA-binding ability than their PEG-functionalised counterparts. In a study with PEGylated poly(2-(dimethylamino)ethyl methacrylate) (pDMAEMA) polymers, Verbaan *et al*., (2004) found that increased grafting densities further weaken interactions with DNA, which they suggested was due to shielding of the positive groups that bind DNA. DNA binding was completely inhibited at very high grafting densities greater than 22%, whereas polymeric NPs with grafting densities lower than 12% were capable of binding DNA. It has been reported that cholesterol (Chol-T) and cholesterol iodide (Chol-Q) liposomes functionalised with a 5% weight ratio of PEG bound pBR322 pDNA at higher ratios than those functionalised with 2% ($^w/_w$) PEG (Daniels *et al*., 2011), similar to what was observed in this study.

The addition of Tf further reduced the DNA binding ability of AuCSTf and AuCSTf-5% PEG NPs. A similar finding was made by Lee *et al*., (2005), who showed that conjugation with Tf increased the ratio at which DNA was fully complexed by PEI NPs. The decreased binding ratio for AuCSTf-2% PEG was unexpected. The addition of Tf may

have modified the PEG conformation in places to make the CS surface more accessible to the pDNA.

4.3.2. Ethidium bromide intercalation assay

Nucleic acid compaction is an important consideration for gene delivery. The DNA should ideally be compacted tight enough to prevent premature dissociation from the NP vector and degradation by serum nucleases. However, if the DNA is bound too tightly, it will interfere with vector unpacking and inhibit transfection (Akinc *et al*., 2005). Thus, the EB intercalation assay was conducted to assess the ability of the FAuNPS to condense and compact pDNA. It utilises EB, a fluorescent dye that intercalates between the bases of DNA. When free in solution, the fluorescence of EB is quenched by solvated oxygen; however, intercalation between the hydrophobic bases of DNA provides protection from quenching, allowing EB to fluoresce (Chib *et al.*, 2014). The fluorescence of intercalated EB is thus 10 times greater than the fluorescence of free EB (Hoy, 2013). The fluorescence of the EB fully intercalated with pDNA is taken as the 100% fluorescence value. FAuNPs are then added in 1 µl aliqouts, leading to formation of the nanocomplex and displacement of EB from the pDNA as it is condensed by the FAuNP. The displaced EB is quenched by oxygen molecules, leading to a decrease in fluorescence. FAuNPs are added until maximum displacement of EB, termed the point of inflection, was observed. These end-point ratios obtained from the EB intercalation assay may not directly correspond with those determined in the band shift assay, as the band shift assays determine the point at which the charge of the pDNA is neutralised by the FAuNPs, while the intercalation assay assesses condensation of the pDNA by FAuNPs.

From Figure 4.6, it is evident that all FAuNPs were able to efficiently condense pDNA, resulting in fluorescence decays of greater than 80%. AuCS displayed the weakest compaction ability of the FAuNPs, but still displaced EB to a significant extent, with a maximum fluorescence decay of approximately 84.7%. PEGylated FAuNPs displayed slightly stronger compaction abilities, with decays of approximately 85.7% for AuCS-2% PEG and 87.8% for AuCS-5% PEG. Tf-targeted FAuNPs displayed endpoints much lower than their corresponding untargeted FAuNPs, and lower than the endpoints obtained in the band shift assay. The fluorescence decays for AuCSTf, AuCSTf-2% PEG, and AuCSTf-5% PEG were approximately 86.8%, 98.9%, and 91.4%, respectively.

AuCSTf-2% PEG thus displayed the greatest ability to condense pDNA. This may correlate with its stronger ability to bind the pDNA, as shown in the band shift assay.
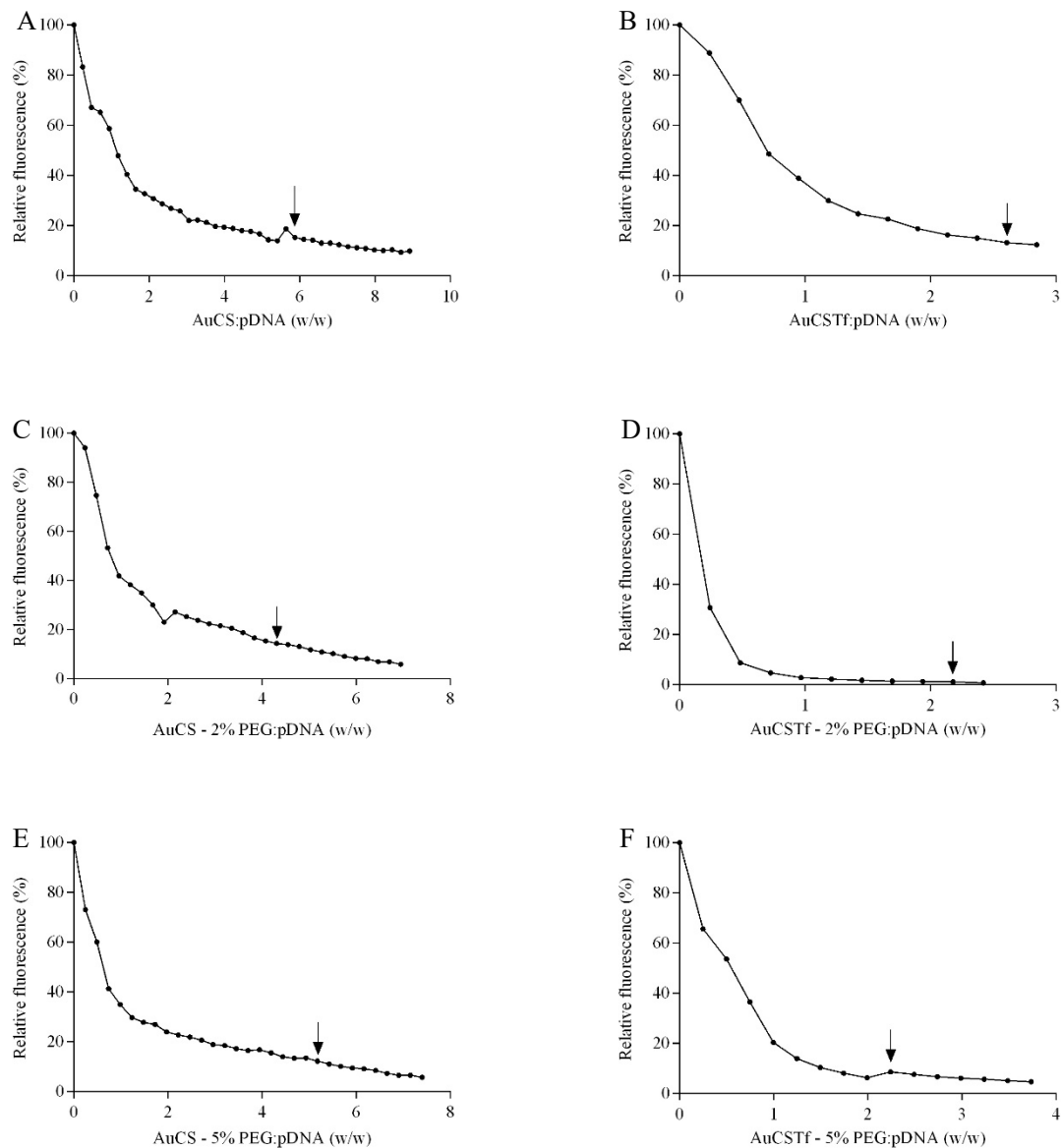
Figure 4.6: EB intercalation assay for A) AuCS, B) AuCSTf, C) AuCS-2% PEG, D) AuCSTf-2% PEG, E) AuCS-5% PEG, and F) AuCSTf-5% PEG.

It has been reported that DNA is efficiently compacted by NPs with a strong positive charge, as the DNA will bend around the NP in a similar manner to how it interacts with histone proteins, whereas weakly charged NPs will not be able to induce the same level of compaction. Furthermore, the transition from extended to compacted DNA occurs when the surface charge of polycations ranges from +5 to +10 (Railsback *et al.*, 2012).

This transition state was investigated by Railsback and co-workers (2012) using weakly positively-charged AuNP with a surface charge of +6. All FAuNPs in this study displayed zeta potentials above +10, with the lowest being +18.8 mV for AuCSTf-5% PEG. Thus, they were all able to efficiently compact the pDNA payload.

The PEGylated NPs displayed a small increase in fluorescence quenching compared to AuCS. Similar observations have been made by Jiang *et al*., (2006) with PEG-grafted CS (CS-*g*-PEG) NPs, where the fluorescence decay was slightly higher for CS-*g*-PEG NPs with a higher PEG grafting density compared to plain CSNPs and CS-*g*-PEG NPs with a lower PEG grafting density. In a study using PEG-PEI vectors conjugated to the RGD peptide, it was found that the RGD-PEG-PEI NPs displaced EB to a greater extent than the RGD-PEI NPs (Kunath *et al*., 2003). It was hence suggested that PEG may also contribute to DNA compaction, although it is less efficient than PEI. Early studies by Lerman, (1971) reported the ability of neutral polymers to induce DNA condensation in the presence of salt, with subsequent studies exploring this ability in PEG (Cheng *et al*., 2015; Froehlich *et al*., 2011). The salts are thought to neutralise the charges on the DNA, preventing electrostatic repulsion and permitting condensation (Cheng *et al*., 2015). It is possible that the PEG on the FAuNPs may have similarly contributed to condensation of the pDNA neutralised by the charges on the CS.

Tf-targeted FAuNPs were able to condense the pDNA to a greater degree than their untargeted counterparts. This increase in fluorescence decay was small for AuCSTf, but more significant for AuCSTf-2% PEG and AuCSTf-5% PEG. A report on higher fluorescence quenching for TAT peptide-conjugated PEG-PEI NPs compared to plain PEI NPs was attributed to the cationic amino acids within the peptide influencing DNA condensation (Kleemann *et al*., 2005). In contrast, Ogris *et al*., (2001) observed that 25 kDa PEI NPs conjugated with Tf showed a reduced ability to condense DNA, as they formed large, fibrous aggregates compared to the spherical, compacted nanocomplexes formed by plain PEI NPs. This may have occurred because the large Tf protein may have inhibited the compaction of nanocomplexes into spherical particles, which would not have occurred with the AuNP. This may account for the observed differences.

The EB intercalation assay can be used as an indication of the protection provided by the vector against degradation by serum nucleases, as tightly compacted DNA will not be

accessible for degradation. However, de Lima *et al*., (2003) noted that this assumption may be erroneous, as EB may be able to access compacted DNA that is inaccessible to nucleases. Thus, the nuclease protection assay is also important to accurately assess the protective capabilities of the FAuNPs.

4.3.3. Nuclease protection assay

Following systemic administration, NP vectors will interact with serum components. These include endonucleases, which may degrade therapeutic nucleic acids. The vector should thus ideally strongly bind its payload and protect it from degradation (Yin *et al*., 2014). The nuclease protection assay was conducted to assess the ability of the FAuNPs to protect pDNA from degradation by serum nucleases. Nanocomplexes at the sub-optimal, optimal, and supra-optimal ratios were incubated with 10% FBS for 4 hours at body temperature (37 °C) and analysed on an agarose gel to assess the extent of degradation. Two controls were used: a positive control composed of undigested pDNA (C1), and a negative control containing pDNA digested under the same conditions as the nanocomplexes (C2).
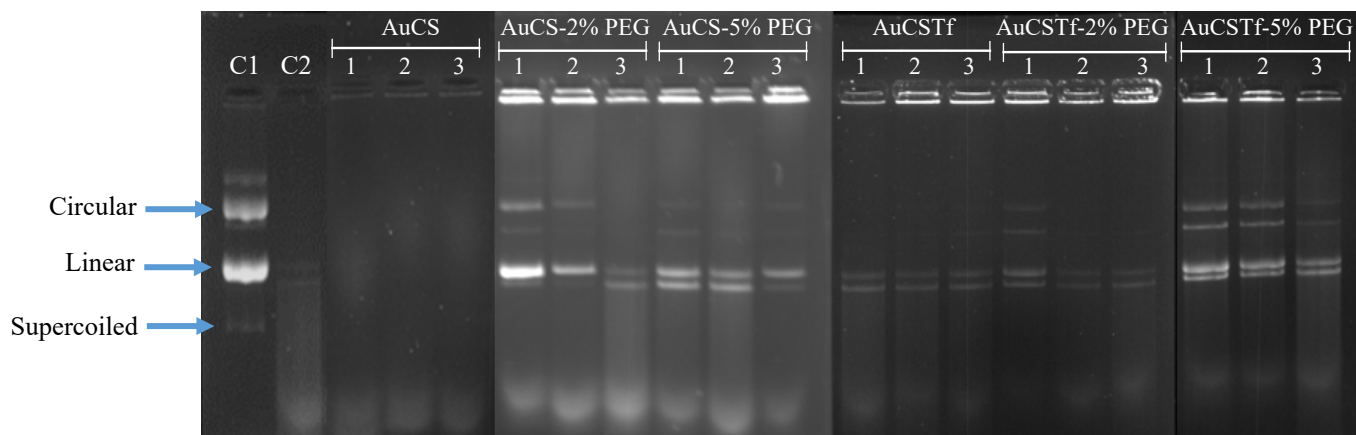
Figure 4.7: The nuclease protection assay in FAuNPs. C1) positive control containing undigested pDNA; C2) negative control containing pDNA digested with 10% FBS; lanes labelled 1, 2, and 3 contain sub-optimal, optimal, and supra-optimal ratios respectively of the indicated FAuNPs, set up as shown in Table 4.4.

From Figure 4.7, it can be noted that AuCS NPs were unable to fully protect the pDNA payload as no intact bands are visible, indicating that the pDNA was degraded to some extent. Both AuCS-2% PEG and AuCS-5% PEG were able to protect pDNA from complete degradation, displaying bands correlating to the linear and circular

conformations of pDNA (C1). All Tf-targeted AuNP were able to protect pDNA to varying extents. However, the supercoiled form was not observed for any FAuNPs. This could be due to nicking of the pDNA into circular and linear forms by the enzymes.

The inability of AuCS to fully protect pDNA may be due to a combination of factors. Despite the strong positive charge of AuCS (+37.8 mV, as shown in Table 4.3), it displayed the weakest compaction ability of the FAuNPs, as demonstrated by the EB intercalation assay (Figure 4.4A). Thus, nucleases may have been able to access and cleave the pDNA to a greater extent than other FAuNPs. The negative charge of the AuCS/pDNA nanocomplex (-17.4mV, as shown in Table 4.3) may have promoted interactions with cationic serum proteins, or positively-charged protein domains. Song *et al*., (2015) observed an increase in the size of negatively-charged DNA-coated AuNP when in media containing serum, which they attributed to the adsorption of serum proteins onto the NP. Thus, the surface charge may have promoted interactions with serum nucleases. DNA displacement has been suggested to occur in lipoplexes which display weakened DNA binding abilities (Simberg *et al*., 2003). It is possible that interactions with serum proteins may have destabilised the pDNA-CS electrostatic bond and resulted in displacement of the pDNA, given the weaker compaction ability of AuCS. The complete degradation of AuCS-bound pDNA was also observed by Lazarus and Singh (2016).

The PEGylated FAuNPs protected the pDNA from degradation, as indicated by the presence of bands for AuCS-2% PEG and AuCS-5% PEG. PEGylation was also able to provide protection despite the stronger negative charges of AuCS-2% PEG and AuCS-5% PEG nanocomplexes (-38.7 mV and -37.6 mV, respectively). PEG is widely used as a steric stabiliser to reduce interactions with serum components, thus preventing opsonisation and interactions with serum nucleases. Tf itself also appears to offer a measure of protection, as can be inferred from the presence of bands for AuCSTf. It has been noted that physical adsorption of Tf onto sulphated polystyrene NPs (PSOSO$_3$H) inhibited interactions with human plasma proteins (Pitek *et al*., 2012). Hence, it is possible that the Tf inhibited interactions with serum nucleases. The increased protection may also be due to the stronger compaction of pDNA by the Tf-targeted FAuNPs, as seen in the EB intercalation assay.

There does not appear to be a significant difference in the protective capabilities of AuCS-2% PEG and AuCS-5% PEG NPs. AuCSTf-5% PEG appeared to provide more protection to degradation than AuCSTf -2% PEG, as the bands appeared more intense. The absence of the supercoiled form could indicate loss of plasmid activity (Zhang and Anchordoquy, 2004). In a study with liposomes synthesised using the lipid DOTAP and varying amounts of cholesterol, Zhang and Anchordoquy, (2004) observed that a significant amount of the supercoil content was degraded after incubation with 10% ($^V/_V$) serum. However, they found no obvious association between transfection efficiency and the loss of the supercoil conformation, and noted that the circular form of plasmids is also capable of transfecting cells. It should also be noted that not all bound pDNA was released from the FAuNPs. SDS was used to release pDNA, however, the presence of fluorescence in the wells of all FAuNPs indicates that much of the pDNA remained NP-bound in the wells. This may have occurred due to the strong compaction of pDNA by these FAuNPs, as demonstrated in the EB intercalation assay (Akinyelu and Singh, 2018).

4.4. *In vitro* cell culture assays

4.4.1. MTT cytotoxicity assay

The MTT assay utilises the yellow 3-(4,5-dimethylthiazol-2-yl)-2,5-diphenyltetrazolium bromide (MTT) dye, which is cleaved by mitochondrial hydrogenases to form purple formazan crystals (Figure 4.8) (Fotakis and Timbrell, 2006). Dissolution of the formazan crystals in DMSO yields a purple solution that can be read spectrophotometrically at 550 nm (Patravale *et al*., 2012). Since MTT is reduced in the mitochondria, the absorbance is indicative of the mitochondrial activity of the cell population, and thus the number of viable cells (van Meerloo *et al*., 2011). Cytotoxicity was assessed in the HEK293, Caco-2, and HeLa cell lines at the sub-optimal, optimal, and supra-optimal ratios obtained in the band shift assay.
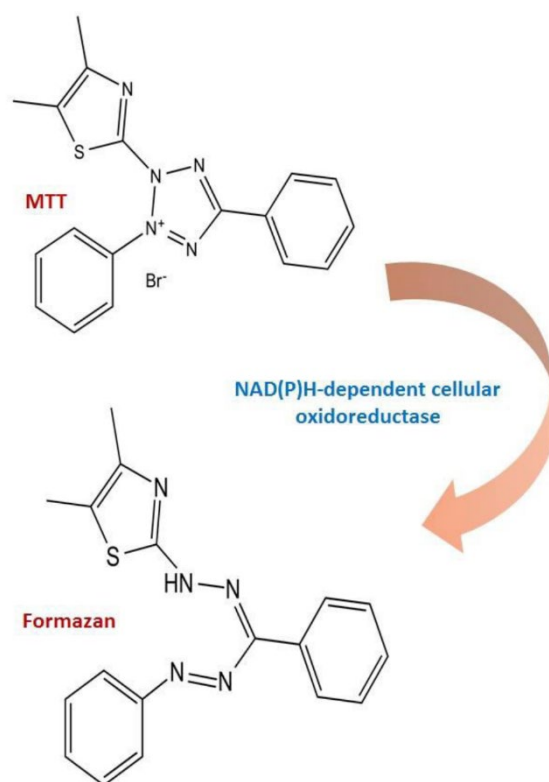
Figure 4.8: The principle of the MTT cytotoxicity assay showing the reduction of MTT to formazan (Bahuguna *et al*., 2017).

From Figures 4.9-4.11 it is evident that the FAuNPs were generally well tolerated in the HeLa and HEK293 cell lines. Cell viabilities were above 70% for most FAuNPs, except for AuCS-2% PEG in HeLa cells, and AuCS-5% PEG in the HEK293 cells. At optimal ratios, these FAuNPs inhibited cell growth by 38% and 46%, respectively. In contrast, AuCSTf-2% PEG and AuCSTf-5% PEG promoted growth in the HEK293 cell line, by 20% and 37% at the optimal binding ratios, respectively. Cell viabilities exceeding 100% were also obtained for certain ratios of AuCSTf and AuCSTf-2% PEG in HeLa cells. Untargeted FAuNPs were generally observed to display greater toxicity in Caco-2 cells than in the other cell lines (Figure 4.10). Cell growth was inhibited by 62% for AuCS, 57% by AuCS-2% PEG, and 48% by AuCS-5% PEG at the optimal ratios. Furthermore, AuCS-2% PEG and AuCS-5% PEG inhibited cell growth in a dose-dependent manner, with the supra-optimal ratios displaying very low viabilities of 19% and 24%, respectively. Tf-targeted AuNP were generally observed to have increased cell viability compared to the untargeted AuNP.
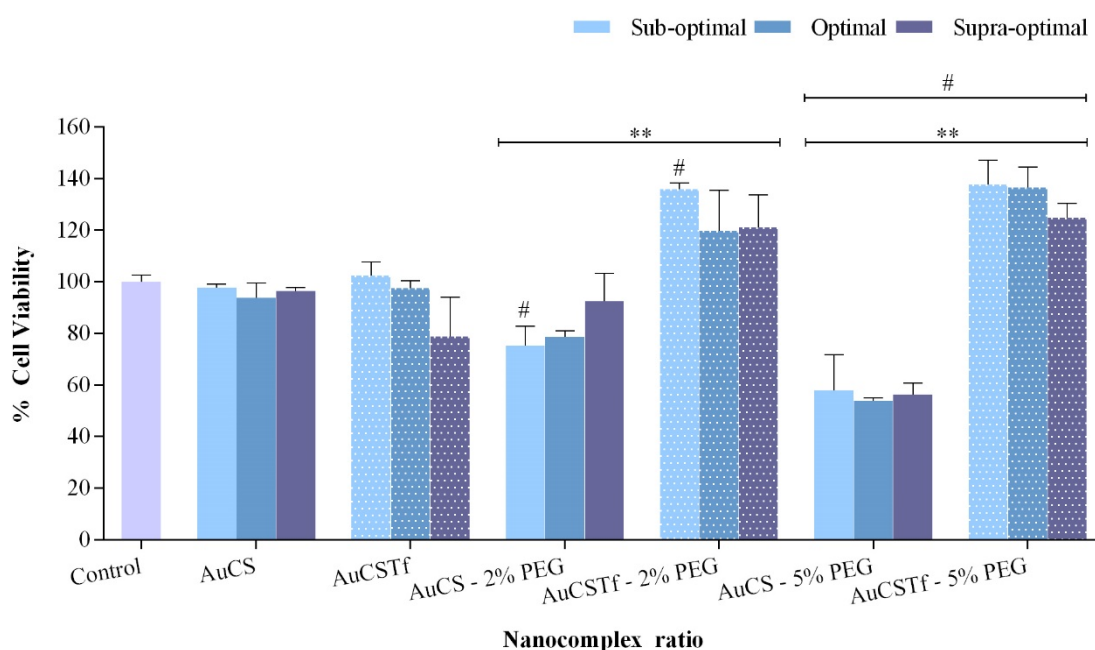
Figure 4.9: MTT cytotoxicity assay in the HEK293 cell line. Data is represented as means ± SD (n=3). **p<0.01 considered statistically significant between corresponding ratios of Tf-targeted and untargeted FAuNPS; #p<0.05 considered statistically significant vs. control.
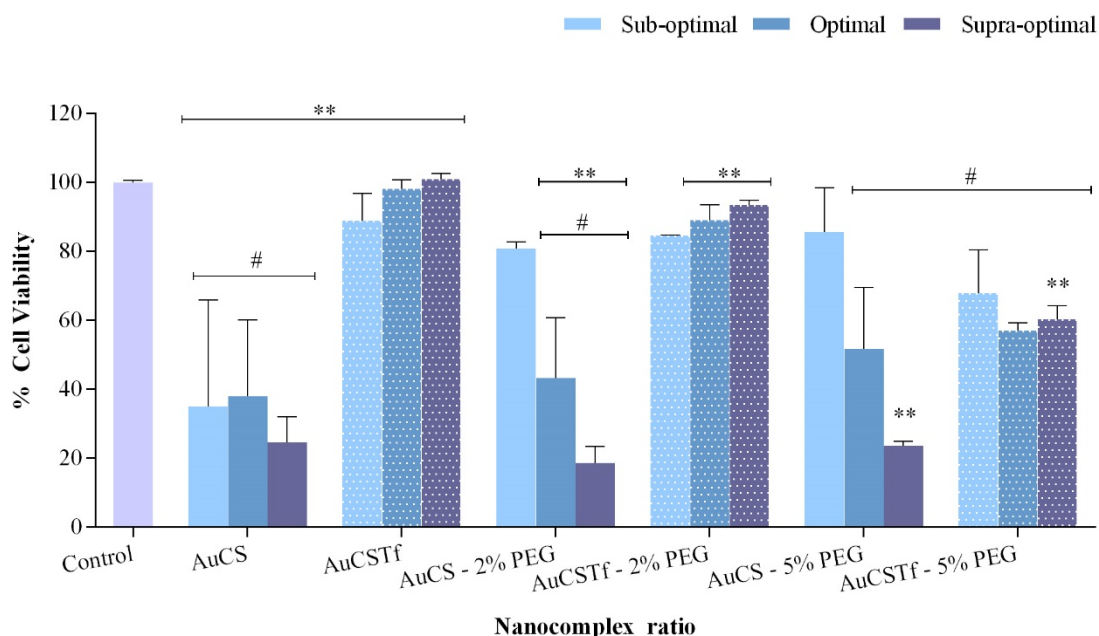
Figure 4.10: MTT cytotoxicity assay in the Caco-2 cell line. Data is represented as means ± SD (n=3). **p<0.01 considered statistically significant between corresponding ratios of Tf-targeted and untargeted FAuNPS; #p<0.05 considered statistically significant vs. control.
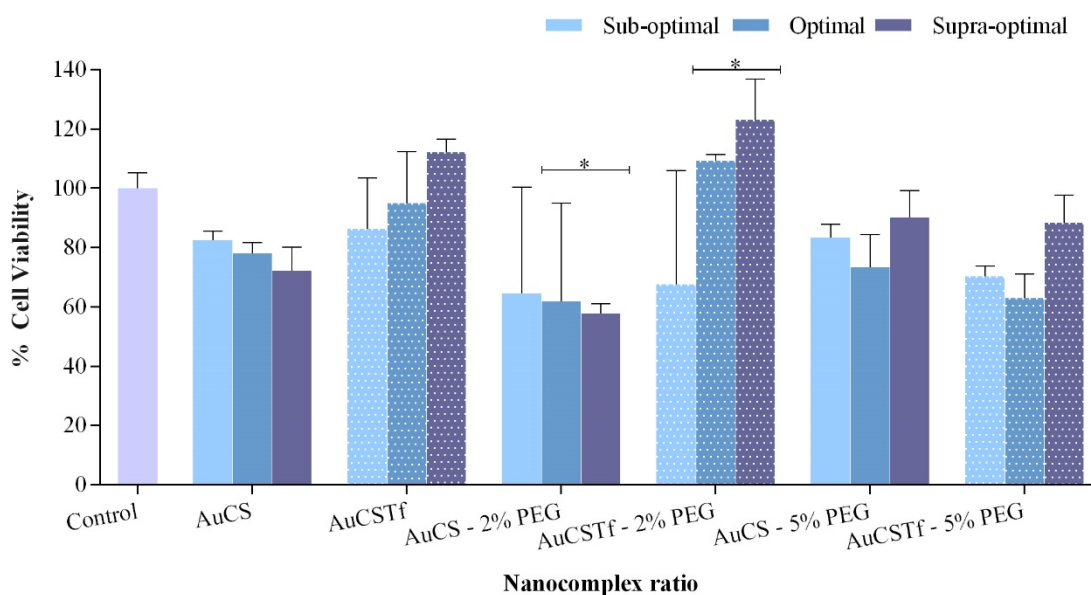
Figure 4.11: MTT cytotoxicity assay in the HeLa cell line. Data is represented as means ± SD (n=3). *p<0.05 considered statistically significant between corresponding ratios of Tf-targeted and untargeted FAuNPS.

Coating AuNP with CS is generally thought to increase the biocompatibility of the NPs and thus improve their transfection efficiency (Rodrigues *et al*., 2012). However, differing results have been obtained regarding the toxicity of AuCS NPs in different cell lines. For example, Boca *et al*., (2011) observed minimal toxicity of AuCS NPs in Chinese hamster ovary (CHO) cells, while Boyles *et al*., (2015) found that AuCS induced cytotoxicity in the human monocyte cell line THP-1. In this study, AuCS was observed to cause minimal cytotoxicity in HeLa and HEK293 cells, but significant toxicity to Caco-2 cells (p<0.05). Martínez-Torres *et al*., (2018) found that AuCS NPs caused cell death in HeLa cells by inducing the formation of reactive oxygen species (ROS), whereas plain citrate-capped AuNP remained non-toxic to cells. The concentrations used by Martínez-Torres *et al*., (2018) were higher than those used in this study, although AuCS did display a small dose-dependent decrease in cell viability across the ratios, similar to the observations made by the authors (Figure 4.11). Studies using AuCS gels and CS-capped AuNRs displayed minimal cytotoxicity in HEK293 cells, similar to the results obtained in this study (Figure 4.9) (Ramezani *et al*., 2014; Manivasagan *et al*., 2018).

Differing results have been obtained regarding the influence of PEG on cell viability. Some studies have found that an increase in the degree of PEGylation reduced the

cytotoxicity of NPs. An increase in the PEGylation of liposomes has been found to reduce their cytotoxicity to HepG2 cells (Chen *et al.*, 2013); while a high density of PEG on CSNPs was seen to reduce cytotoxicity in monkey kidney epithelial cells (Vero) compared to a lower density of PEG (De Matteis *et al.*, 2016). In the HeLa cell line, AuCS-5% PEG displayed an increase in cell viability compared to AuCS-2% PEG ($p < 0.01$ for the optimal and supra-optimal ratios). AuCS-5% PEG showed a marginal, and statistically insignificant, increase in cell viability compared to AuCS-2% PEG in Caco-2 cells. However, in the HEK293 cell line, AuCS-5% PEG displayed a significantly lower cell viability ($p < 0.05$) than AuCS-2% PEG. The administration of PEG$_{5000}$ coated AuNP coated were reported to induce apoptosis in liver cells of mice *in vivo* (Cho *et al.*, 2009). PEGylated AuNP have also been observed to decrease the viability of HEK293 cells (Tlotleng *et al.*, 2016).

Untargeted FAuNPs appeared to demonstrate cell-specific growth inhibition in the Caco-2 cell line. Treatment with AuCS ($p < 0.05$), optimal and supra-optimal ratios of AuCS-2% PEG and AuCS-5% PEG ($p < 0.05$), and AuCSTf-5% PEG ($p < 0.05$) resulted in significant decreases in cell viability. In a study using silver nanoparticles (AgNPs), van der Zande *et al.*, (2016) observed that Caco-2 cells were more sensitive than human breast cancer epithelial cell line (MCF-7) to the toxic effects of AgNPs. They suggested that this increased sensitivity was due to the higher uptake of AgNPs by Caco-2 cells. This correlates with the results of the transfection assay, as Caco-2 cells displayed the highest transfection efficiencies. Thus, the higher cytotoxicities exhibited by Caco-2 may be due their increased uptake of FAuNPs relative to the HeLa and HEK293 cells. This increased uptake may have exacerbated any toxic effects exhibited by CS, PEG, or the AuNP themselves. AuNP have been reported to induce apoptosis in Caco-2 cells (Nady, 2017). CSNPs have also been found by to induce damage to Caco-2 cell mitochondrial membranes (Loh *et al.*, 2012).

The Tf-targeted AuNP displayed favourable cell viabilities, and in some cases increased viability compared to their untargeted counterparts. This increase was significant for AuCSTf-2% PEG ($p < 0.05$) and AuCSTf-5% PEG ($p < 0.01$) in the HEK293 cell line, AuCSTf in Caco-2 ($p < 0.01$), certain ratios of AuCSTf -2% PEG and AuCSTf-5% PEG in Caco-2 ($p < 0.01$), and AuCSTf-2% PEG in HeLa ($p < 0.05$). AuCSTf and AuCSTf-2% PEG were seen to increase cell viability in a dose-dependent manner in Caco-2 and HeLa

cell lines. This increased cell viability is especially noteworthy in the Caco-2 cell line and for AuCSTf-5% PEG in HEK293, as it suggests that conjugation with Tf curbed the cytotoxic aspects of the untargeted FAuNPs. Lee *et al*., (2005) reported that Jurkat and HeLa cells treated with Tf-conjugated PEI NPs displayed increased viability compared to those treated with PEI NPs. The growth promotion may also have been due to the delivery of iron to the cells via the holoTf proteins.

Caco-2 cells, being colorectal cancer cells, are often used as a model for intestinal cells, and may be used to assess the effect NPs may have on the gastrointestinal system (Chen *et al*., 2016). The results obtained suggest that the untargeted AuNP might have adverse effects on the gastrointestinal system. Moreover, assessing the cytotoxicity of NPs in the HEK293 cell line may be an indication of the cellular interactions of NPs with kidney cells *in vivo* (Tlotleng *et al*., 2016). This is important as the kidney represents an organ where NPs tend to accumulate following systemic administration. All FAuNPs displayed favourable cell viabilities in the HEK293, suggesting that they may not produce renal toxicity *in vivo*. However, it should be noted that, while treatment with AuCS-5% PEG resulted in cell viabilities around 60%, the significant reduction in cell viability observed may limit their use *in vivo*.

4.4.2. Apoptotic studies

Apoptotic studies were conducted to determine the mechanism of action by which cell viability is reduced following treatment with the FAuNPs. This was done using the dual ethidium bromide/acridine orange (EB/AO) assay, which is advantageous over MTT in that it allows for differentiation between necrotic and apoptotic cells (Liu *et al*., 2015). The EB/AO assay is dependent on the differential staining of the intercalating EB and AO dyes. AO is able to penetrate the cell membrane, and stain the nucleus green, while EB is only capable of entering cells and staining the nucleus orange following membrane disruption (Ribble *et al*., 2005). Thus, live and early apoptotic (EA) cells, which have intact cell membranes, appear green, with cells in EA fluoresce a brighter green with visible condensed chromatin (Kasibhatla *et al*., 2006). Late apoptotic (LA) and necrotic cells have damaged membranes and thus fluoresce orange, with cells in LA displaying condensed chromatin (Ribble *et al*., 2005). The assay was carried out for the optimal

ratios that showed the lowest viabilities in the MTT cell viability assay, viz. AuCS in Caco-2; AuCS-5% PEG in HEK293; and AuCS-2% PEG in HeLa cells.

Figure 4.12 shows that all cell lines contained cells in various stages of apoptosis, indicating that exposure to the FAuNPs may have induced apoptosis. Cells in early apoptosis, fluorescing a much brighter green than live cells, can be seen in all three cell lines, with Caco-2 displaying cells in late apoptosis. HEK293 cells were observed to display the lowest apoptotic index, followed by Caco-2 and HeLa cells, respectively. The apoptotic indices (Table 4.5) are noticeably lower than the cell viabilities obtained in the MTT assay. This may be due to the difference in incubation times: cells were incubated with nanocomplexes for 48 hours in the MTT cytotoxicity assay, but were only incubated for 24 hours for the EB/AO assay. The much lower apoptotic index of the HEK293 cells may be due to the slower growth of the non-cancerous cells.

Table 4.5: Apoptotic indices for AuCS-5% PEG, AuCS-2% PEG, and AuCS in HEK293, HeLa and Caco-2 cell lines, respectively

Cell lines	Apoptotic index
HEK293	0.07
HeLa	0.19
Caco-2	0.15
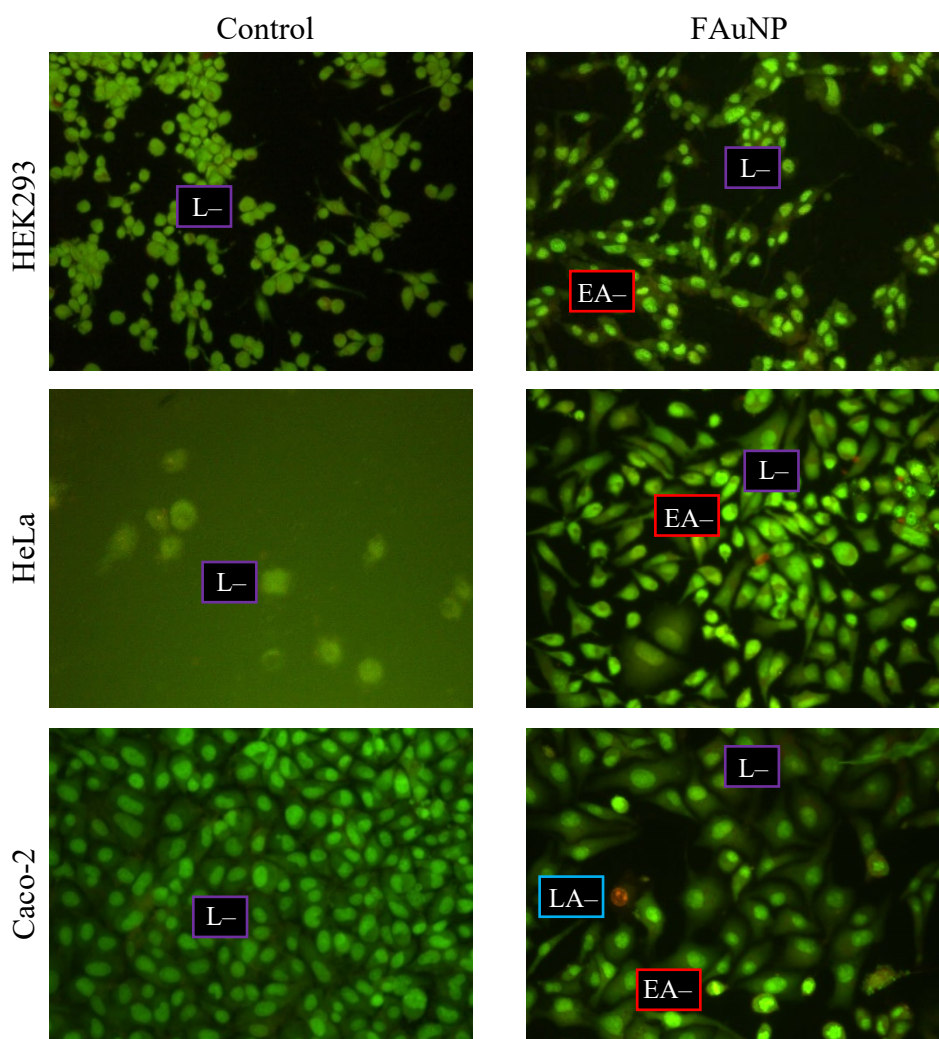
Figure 4.12: Flourescent images of the ethidium bromide/acridine orange assay in HEK293, HeLa and Caco-2 cell lines at 20x magnification; L = live cells, EA = early apoptosis, LA = late apoptosis.

4.4.3. Transfection studies

The transfection efficiency of the FAuNPs was assessed using the luciferase reporter gene assay. The assay utilises the firefly luciferase protein, a 61 kDa protein that does not require post-translational modifications, facilitating its use as a reporter protein (Fan and Wood, 2007). In the presence of ATP, magnesium, and oxygen, luciferase catalyses the oxidation of luciferin to produce oxyluciferin, carbon dioxide (CO_2), inorganic phosphate (PPi), and light that absorbs maximally at 560 nm (Fan and Wood, 2007; Herschman, 2004; Pandolfi and Stecca, 2015). This reaction is split into two stages, shown below (de Wet *et al*., 1987):

1) Luciferase + luciferin + ATP $\xleftrightarrow{\text{Mg}^{2+}}$ Luciferase.luciferyl-AMP + PPi

2) Luciferase.luciferyl-AMP + O_2 $\longrightarrow$ Luciferase + oxyluciferin + AMP + CO_2 + light

Cells transfected with the *luc* gene encoding firefly luciferase will thus produce luminescence, which can be measured in relative light units (RLU). The intensity of the luminescence produced is proportional to the amount of luciferase protein produced, and thus can be used as a measure of transfection efficiency (Pandolfi and Stecca, 2015). Results are presented as RLU normalised against the protein content of the cells (RLU/mg protein). Two controls are used to determine background luminescence: a negative, cell-only control, to which no pDNA is added (designated C1), and a positive control, to which free pDNA in the absence of FAuNPs is added (designated C2).

The results for the luciferase assay in HEK293, Caco-2, and HeLa cell lines are presented in Figures 4.13, 4.14, and 4.15, respectively. All FAuNPs were capable of transfecting cells, leading to luminescence values higher than those achieved by transfection with free pDNA. The highest transfection efficiencies were observed in the Caco-2 cell line, with luciferase activities ranging from 8.67×10^5 RLU/mg protein for the sub-optimal AuCS ratio to 1.54×10^5 RLU/mg protein for the optimal ratio of AuCSTf -5% PEG. Luciferase activities ranged from 1.87×10^5 RLU/mg protein for the sub-optimal ratio of AuCSTf-5% PEG to 5.27×10^4 RLU/mg protein for the sub-optimal ratio of AuCS-2% PEG in the HeLa cells. Transfection efficiencies were generally lower in HEK293 cells, ranging from 7.1×10^4 RLU/mg protein for the supra-optimal ratio of AuCS-2% PEG to 3.24×10^4 RLU/mg protein for the sub-optimal ratio of AuCSTf-5% PEG. A general trend was observed where the PEGylated FAuNPs produced lower transfection efficiencies compared to the unPEGylated AuCS NPs.
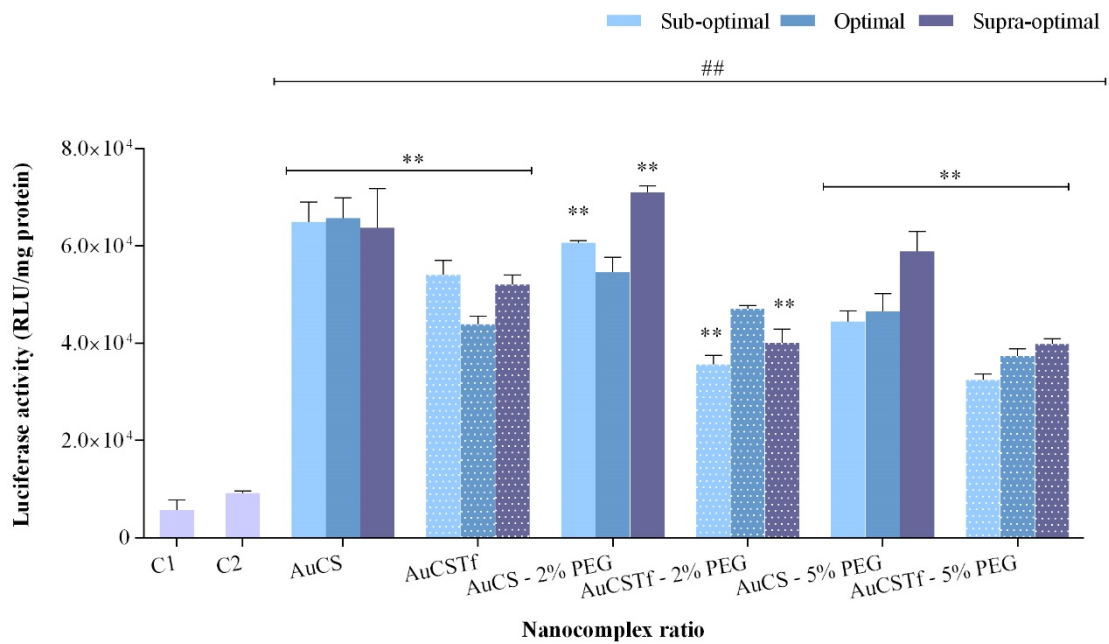
Figure 4.13: Luciferase assay in the HEK293 cell line. Data is represented as means ± SD (n=3). **p<0.01 considered statistically significant between corresponding ratios of Tf-targeted and untargeted FAuNPS; ##p<0.01 considered statistically significant vs. C2.
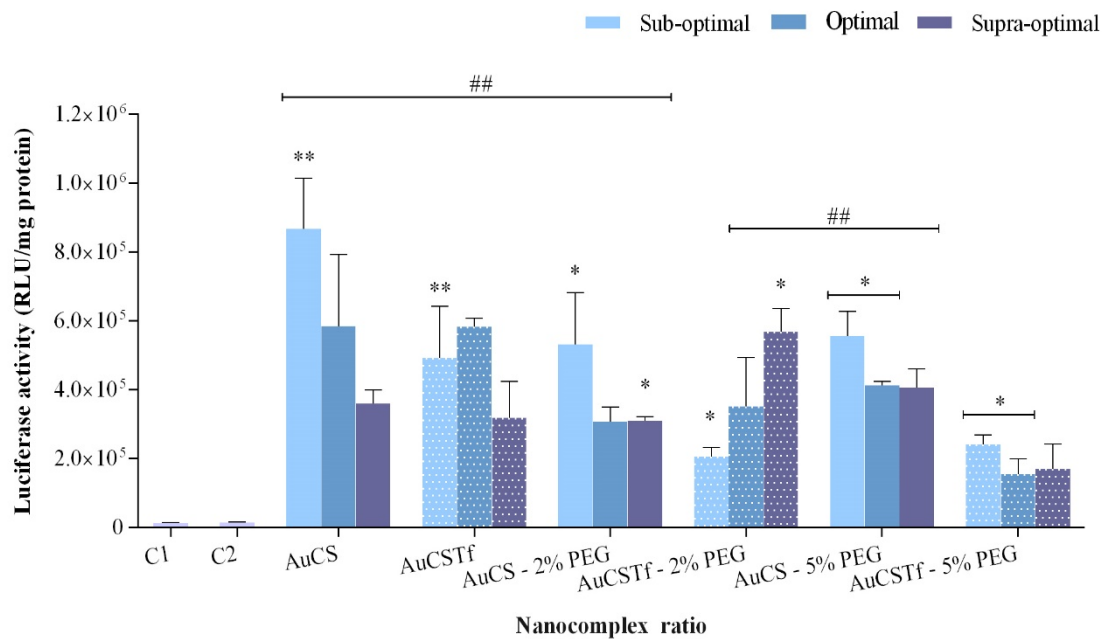
Figure 4.14: Luciferase assay in the Caco-2 cell line. Data is represented as means ± SD (n=3). *p<0.05 and **p<0.01 considered statistically significant between corresponding ratios of Tf-targeted and untargeted FAuNPS; ##p<0.01 considered statistically significant vs. C2.
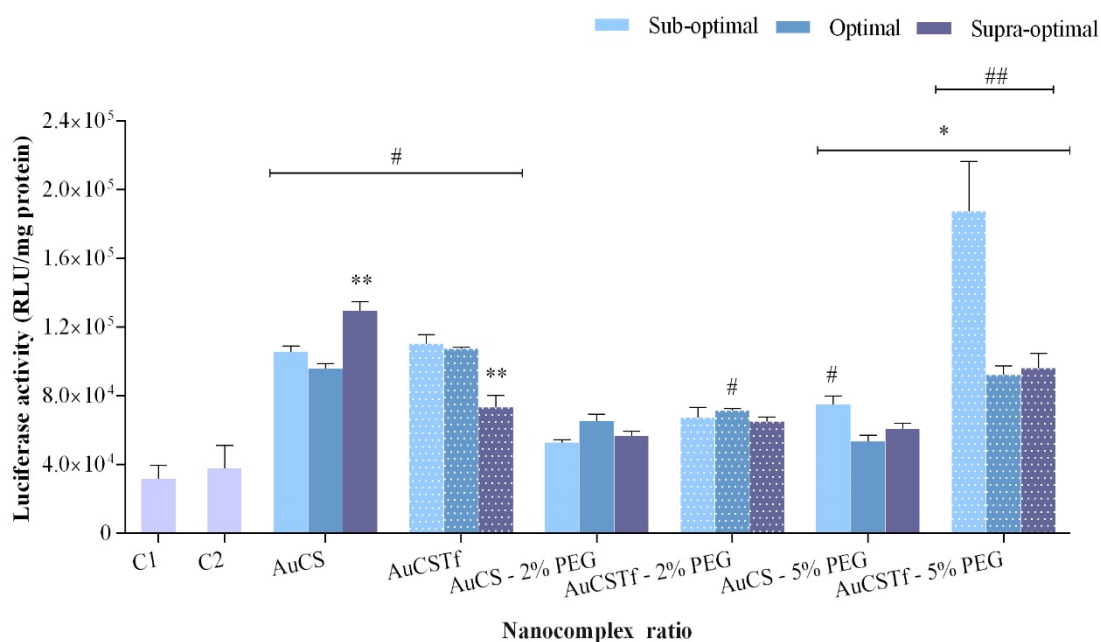
Figure 4.15: Luciferase assay in the HeLa cell line. Data is represented as means ± SD (n=3). *p<0.05 and **p<0.01 considered statistically significant between corresponding ratios of Tf-targeted and untargeted FAuNPS; ##p<0.05 and ##p<0.01 considered statistically significant vs. C2.

Transfection efficiency is influenced by many factors, such as the cell viability, NP interactions with DNA, properties of the NPs including their size and zeta potentials, and the cell type. Different cell types may display many different characteristics that affect how the NP is internalised and processed within the cell, ultimately influencing their transfection efficiency. Differences in cell membrane compositions influence the endocytic pathways used to internalise NPs, and thus their intracellular fate; for example, some cells, such as neurons and HepG2, lack the caveolae1 protein and thus cannot carry out caveolin-dependent endocytosis (Behzadi *et al*., 2017). Variations in cell division rates not only influence the ability of NPs to access the DNA, but have also been shown by Kim *et al*., (2012a) to affect the NP load in cells, as the internalised NPs are split between the daughter cells following cell division. These cellular differences may account for the variations in transfection efficiency observed across the three cell lines, where different ratios for each FAuNP were observed to perform optimally.

There are differing reports regarding the effects of serum on NP stability and transfection efficiency. The transfection efficiency of cationic liposomes has been observed to decrease markedly upon exposure to serum, as their positive charge promotes interactions

with serum proteins, leading to aggregation and dissociation of lipoplexes (Misra *et al.*, 2013; Sato *et al.*, 2001). However, serum has also been reported to improve the transfection ability of CSNPs. Sato *et al.*, (2001) reported increased transfection of CSNPs in medium containing 10% and 20% FBS compared to serum-free medium, which they attributed to an increase in cell growth in response to the added serum. Increased transfection of PEI polyplexes in medium supplemented with 10% ($^V/_V$) foetal calf serum (FCS) has also been reported (Kneuer *et al.*, 2000). All FAuNP nanocomplexes were able to transfect cells in the presence of 10% ($^V/_V$) serum. This is advantageous as NPs will be exposed to such conditions *in vivo* (Misra *et al.*, 2013). The FAuNPs can be inferred to maintain their stability and transfection abilities in the presence of serum proteins.

While it is generally accepted that a positive surface charge is a requirement for efficient transfection, as it promotes interactions with negative membrane proteoglycans, several studies have shown anionic nanocomplexes to be capable of transfecting cells (Akinc and Battaglia, 2013). Cebrián *et al.*, (2011) and Kneuer *et al.*, (2000), for example, reported transfection with anionic PEI-AuNP and silica nanocomplexes, respectively. The nanocomplexes in this study all showed strong negative charges, ranging from -41 to -17.4 mV, yet were still capable of efficiently transfecting cells. It has been reported that anionic NPs show reduced uptake compared to cationic NPs (Fröhlich, 2012). The reported analysis of the cellular uptake of anionic, cationic, and neutral dendrimers in human lung carcinoma (A549) cells showed that cationic dendrimers had the fastest rate of cellular entry, followed by anionic and neutral dendrimers, respectively (Perumal *et al.*, 2008). This may correlate with the results of Lazarus and Singh, (2016), where cationic AuCS nanocomplexes bearing a charge of +28.4 mV produced higher transfection efficiencies in HeLa cells than those observed in this study, with luciferase activities approximately 3-4 orders of magnitude higher.

The size of the nanocomplex also plays an important role in influencing the transfection efficiency of the FAuNPs. Studies suggest that different cell types display different optimal sizes for transfection (Shang *et al.*, 2014). It was reported that, from a range of 14, 30, 50, 74, and 100 nm AuNP, the 50 nm AuNP showed maximal uptake into HeLa cells (Chithrani *et al.*, 2006). However, studies investigating the uptake of poly(lactic-coglycolic acid) (PLGA) NPs in Caco-2 cells, showed that cellular uptake was lowest for

50 nm NPs, with maximum cell uptake observed for 100 nm PLGA NPs. Decreased uptake was observed for larger NPs (200, 500, and 1000 nm); however, their uptake remained higher than that of the 50 nm NPs (Win and Feng, 2005). This observation may account for the higher transfection levels observed in Caco-2 cells, as all nanocomplexes were above 100 nm in diameter.

It should be noted that the zeta potentials and hydrodynamic diameters of the nanocomplexes may be different in cell culture medium. Zeta potentials were determined in 18 Mohm water; however, the presence of ions in the medium will influence the slipping plane, and thus the zeta potentials, of the nanocomplexes. Ji *et al.*, (2010) have reported that DMEM contains a high concentration of cations such as Ca^{2+}, Na^+, and K^+, which may interact with and screen the negative charge of the nanocomplexes, allowing for interactions with positive compounds (Boyles *et al.*, 2015). Zeta potential measurements taken for liposome-polymer nanocomplexes in serum-free medium have been found to accurately correlate with their transfection efficiency (Son *et al.*, 2000). It has also been suggested that size measurements be taken in medium, to determine the level of NP aggregation or protein adsorption (Shang *et al.*, 2014).

Another important factor influencing cellular uptake and transfection efficiency is the presence of ligands on the vector. It is established that PEGylation interferes with transfection, in what is referred to as the PEG dilemma. This phenomenon has been widely reported for different types of nanoparticles. The PEGylation of β-cyclodextrin-containing polymer (βCDP) and branched PEI (bPEI) NPs led to reduced transfection compared to unPEGylated NPs, through different mechanisms (Mishra *et al.*, 2004). Although PEG-βCDP NPs displayed reduced uptake compared to unPEGylated NPs, PEGylation of bPEI NPs was not observed to inhibit uptake. This lead Mishra *et al.*, (2004) to suggest that the aggregated bPEI NPs may distort endosomal membranes to a greater extent than PEGylated NPs, inducing endosomal escape. Thus, PEGylation interfered with endosomal escape. Studies have also shown that PEGylation reduces transfection in a dose-dependent manner, with larger amounts of PEG leading to further reductions in transfection efficiency (Chan *et al.*, 2012; Gjetting *et al.*, 2010; Zhang *et al.*, 2010). In agreement with these studies, the addition of PEG led to a decrease in transfection efficiency in this study. This general trend was observed in all three cell lines. However, AuCS-5% PEG was observed to produce lower transfection than AuCS-2%

PEG in HEK293 cells only. This decreased transfection was significant for the sub- and supra-optimal ratios (p<0.01). In contrast, AuCS-5% PEG produced similar luciferase activities compared to AuCS-2% PEG in Caco-2 and HeLa cells. This unexpected result may correlate with the lower cell viability of AuCS-5% PEG in HEK293 cells, which may have led to decreased luminescence in these cells, whereas AuCS-5% PEG produced higher or similar cell viabilities in the HeLa and Caco-2 cell lines. The much smaller size of the AuCS-5% PEG nanocomplexes compared to AuCS-2% PEG (139.8 nm vs 268.8 nm) may also have contributed to its increased transfection.

A trend can be seen in the HEK293 cell line, where the addition of Tf onto FAuNPs resulted in decreased transfection activity. This may have occurred due to the presence of the extra ligand inhibiting interactions with the cell membrane, thus leading to reduced cellular uptake. This trend also correlates with the EB intercalation assay, where Tf-targeted FAuNPs displayed an increased ability to condense pDNA compared to the untargeted FAuNPs. Increased nucleic acid condensation may interfere with "vector unpacking", the ability of the nanocomplex to dissociate from its nucleic acid payload. This is a requirement for the binding of transcription factors and expression of the therapeutic gene (Schaffer *et al*., 2000). Bolhassani and Saleh, (2013) also noted that large targeting ligands may interfere with unpacking of the vector, and thus the presence of the large ~80kDa Tf protein may have hindered nucleic acid dissociation.

These factors (the PEG dilemma and inhibited vector unpacking) may explain why the AuCS ratios tended to display the highest overall transfection efficiency compared to other nanocomplexes in all cell lines. The luciferase activity of AuCS is higher than AuCSTf-5% PEG in TfR-negative HEK293 and Caco-2 cells, despite AuCSTf-5% PEG nanocomplexes displaying a similar zeta potential (-17.8 mV), smaller size (104 nm), and increased cell viabilities in these cell lines.

Most NPs are internalised via endocytosis, rather than through passive mechanisms (Fröhlich, 2012). The characteristics of the FAuNPs such as size, zeta potentials, and associated ligands, strongly influence which endocytic pathway they will exploit to enter cells. Studies also have shown that anionic, neutral, and cationic NPs may enter through different pathways (Perumal *et al*., 2008). The uptake of 50, 100, 200, 500 and 1000 nm latex beads in murine melanoma B16 cells showed that beads of 200 nm or less were

internalised via CME, while CvME internalised 500 nm beads. CvME was suggested to be the major uptake pathway for beads between 200 and 1000 nm (Rejman *et al*., 2004). Hence, it is possible that all FAuNPs, except AuCS-2% PEG, may predominantly enter via CME. AuCS-2% PEG, with a nanocomplex size of 268.8 nm, may have been taken up by CvME. However, the presence of CS may induce uptake by CME, as CSNPs have been observed to enter A549 and Caco-2 cells via CME (Sahay *et al*., 2010). It is also possible that the FAuNPs may utilise multiple internalisation pathways simultaneously. RME internalises NPs ranging from 100 to 200 nm in size (Win and Feng, 2005). All Tf-targeted nanocomplexes were within this size range, with diameters of 154.4, 118.4, and 104 nm for AuCSTf, AuCSTf -2% PEG, and AuCSTf-5% PEG, respectively, signifying their potential use for targeted gene delivery.

It was expected that the Tf-targeted FAuNPs would display higher transfection than their untargeted counterparts in the TfR-positive HeLa cell line, as this would suggest that the NPs are entering cells via RME (Akinyelu and Singh, 2018). However, the AuCSTf did not display increased transfection compared to the AuCS, with the supra-optimal ratio of AuCSTf instead showing a significant decrease compared to AuCS (p<0.01). A possible reason for the high transfection of AuCS compared to AuCSTf is offered by Chithrani *et al*., (2006), who reported that the uptake of negatively-charged citrate-capped AuNP was three times higher than Tf-conjugated AuNP in HeLa cells. Further investigations revealed that the citrate-capped AuNP became coated with proteins following incubation in serum-containing DMEM. These serum proteins were then able to induce cellular uptake via RME. They suggested that uptake of the citrate-capped AuNP was higher due to the presence of many different serum proteins targeting different receptors, whereas the Tf-conjugated AuNP could only target the TfR. It is possible that serum proteins may have interacted with the AuCS and promoted cellular uptake, as these FAuNPs carried no ligands that inhibit interactions with serum components.

The majority of serum proteins are anionic and would thus not be expected to interact with the anionic AuCS nanocomplexes (Boyles *et al*., 2015). However, multiple studies have reported that serum proteins can interact with, and form a protein corona around, anionic NPs. Bewersdorff *et al*., (2017) analysed the protein coronas of AuNP functionalised with sulphated and non-sulphated dendritic polyglycerols (dPG). They found that AuNP carrying sulphated dPG bore a negative charge, and formed larger and

more varied coronas than their cationic non-sulphated counterparts. These serum proteins were also found to facilitate uptake via RME. Dissimilar results were obtained by Boyles *et al*., (2015), comparing anionic citrate-capped AuNP and cationic AuCS NPs, and Deng *et al*., (2012), comparing anionic poly(acrylic acid)-coated AuNP to cationic poly(N-(2-aminoethyl)acrylamide)-coated AuNP. Both these studies observed that the protein corona increased as the positive charge increased, nevertheless, serum proteins were observed to interact with the anionic NPs. It is also possible that the zeta potentials differed in the medium, as mentioned above, and allowed interactions with serum proteins.

The AuCSTf-2% PEG, similarly to the AuCSTF, displayed similar transfection levels compared to the untargeted AuCS-2% PEG, producing only marginal increases in luciferase activity. The AuCSTf-5% PEG was the only targeted NP to produce significantly increased transfection compared to its untargeted counterpart (p<0.05). This would suggest that the AuCSTf-5% PEG nanocomplexese entered the cells by RME, although it should be noted that the lower transfection of AuCSTf and AuCSTf-2% PEG does not exclude RME as a method of entry. A potential reason for the lowered expression of AuCSTf-2% PEG could be its ability to strongly condense the pDNA. Thus, to verify uptake by RME, a competition binding assay was conducted.

4.4.4. Competition binding assay

The competition binding assay was carried out for the Tf-targeted FAuNPs. The assay involved flooding the TfR-positive HeLa cells with excess free holoTf, thus binding to and blocking the receptors, thereby preventing NP uptake via RME. A drop in luciferase activity following the assay was an indication that NPs are being taken up by RME.

AuCSTf displayed significant decreases (p<0.01) in luciferase activity in the competition assay, indicating that the main entry mechanism of AuCSTf NPs was RME (Figure 4.16A). The greatest reduction was observed for the optimal ratio, which displayed a 6.9-fold decease in luciferase activity upon addition of free Tf. The sub-optimal and supra-optimal ratios decreased by approximately 4.6 and 3-fold, respectively. In contrast to the AuCSTf, the PEGylated Tf-targeted FAuNPs did not display such significant decreases in transfection. A small ~1.8-fold decrease was observed for the optimal ratio of AuCSTf-2% PEG. However, the sub- and supra-optimal ratios did not decrease upon addition of free Tf, indicating that they do not enter cells via RME (Figure 4.16B). Despite the

significantly increased uptake of AuCSTf-5% PEG in HeLa cells compared to their untargeted counterparts, only the sub-optimal ratio displayed a significant ~2.9-fold decrease in luciferase activity ($p < 0.01$), with the supra-optimal ratio displaying a smaller ~2.3-fold decrease (Figure 4.16C).
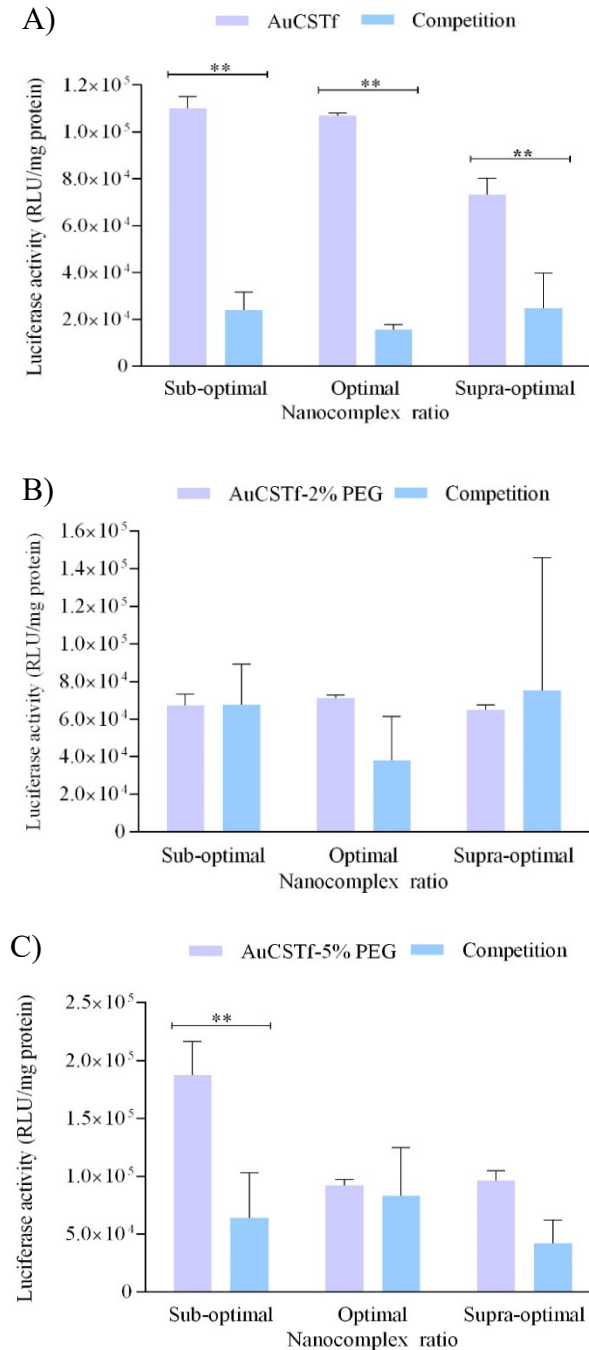
Figure 4.16: Competition binding assays for A) AuCSTf, B) AuCSTf-2% PEG, and C) AuCSTf-5% PEG. Data is represented as means ± SD (n=3). **$p < 0.01$ considered statistically significant.

There are a number of reasons why targeting may have failed for the AuCSTf-2% PEG NPs. It has been noted that strong positive or negative zeta potentials may promote the formation of a protein corona around NPs, which may prevent the targeting ligand from binding to its receptor (Wiley *et al.*, 2013). However, both PEG and Tf have been observed to inhibit serum protein interactions. Moreover, this effect was not observed for AuCSTf, which also displayed a strong negative zeta potential. It is also not likely that the failure of AuCSTF-2% PEG to enter cells via RME was due to failure of the Tf to conjugate to the NP, as AuCSTf-2% PEG consistently displayed dissimilar results to AuCS-2% PEG. It is therefore likely that PEGylation itself interfered with receptor binding.

PEGylation may hamper uptake via RME by blocking the active sites of the targeting ligand and preventing it from binding to the receptor. Managit *et al.*, (2003) analysed the effect of two PEG chain lengths, PEG_{350} and PEG_{2000}, for *in vivo* liver uptake of galactosylated liposomes (Gal-liposomes). PEGylation of the Gal-liposomes appeared to inhibit receptor-mediated uptake relative to the unPEGylated Gal-liposomes, as the PEG_{350}-Gal-liposomes and PEG_{2000}-Gal liposomes displayed 10- and 100-times lower uptake than Gal-liposomes, respectively. PEG_{2000} almost abolished the increased uptake of the targeted liposomes, displaying similar levels of hepatic uptake as untargeted PEG_{2000}-liposomes. This is similar to what was observed with the AuCSTf-2% PEG NPs. Managit *et al.*, (2003) suggested that the longer PEG_{2000} chains interfered with binding of the galactose moiety to its receptor. They also noted that, since PEGylation inhibits the interactions of vectors with biological compounds, it was expected to inhibit receptor-mediated uptake. Researchers also noted that binding of PEG and targeting molecules to the same reactive sites on the NP surface may lead to steric hindrance of receptor binding (Jokerst *et al.*, 2011).

The effects of PEG grafting density on the targeting efficiency of the RGD peptide, using NPs coated with increasing amounts of DSPE-PEG_{2000} and maleimide-DSPE-PEG_{2000} have been investigated (Hak *et al.*, 2012). Cellular uptake of targeted nanoparticles with 5 and 10 mol% PEG was observed to be increased compared to non-targeted NPs; however, grafting densities of 20 mol% and higher resulted in reduced cellular uptake compared to the lower grafting densities. In this study, the opposite was seen, where the lower grafting density of PEG inhibited receptor-mediated uptake. This discrepancy may

be due to the method used to conjugate the targeting ligand to the NP. Hak *et al*., (2012) bound the RGD peptide to the end of the PEG chain, whereas the Tf was adsorbed onto the surface of the NP in this study. It is possible that the lower grafting density of 2% ($^W/_W$) PEG may have assumed a more folded or mushroom conformation than the 5% ($^W/_W$) PEG. When the large Tf protein adsorbed onto the surface of the FAuNP, the folded PEG chains may have partially or totally covered the Tf, interfering with receptor binding, as noted by Jokerst *et al*., (2011). It is possible that the higher transfection of AuCSTf-5% occurred due to the formation of 'protein patches', as has been suggested by Cai *et al*., (2018). These patches may have promoted receptor-mediated uptake, as there may have been less interference from neighbouring PEG chains.

A possible method of overcoming the problems experienced with PEGylation and targeting is to conjugate the Tf directly onto the PEG chains, rather than onto the NP. This technique has been employed by several studies, with success. Kim *et al*., (2012b) used a PEG_{10000} linker to join Tf to the TNF-related apoptosis-inducing ligand (TRAIL) and observed that the resulting $Tf-PEG_{10000}$-TRAIL displayed a similar binding affinity for TfR as free holoTf. Huang *et al*., (2007) conducted *in vivo* biodistribution studies and *in vitro* gene expression studies in brain capillary endothelial cells using PEG_{3400}-linked PAMAM-Tf dendrimers. These dendrimers showed significantly increased brain uptake *in vivo*. *In vitro* studies revealed that, although the PAMAM-PEG-Tf dendrimers showed the lowest cellular uptake compared to PAMAM and PAMAM-PEG complexes, they produced the highest levels of gene expression. These studies utilise bi-functional PEG molecules, which carry functional groups at both ends of the chain, allowing for conjugation to both the Tf and NP.

Chapter 5
Conclusion

The difficulties faced in the treatment of aggressive brain cancers using conventional methods has driven the search for novel therapies that can selectively and efficiently eliminate cancerous cells. Gene therapy holds great promise in treating these cancers; however, numerous challenges are faced in designing vectors capable of transporting therapeutic genes into the brain. Over the years, issues with vector toxicity and immunogenicity has shifted interest from viral to non-viral vectors and, in particular, NP vectors. AuNP are popular due to their ease of synthesis and low toxicity. Furthermore, the ease with which they can be functionalised allows for conjugation with stealth and targeting ligands, valuable ligands for brain delivery. PEGylation is the most commonly used strategy to produce stealth NPs that can escape detection by the immune system and remain in circulation for longer periods of time, while the addition of targeting ligands allows the vector to exploit the RMT process to cross the BBB.

In this study, AuNP were successfully synthesised using the citrate reduction method, and functionalised. Morphological characterisation with TEM revealed AuNP to be spherical and small in size (<20 nm), while NTA showed that all FAuNPs displayed favourable sizes for transfection and zeta potentials for complexation of pDNA and cellular uptake. FAuNPs were further shown to partially protect their payload from degradation by serum nucleases. The FAuNP nanocomplexes successfully transfected cells *in vitro*, with interactions that appeared to be strongly influenced by cell type. Highest transgene expression was noted in Caco-2 cells compared to the HEK293 and HeLa cells. Untargeted FAuNPs were generally well tolerated in the HEK293 and HeLa cell lines as shown in the MTT cytotoxicity assay, but demonstrated significant cytotoxicity in Caco-2 cells. These cell-specific interactions are important to consider when designing vectors to transfect specific cells or tissues. Furthermore, they may ultimately influence the method of administration of the gene delivery vector, given that Caco-2 is often used to model intestinal cells.

When compared to the unPEGylated AuCS NPs, PEGylation or steric stabilisation was observed to reduce the pDNA binding abilities of the FAuNPs, due to shielding the positive charges on the CS. However, it enhanced the ability of the FAuNPs to condense

and protect pDNA, as shown in the EB intercalation and nuclease protection assays. Despite these advantageous characteristics, PEGylation resulted in measurable decreases in the transfection efficiencies of the FAuNPs compared to the AuCS nanocomplexes. Many different PEGylation techniques have been developed in attempts to overcome the PEG dilemma, and future studies may utilise them to avoid reductions in transfection efficiency. These techniques include the use of PEG bound to NPs via cleavable or acid-labile bonds, which separate from the NP in acidic conditions, or mixed layers of high MW and low MW PEG.

An important parameter that requires optimisation is the grafting density of PEG on the NP surface. Comparison of the two PEGylated FAuNPs (AuCS-2% PEG and AuCS-5% PEG) reveals that they displayed a similar ability to bind, condense, protect, and deliver pDNA. Functionalisation with 5% ($^{\mathrm{w}}/_{\mathrm{w}}$) PEG led to a greater reduction in zeta potential; however, the DNA binding ability of AuCS-5% PEG NPs was not compromised, and they were still capable of fully complexing pDNA. While the AuCS-5% PEG produced significantly higher cell viabilites than AuCS-2% PEG in HeLa cells, it is noteworthy that they displayed significantly higher cytotoxicities in the non-cancerous HEK293 cells. These results suggest that a 2% weight ratio of PEG is an adequate grafting density for the FAuNPs produced in this study, although further studies could be conducted to evaluate the ability of the different grafting densities to prevent serum protein binding, as well as to improve their biodistribution *in vivo*.

Targeting was facilitated by the holoTf protein, binding to the TfR expressed on the BBB. In many cases, the Tf-targeted FAuNPs displayed favourable results compared to their untargeted counterparts. They were capable of condensing pDNA to greater degrees and were able to partially protect pDNA, as evidenced by the AuCSTf FAuNPs. Moreover, they were well tolerated in all cell lines and, in some cases, demonstrated increased cell viability compared to untargeted FAuNPs. The competition binding assay further confirmed uptake of AuCSTf and AuCSTf-5% PEG NPs via RME, demonstrating their potential as gene delivery vectors for the treatment of brain cancers. However, the addition of PEG was observed to inhibit uptake by RME, with the 2% ($^{\mathrm{w}}/_{\mathrm{w}}$) grafting density almost completely abolishing receptor-mediated internalisation. This demonstrates the importance of *in vitro* studies to optimise vector design, especially to determine the factors influencing targeting efficiency. These results suggest that the

AuCSTf NPs are optimal for receptor targeting, as they displayed favourable uptake via RME at the optimal ratio, and, despite the lack of steric stabilisers, were able to protect their payload from complete degradation. To overcome the issues of PEG interfering with receptor binding, future studies may utilise shorter PEG chains, such as PEG_{350} or PEG_{750}, or explore different methods of conjugating the targeting ligand to the PEG chains.

Worldwide, brain cancer is a huge socio-economic burden, as treatments are often expensive and ineffective. The FAuNPs produced in this study were cheaply and easily synthesised, with AuCSTf able to efficiently enter cells by RME. They thus represent a cheaper and safer alternative to conventional treatments for brain cancers, and have the potential to reduce the socio-economic burden and increase the quality of life experienced by cancer patients.

Overall, the FAuNPs synthesised in this study demonstrated their potential as gene delivery vectors, being capable of efficiently complexing pDNA and transfecting cells *in vitro*, with AuCSTf and AuCSTf-5% PEG NPs able to exploit RME to enter cells. These FAuNPs show promise for future use as gene delivery vectors, and, with further optimisation and *in vivo* evaluation, may be used further in preclinical trials.

References

Abbott, N. J. (2013). Blood–brain barrier structure and function and the challenges for CNS drug delivery. *Journal of Inherited Metabolic Disease*, *36*(3), 437–449.

Abuchowski, A., McCoy, J. R., Palczuk, N. C., van Es, T. and Davis, F. F. (1977). Effect of covalent attachment of polyethylene glycol on immunogenicity and circulating life of bovine liver catalase. *The Journal of Biological Chemistry*, *252*(11), 3582–3586.

Akinc, A. and Battaglia, G. (2013). Exploiting Endocytosis for Nanomedicines. *Cold Spring Harbor Perspectives in Biology*, *5*(11), a016980.

Akinc, A., Thomas, M., Klibanov, A. M. and Langer, R. (2005). Exploring polyethylenimine-mediated DNA transfection and the proton sponge hypothesis. *The Journal of Gene Medicine*, *7*(5), 657–663.

Akinyelu, J. and Singh, M. (2018). Chitosan Stabilized Gold-Folate-Poly(lactide-co-glycolide) Nanoplexes Facilitate Efficient Gene Delivery in Hepatic and Breast Cancer Cells. *Journal of Nanoscience and Nanotechnology*, *18*(7), 4478–4486.

Akiyama, Y., Mori, T., Katayama, Y. and Niidome, T. (2009). The effects of PEG grafting level and injection dose on gold nanorod biodistribution in the tumor-bearing mice. *Journal of Controlled Release*, *139*(1), 81–84.

Alsaggar, M. and Liu, D. (2015). Physical Methods for Gene Transfer. In L. Huang, D. Liu and E. Wagner (Eds.), *Nonviral Vectors for Gene Therapy* (Vol. 89, pp. 1–24). Academic Press.

Alyautdin, R., Khalin, I., Nafeeza, M. I., Haron, M. H. and Kuznetsov, D. (2014). Nanoscale drug delivery systems and the blood-brain barrier. *International Journal of Nanomedicine*, *9*(1), 795–811.

Armulik, A., Genove, G., Mae, M., Nisancioglu, M. H., Wallgard, E., Niaudet, C., … Betsholtz, C. (2010). Pericytes regulate the blood-brain barrier. *Nature*, *468*(7323), 557–561.

Artusi, S., Miyagawa, Y., Goins, W., Cohen, J., Glorioso, J., Artusi, S., … Glorioso, J. C. (2018). Herpes Simplex Virus Vectors for Gene Transfer to the Central Nervous System. *Diseases*, *6*(3), 74.

Aryal, M., Vykhodtseva, N., Zhang, Y.-Z., Park, J. and McDannold, N. (2013). Multiple treatments with liposomal doxorubicin and ultrasound-induced disruption of blood–tumor and blood–brain barriers improve outcomes in a rat glioma model. *Journal of Controlled Release*, *169*(1–2), 103–111.

Asadi-Moghaddam, K. and Chiocca, E. A. (2009). Gene- and viral-based therapies for brain tumors. Neurotherapeutics: *The Journal of the American Society for Experimental NeuroTherapeutics*, *6*(3), 547–557.

Bahuguna, A., Khan, I., Bajpai, V. K. and Kang, S. C. (2017). MTT assay to evaluate the cytotoxic potential of a drug. *Bangladesh Journal of Pharmacology*, *12*(2), 115–118.

Banks, W. A. (2016). From blood–brain barrier to blood–brain interface: new opportunities for CNS drug delivery. *Nature Reviews Drug Discovery*, *15*(4), 275–292.

Barar, J., Rafi, M. A., Pourseif, M. M. and Omidi, Y. (2016). Blood-brain barrier transport machineries and targeted therapy of brain diseases. *BioImpacts: BI*, *6*(4), 225–248.

Behr, J.-P. (1997). The Proton Sponge: a Trick to Enter Cells the Viruses Did Not Exploit. *CHIMIA International Journal for Chemistry*, *51*(1–2), 34–36.

Behzadi, S., Serpooshan, V., Tao, W., Hamaly, M. A., Alkawareek, M. Y., Dreaden, E. C., … Mahmoudi, M. (2017). Cellular uptake of nanoparticles: journey inside the cell. *Chemical Society Reviews*, *46*(14), 4218–4244.

Benjaminsen, R. V, Mattebjerg, M. A., Henriksen, J. R., Moghimi, S. M. and Andresen, T. L. (2013). The Possible "Proton Sponge " Effect of Polyethylenimine (PEI) Does Not Include Change in Lysosomal pH. *Molecular Therapy*, *21*(1), 149–157.

Bewersdorff, T., Vonnemann, J., Kanik, A., Haag, R. and Haase, A. (2017). The influence of surface charge on serum protein interaction and cellular uptake: studies with dendritic polyglycerols and dendritic polyglycerol-coated gold nanoparticles. *International Journal of Nanomedicine*, *12*, 2001–2019.

Bhatia, S. (2016). Nanoparticles Types, Classification, Characterization, Fabrication Methods and Drug Delivery Applications. In *Natural Polymer Drug Delivery Systems* (pp. 33–93). Cham: Springer International Publishing.

Bhattacharjee, S. (2016). DLS and zeta potential – What they are and what they are not? *Journal of Controlled Release*, *235*, 337–351.

Bicker, J., Alves, G., Fortuna, A. and Falcão, A. (2014). Blood–brain barrier models and their relevance for a successful development of CNS drug delivery systems: A review. *European Journal of Pharmaceutics and Biopharmaceutics*, *87*(3), 409–432.

Bien-Ly, N., Yu, Y. J., Bumbaca, D., Elstrott, J., Boswell, C. A., Zhang, Y., … Watts, R. J. (2014). Transferrin receptor (TfR) trafficking determines brain uptake of TfR antibody affinity variants. *The Journal of Experimental Medicine*, *211*(2), 233–244.

Bitsikas, V., Corrêa, I. R. and Nichols, B. J. (2014). Clathrin-independent pathways do not contribute significantly to endocytic flux. *ELife*, *3*, e03970.

Blanco, E., Shen, H. and Ferrari, M. (2015). Principles of nanoparticle design for overcoming biological barriers to drug delivery. *Nature Biotechnology*, *33*(9), 941–951.

Blattman, J. N. and Greenberg, P. D. (2004). Cancer immunotherapy: a treatment for the masses. *Science*, *305*(5681), 200–205.

Bleil, J. D. and Bretscher, M. S. (1982). Transferrin receptor and its recycling in HeLa cells. *The EMBO Journal*, *1*(3), 351–355.

Boca, S. C., Potara, M., Toderas, F., Stephan, O., Baldeck, P. L. and Astilean, S. (2011). Uptake and biological effects of chitosan-capped gold nanoparticles on Chinese Hamster Ovary cells. *Materials Science and Engineering: C*, *31*(2), 184–189.

Bolhassani, A. and Saleh, T. (2013). Challenges in Advancing the Field of Cancer Gene Therapy: An Overview of the Multi-Functional Nanocarriers. In W. Ming and D. Good (Eds.), *Novel Gene Therapy Approaches* (pp. 197–259).

Bonakdar, M., Wasson, E. M., Lee, Y. W. and Davalos, R. V. (2016). Electroporation of Brain Endothelial Cells on Chip toward Permeabilizing the Blood-Brain Barrier. *Biophysical Journal*, *110*(2), 503–513.

Bonifacino, J. S. and Rojas, R. (2006). Retrograde transport from endosomes to the trans-Golgi network. *Nature Reviews Molecular Cell Biology*, *7*(8), 568–579.

Boyles, M. S. P., Kristl, T., Andosch, A., Zimmermann, M., Tran, N., Casals, E., … Duschl, A. (2015). Chitosan functionalisation of gold nanoparticles encourages particle uptake and induces cytotoxicity and pro-inflammatory conditions in phagocytic cells, as well as enhancing particle interactions with serum components. Journal of *Nanobiotechnology*, *13*(1), 84–103.

Bray, F., Ferlay, J., Soerjomataram, I., Siegel, R. L., Torre, L. A. and Jemal, A. (2018). Global cancer statistics 2018: GLOBOCAN estimates of incidence and mortality worldwide for 36 cancers in 185 countries. *CA: A Cancer Journal for Clinicians*, *68*(6), 394–424.

Brown, C. E., Alizadeh, D., Starr, R., Weng, L., Wagner, J. R., Naranjo, A., … Badie, B. (2016). Regression of Glioblastoma after Chimeric Antigen Receptor T-Cell Therapy. *New England Journal of Medicine*, *375*(26), 2561–2569.

Brust, M., Walker, M., Bethell, D., Schiffrin, D. J. and Whyman, R. (1994). Synthesis of thiol-derivatised gold nanoparticles in a two-phase Liquid–Liquid system. *Journal of the Chemical Society, Chemical Communications*, *0*(7), 801–802.

Burdo, J. R., Antonetti, D. A., Wolpert, E. B. and Connor, J. R. (2003). Mechanisms and regulation of transferrin and iron transport in a model blood–brain barrier system. *Neuroscience*, *121*(4), 883–890.

Cai, C., Wang, M., Wang, X., Wang, B., Chen, H., Chen, J., … Feng, W. (2018). Transferrin Adsorbed on PEGylated Gold Nanoparticles and Its Relevance to Targeting Specificity. *Journal of Nanoscience and Nanotechnology*, *18*(8), 5306–5313.

Canton, I. and Battaglia, G. (2012). Endocytosis at the nanoscale. *Chemical Society Reviews*, *41*(7), 2718–2739.

Cebrián, V., Martín-Saavedra, F., Yagüe, C., Arruebo, M., Santamaría, J. and Vilaboa, N. (2011). Size-dependent transfection efficiency of PEI-coated gold nanoparticles. *Acta Biomaterialia*, *7*(10), 3645–3655.

Chan, C.-L., Majzoub, R. N., Shirazi, R. S., Ewert, K. K., Chen, Y.-J., Liang, K. S. and Safinya, C. R. (2012). Endosomal escape and transfection efficiency of PEGylated

cationic liposome-DNA complexes prepared with an acid-labile PEG-lipid. *Biomaterials*, *33*(19), 4928–4935.

Chan, K. T., Choi, M. Y., Lai, K. K. Y., Tan, W., Tung, L. N., Lam, H. Y., … Law, S. (2014). Overexpression of transferrin receptor CD71 and its tumorigenic properties in esophageal squamous cell carcinoma. *Oncology Reports*, *31*(3), 1296–1304.

Chandran, P., Riviere, J. E. and Monteiro-Riviere, N. A. (2017). Surface chemistry of gold nanoparticles determines the biocorona composition impacting cellular uptake, toxicity and gene expression profiles in human endothelial cells. *Nanotoxicology*, *11*(4), 507–519.

Chen, N., Song, Z.-M., Tang, H., Xi, W.-S., Cao, A., Liu, Y. and Wang, H. (2016). Toxicological Effects of Caco-2 Cells Following Short-Term and Long-Term Exposure to Ag Nanoparticles. *International Journal of Molecular Sciences*, *17*(6), 974–990.

Chen, Y.-S., Hung, Y.-C., Liau, I. and Huang, G. S. (2009). Assessment of the In Vivo Toxicity of Gold Nanoparticles. *Nanoscale Research Letters*, *4*(8), 858–864.

Chen, Y. and Liu, L. (2012). Modern methods for delivery of drugs across the blood-brain barrier. *Advanced Drug Delivery Reviews*, *64*(7), 640–665.

Chen, Y., Sun, J., Lu, Y., Tao, C., Huang, J., Zhang, H., … Zhong, Y. (2013). Complexes containing cationic and anionic pH-sensitive liposomes: comparative study of factors influencing plasmid DNA gene delivery to tumors. International Journal of *Nanomedicine*, *8*, 1573–1593.

Cheng, C., Jia, J. L. and Ran, S. Y. (2015). Polyethylene glycol and divalent salt-induced DNA reentrant condensation revealed by single molecule measurements. *Soft Matter*, *11*(19), 3927–3935.

Cheng, Y., Zak, O., Aisen, P., Harrison, S. C. and Walz, T. (2004). Structure of the human transferrin receptor-transferrin complex. *Cell*, *116*(4), 565–576.

Chhabra, R., Tosi, G. and Grabrucker, A. (2015). Emerging Use of Nanotechnology in the Treatment of Neurological Disorders. *Current Pharmaceutical Design*, *21*(22), 3111–3130.

Chib, R., Raut, S., Sabnis, S., Singhal, P., Gryczynski, Z. and Gryczynski, I. (2014). Associated Anisotropy Decays of Ethidium Bromide Interacting with DNA. Methods and *Applications in Fluorescence*, *2*(1), 015003.

Chira, S., Jackson, C. S., Oprea, I., Ozturk, F., Pepper, M. S., Diaconu, I., … Berindan-Neagoe, I. (2015). Progresses towards safe and efficient gene therapy vectors. *Oncotarget*, *6*(31), 30675–30703.

Chithrani, B. D., Ghazani, A. A. and Chan, W. C. W. (2006). Determining the Size and Shape Dependence of Gold Nanoparticle Uptake into Mammalian Cells. *Nano Letters*, *6*(4), 662–668.

Cho, W.-S., Cho, M., Jeong, J., Choi, M., Cho, H.-Y., Han, B. S., ... Jeong, J. (2009). Acute toxicity and pharmacokinetics of 13 nm-sized PEG-coated gold nanoparticles. *Toxicology and Applied Pharmacology*, *236*(1), 16–24.

Chou, L. Y. T., Ming, K. and Chan, W. C. W. (2011). Strategies for the intracellular delivery of nanoparticles. *Chemical Society Reviews*, *40*(1), 233–245.

Choudhury, H., Pandey, M., Chin, P. X., Phang, Y. L., Cheah, J. Y., Ooi, S. C., ... Gorain, B. (2018). Transferrin receptors-targeting nanocarriers for efficient targeted delivery and transcytosis of drugs into the brain tumors: a review of recent advancements and emerging trends. *Drug Delivery and Translational Research*, *8*(5), 1545–1563.

Choudhury, S. R., Hudry, E., Maguire, C. A., Sena-Esteves, M., Breakefield, X. O. and Grandi, P. (2017). Viral vectors for therapy of neurologic diseases. Neuropharmacology, *120*, 63–80.

Chow, B. W. and Gu, C. (2015). The molecular constituents of the blood-brain barrier. *Trends in Neurosciences*, *38*(10), 598–608.

Clark, A. J. and Davis, M. E. (2015). Increased brain uptake of targeted nanoparticles by adding an acid-cleavable linkage between transferrin and the nanoparticle core. *Proceedings of the National Academy of Sciences of the United States of America*, *112*(40), 12486–12491.

Colombo, M., Fiandra, L., Alessio, G., Mazzucchelli, S., Nebuloni, M., De Palma, C., ... Prosperi, D. (2016). Tumour homing and therapeutic effect of colloidal nanoparticles depend on the number of attached antibodies. Nature *Communications*, *7*, 13818.

Cross, D. and Burmester, J. K. (2006). Gene Therapy for Cancer Treatment: Past, Present and Future. *Clinical Medicine & Research*, *4*(3), 1–10.

Cwetsch, A. W., Pinto, B., Savardi, A. and Cancedda, L. (2018). In vivo methods for acute modulation of gene expression in the central nervous system. *Progress in Neurobiology*, *168*, 69–85.

Daneman, R. and Prat, A. (2015). The blood-brain barrier. *Cold Spring Harbor Perspectives in Biology*, *7*(1), a020412.

Danhier, F., Feron, O. and Préat, V. (2010). To exploit the tumor microenvironment: Passive and active tumor targeting of nanocarriers for anti-cancer drug delivery. *Journal of Controlled Release*, *148*(2), 135–146.

Daniel, M.-C. and Astruc, D. (2004). Gold nanoparticles: assembly, supramolecular chemistry, quantum-size-related properties, and applications toward biology, catalysis, and nanotechnology. *Chemical Reviews*, *104*(1), 293–346.

Daniel, M.-C., Grow, M. E., Pan, H., Bednarek, M., Ghann, W. E., Zabetakis, K. and Cornish, J. (2011). Gold nanoparticle-cored poly(propyleneimine) dendrimers as a new platform for multifunctional drug delivery systems. *New Journal of Chemistry*, *35*(10), 2366–2374.

Daniels, A., Noor-Mahomed, N., Singh, M. and Ariatti, M. (2011). Cytofectin amine head group modification and degree of liposome pegylation: factors influencing gene transfer. *Indian Journal of Pharmaceutical Sciences*, *73*(4), 381–386.

Daniels, T. R., Bernabeu, E., Rodríguez, J. A., Patel, S., Kozman, M., Chiappetta, D. A., … Penichet, M. L. (2012). The transferrin receptor and the targeted delivery of therapeutic agents against cancer. *Biochimica et Biophysica Acta (BBA) - General Subjects*, *1820*(3), 291–317.

De Bock, M., Van Haver, V., Vandenbroucke, R. E., Decrock, E., Wang, N. and Leybaert, L. (2016). Into rather unexplored terrain-transcellular transport across the blood-brain barrier. *Glia*, *64*(7), 1097–1123.

De Jong, W. H., Hagens, W. I., Krystek, P., Burger, M. C., Sips, A. J. A. M. and Geertsma, R. E. (2008). Particle size-dependent organ distribution of gold nanoparticles after intravenous administration. *Biomaterials*, *29*(12), 1912–1919.

de Lima, M., Neves, S., Filipe, A., Duzgunes, N. and Simoes, S. (2003). Cationic Liposomes for Gene Delivery: From Biophysics to Biological Applications. *Current Medicinal Chemistry*, *10*(14), 1221–1231.

De Matteis, L., Alleva, M., Serrano-Sevilla, I., García-Embid, S., Stepien, G., Moros, M. and De La Fuente, J. M. (2016). Controlling properties and cytotoxicity of chitosan nanocapsules by chemical grafting. *Marine Drugs*, *14*(10), 175–189.

De Vry, J., Martínez-Martínez, P., Losen, M., Bode, G. H., Temel, Y., Steckler, T., … Prickaerts, J. (2010a). Low Current-driven Micro-electroporation Allows Efficient In Vivo Delivery of Nonviral DNA into the Adult Mouse Brain. *Molecular Therapy*, *18*(6), 1183–1191.

De Vry, J., Martínez-Martínez, P., Losen, M., Temel, Y., Steckler, T., Steinbusch, H. W. M., … Prickaerts, J. (2010b). In vivo electroporation of the central nervous system: A non-viral approach for targeted gene delivery. *Progress in Neurobiology*, *92*(3), 227–244.

de Wet, J. R., Wood, K. V, DeLuca, M., Helinski, D. R. and Subramani, S. (1987). Firefly luciferase gene: structure and expression in mammalian cells. *Molecular and Cellular Biology*, *7*(2), 725–737.

Deng, Z. J., Liang, M., Toth, I., Monteiro, M. and Minchin, R. F. (2012). Plasma protein binding of positively and negatively charged polymer-coated gold nanoparticles elicits different biological responses. *Nanotoxicology*, *7*(3), 314–322.

Descamps, L., Dehouck, M. P., Torpier, G. and Cecchelli, R. (1996). Receptor-mediated transcytosis of transferrin through blood-brain barrier endothelial cells. *American Journal of Physiology-Heart and Circulatory Physiology*, *270*(4), H1149–H1158.

Ding, Y., Jiang, Z., Saha, K., Kim, C. S., Kim, S. T., Landis, R. F. and Rotello, V. M. (2014a). Gold Nanoparticles for Nucleic Acid Delivery. *Molecular Therapy*, *22*(6), 1075–1083.

Ding, Y., Liang, J.-J., Geng, D.-D., Wu, D., Dong, L., Shen, W.-B., … Zhang, C. (2014b). Development of a Liver-Targeting Gold-PEG-Galactose Nanoparticle Platform and a Structure-Function Study. *Particle & Particle Systems Characterization*, *31*(3), 347–356.

Dixit, S., Novak, T., Miller, K., Zhu, Y., Kenney, M. E. and Broome, A.-M. (2015). Transferrin receptor-targeted theranostic gold nanoparticles for photosensitizer delivery in brain tumors. *Nanoscale*, *7*(5), 1782–1790.

Domínguez, A., Álvarez, A., Hilario, E., Suarez-Merino, B. and Goñi-de-Cerio, F. (2013). Central nervous system diseases and the role of the blood-brain barrier in their treatment. *Neuroscience Discovery*, *1*(1), 3–13.

Dong, X. (2018). Current Strategies for Brain Drug Delivery. *Theranostics*, *8*(6), 1481–1493.

Dreaden, E. C., Alkilany, A. M., Huang, X., Murphy, C. J. and El-Sayed, M. A. (2012). The golden age: gold nanoparticles for biomedicine. *Chemical Society Reviews*, *41*(7), 2740–2779.

Duck, K. A., Simpson, I. A. and Connor, J. R. (2017). Regulatory mechanisms for iron transport across the blood-brain barrier. *Biochemical and Biophysical Research Communications*, *494*(1–2), 70–75.

Dykman, L. A. and Khlebtsov, N. G. (2011). Gold nanoparticles in biology and medicine: recent advances and prospects. *Acta Naturae*, *3*(2), 34–55.

Eckenroth, B. E., Steere, A. N., Chasteen, N. D., Everse, S. J. and Mason, A. B. (2011). How the binding of human transferrin primes the transferrin receptor potentiating iron release at endosomal pH. *Proceedings of the National Academy of Sciences of the United States of America*, *108*(32), 13089–13094.

El Hage Chahine, J.-M., Hémadi, M. and Ha-Duong, N.-T. (2012). Uptake and release of metal ions by transferrin and interaction with receptor 1. *Biochimica et Biophysica Acta (BBA) - General Subjects*, *1820*(3), 334–347.

Elahi, N., Kamali, M. and Baghersad, M. H. (2018). Recent biomedical applications of gold nanoparticles: A review. *Talanta*, *184*, 537–556.

Elkin, S. R., Lakoduk, A. M. and Schmid, S. L. (2016). Endocytic pathways and endosomal trafficking: a primer. *Wiener Medizinische Wochenschrift*, *166*(7–8), 196–204.

Escors, D. and Breckpot, K. (2010). Lentiviral vectors in gene therapy: their current status and future potential. *Archivum Immunologiae et Therapiae Experimentalis*, *58*(2), 107–119.

Fan, F. and Wood, K. V. (2007). Bioluminescent Assays for High-Throughput Screening. *Assay and Drug Development Technologies*, *5*(1), 127–136.

Fan, J. H., Hung, W. I., Li, W. T. and Yeh, J. M. (2009). Biocompatibility Study of Gold Nanoparticles to Human Cells. In J. C. H. Goh and C. T. Lim (Eds.), *13th International Conference on Biomedical Engineering* (pp. 870–873). Springer Berlin Heidelberg.

Fang, Y., Xue, J., Gao, S., Lu, A., Yang, D., Jiang, H., … Shi, K. (2017). Cleavable PEGylation: a strategy for overcoming the "PEG dilemma" in efficient drug delivery. *Drug Delivery*, *24*(2), 22–32.

Farkas, J., Christian, P., Urrea, J. A. G., Roos, N., Hassellöv, M., Tollefsen, K. E. and Thomas, K. V. (2010). Effects of silver and gold nanoparticles on rainbow trout (Oncorhynchus mykiss) hepatocytes. *Aquatic Toxicology*, *96*(1), 44–52.

Faulk, W. P. and Taylor, G. M. (1971). An immunocolloid method for the electron microscope. *Immunochemistry*, *8*(11), 1081–1083.

Fesnak, A. D., June, C. H. and Levine, B. L. (2016). Engineered T cells: the promise and challenges of cancer immunotherapy. *Nature Reviews Cancer*, *16*(9), 566–581.

Fioretti, D., Iurescia, S., Fazio, V. M. and Rinaldi, M. (2010). DNA vaccines: developing new strategies against cancer. *Journal of Biomedicine & Biotechnology*, *2010*, 174378.

Forest, V. and Pourchez, J. (2017). Preferential binding of positive nanoparticles on cell membranes is due to electrostatic interactions: A too simplistic explanation that does not take into account the nanoparticle protein corona. *Materials Science and Engineering: C*, *70*, 889–896.

Forrest, M. L. and Pack, D. W. (2002). On the Kinetics of Polyplex Endocytic Trafficking: Implications for Gene Delivery Vector Design. *Molecular Therapy*, *6*(1), 57–66.

Fotakis, G. and Timbrell, J. A. (2006). In vitro cytotoxicity assays: Comparison of LDH, neutral red, MTT and protein assay in hepatoma cell lines following exposure to cadmium chloride. *Toxicology Letters*, *160*(2), 171–177.

Frens, G. (1973). Controlled Nucleation for the Regulation of the Particle Size in Monodisperse Gold Suspensions. *Nature Physical Science*, *241*(105), 20–22.

Froehlich, E., Mandeville, J. S., Arnold, D., Kreplak, L. and Tajmir-Riahi, H. A. (2011). PEG and mPEG-anthracene induce DNA condensation and particle formation. *Journal of Physical Chemistry B*, *115*(32), 9873–9879.

Fröhlich, E. (2012). The role of surface charge in cellular uptake and cytotoxicity of medical nanoparticles. *International Journal of Nanomedicine*, *7*, 5577–5591.

Fullstone, G., Nyberg, S., Tian, X. and Battaglia, G. (2016). From the Blood to the Central Nervous System: A Nanoparticle's Journey Through the Blood–Brain Barrier by Transcytosis. In K. T. Al-Jamal (Ed.), *International Review of Neurobiology* (Vol. 130, pp. 41–72). Academic Press.

Furtado, D., Björnmalm, M., Ayton, S., Bush, A. I., Kempe, K. and Caruso, F. (2018). Overcoming the Blood-Brain Barrier: The Role of Nanomaterials in Treating Neurological Diseases. *Advanced Materials*, *30*(46), 1801362.

Gallego, O. (2015). Nonsurgical treatment of recurrent glioblastoma. *Current Oncology*, *22*(4), e273-281.

Gammella, E., Buratti, P., Cairo, G. and Recalcati, S. (2017). The transferrin receptor: the cellular iron gate. *Metallomics*, *9*(10), 1367–1375.

Ginn, S. L., Amaya, A. K., Alexander, I. E., Edelstein, M. and Abedi, M. R. (2018). Gene therapy clinical trials worldwide to 2017: An update. *The Journal of Gene Medicine*, *20*(5), e3015.

Gjetting, T., Arildsen, N. S., Christensen, C. L., Poulsen, T. T., Roth, J. A., Handlos, V. N. and Poulsen, H. S. (2010). In vitro and in vivo effects of polyethylene glycol (PEG)-modified lipid in DOTAP/cholesterol-mediated gene transfection. *International Journal of Nanomedicine*, *5*(1), 371–383.

Grabrucker, A. M., Chhabra, R., Belletti, D., Forni, F., Vandelli, M. A., Ruozi, B. and Tosi, G. (2014). Nanoparticles as Blood--Brain Barrier Permeable CNS Targeted Drug Delivery Systems. In G. Fricker, M. Ott and A. Mahringer (Eds.), *The Blood Brain Barrier (BBB)* (pp. 71–89). Springer Berlin Heidelberg.

Grant, B. D. and Donaldson, J. G. (2009). Pathways and mechanisms of endocytic recycling. *Nature Reviews Molecular Cell Biology*, *10*(9), 597–608.

Gref, R., Lück, M., Quellec, P., Marchand, M., Dellacherie, E., Harnisch, S., … Müller, R. . (2000). 'Stealth' corona-core nanoparticles surface modified by polyethylene glycol (PEG): influences of the corona (PEG chain length and surface density) and of the core composition on phagocytic uptake and plasma protein adsorption. *Colloids and Surfaces B: Biointerfaces*, *18*(3–4), 301–313.

Habashy, H. O., Powe, D. G., Staka, C. M., Rakha, E. A., Ball, G., Green, A. R., … Gee, J. M. W. (2010). Transferrin receptor (CD71) is a marker of poor prognosis in breast cancer and can predict response to tamoxifen. *Breast Cancer Research and Treatment*, *119*(2), 283–293.

Hacein-Bey-Abina, S., Von Kalle, C., Schmidt, M., McCormack, M. P., Wulffraat, N., Leboulch, P., … Cavazzana-Calvo, M. (2003). LMO2-Associated Clonal T Cell Proliferation in Two Patients after Gene Therapy for SCID-X1. *Science*, *302*(5644), 415–419.

Hak, S., Helgesen, E., Hektoen, H. H., Huuse, E. M., Jarzyna, P. A., Mulder, W. J. M., … Davies, C. de L. (2012). The effect of nanoparticle polyethylene glycol surface density on ligand-directed tumor targeting studied in vivo by dual modality imaging. *ACS Nano*, *6*(6), 5648–5658.

Halabalová, V. and Šimek, L. (2006). A Study of the Interaction between Chitosan and Poly(Ethylene Glycol) by Viscosity Method. *International Journal of Polymer Analysis and Characterization*, *11*(3), 185–195.

Hall, J. B., Dobrovolskaia, M. A., Patri, A. K. and McNeil, S. E. (2007). Characterization of nanoparticles for therapeutics. *Nanomedicine*, *2*(6), 789–803.

Han, G., Martin, C. T. and Rotello, V. M. (2006). Stability of Gold Nanoparticle-Bound DNA toward Biological, Physical, and Chemical Agents. *Chemical Biology & Drug Design*, *67*(1), 78–82.

Hanahan, D. and Weinberg, R. A. (2011). Hallmarks of Cancer: The Next Generation. *Cell*, *144*(5), 646–674.

Hansen, M., Smith, M. C., Crist, R. M., Clogston, J. D. and McNeil, S. E. (2015). Analyzing the influence of PEG molecular weight on the separation of PEGylated gold nanoparticles by asymmetric-flow field-flow fractionation. *Analytical and Bioanalytical Chemistry*, *407*(29), 8661–8672.

Hardee, C. L., Arévalo-Soliz, L. M., Hornstein, B. D. and Zechiedrich, L. (2017). Advances in Non-Viral DNA Vectors for Gene Therapy. *Genes*, *8*(2), 65–86.

Hatakeyama, H., Akita, H. and Harashima, H. (2013). The polyethyleneglycol dilemma: advantage and disadvantage of PEGylation of liposomes for systemic genes and nucleic acids delivery to tumors. *Biological & Pharmaceutical Bulletin*, *36*(6), 892–899.

Helander, A. and Beck, O. (2008). Analytical markers of acute and chronic alcohol consumption. In M.J. Bogusz (Ed.), *Handbook of Analytical Separations* (Vol. 6, pp. 567–588). Elsevier Science B.V.

Herizchi, R., Abbasi, E., Milani, M. and Akbarzadeh, A. (2016). Current methods for synthesis of gold nanoparticles. *Artificial Cells, Nanomedicine, and Biotechnology*, *44*(2), 596–602.

Herschman, H. R. (2004). Noninvasive imaging of reporter gene expression in living subjects. *Advances in Cancer Research*, *92*, 29–80.

Hillyer, J. F. and Albrecht, R. M. (2001). Gastrointestinal persorption and tissue distribution of differently sized colloidal gold nanoparticles. *Journal of Pharmaceutical Sciences*, *90*(12), 1927–1936.

Hopkins, C. R. and Trowbridge, I. S. (1983). Internalization and processing of transferrin and the transferrin receptor in human carcinoma A431 cells. *The Journal of Cell Biology*, *97*(2), 508–521.

Hoy, M. A. (2013). Some Basic Tools: How to Cut, Paste, Copy, Measure, Visualize, and Clone DNA. In M. A. Hoy (Ed.), *Insect Molecular Genetics* (3rd ed., pp. 183–214). Academic Press.

Huang, M., Khor, E. and Lim, L.-Y. (2004). Uptake and Cytotoxicity of Chitosan Molecules and Nanoparticles: Effects of Molecular Weight and Degree of Deacetylation. *Pharmaceutical Research*, *21*(2), 344–353.

Huang, R.-Q., Qu, Y.-H., Ke, W.-L., Zhu, J.-H., Pei, Y.-Y. and Jiang, C. (2007). Efficient gene delivery targeted to the brain using a transferrin-conjugated polyethyleneglycol-modified polyamidoamine dendrimer. *The FASEB Journal*, *21*(4), 1117–1125.

Huang, X. and El-Sayed, M. A. (2010). Gold nanoparticles: Optical properties and implementations in cancer diagnosis and photothermal therapy. *Journal of Advanced Research*, *1*(1), 13–28.

Hulou, M. M., Cho, C.-F., Chiocca, E. A. and Bjerkvig, R. (2016). Experimental therapies: gene therapies and oncolytic viruses. In *Handbook of Clinical Neurology* (Vol. 134, pp. 183–197).

Ibraheem, D., Elaissari, A. and Fessi, H. (2014). Gene therapy and DNA delivery systems. *International Journal of Pharmaceutics*, *459*(1–2), 70–83.

Immordino, M. L., Dosio, F. and Cattel, L. (2006). Stealth liposomes: review of the basic science, rationale, and clinical applications, existing and potential. *International Journal of Nanomedicine*, *1*(3), 297–315.

Ivanov, M. R., Bednar, H. R. and Haes, A. J. (2009). Investigations of the mechanism of gold nanoparticle stability and surface functionalization in capillary electrophoresis. *ACS Nano*, *3*(2), 386–394.

James, A. E. and Driskell, J. D. (2013). Monitoring gold nanoparticle conjugation and analysis of biomolecular binding with nanoparticle tracking analysis (NTA) and dynamic light scattering (DLS). *The Analyst*, *138*(4), 1212–1218.

Jayant, R. D., Sosa, D., Kaushik, A., Atluri, V., Vashist, A., Tomitaka, A. and Nair, M. (2016). Current status of non-viral gene therapy for CNS disorders. *Expert Opinion on Drug Delivery, 13*(10), 1433–1445.

Jefferies, W. A., Brandon, M. R., Hunt, S. V., Williams, A. F., Gatter, K. C. and Mason, D. Y. (1984). Transferrin receptor on endothelium of brain capillaries. *Nature*, *312*(5990), 162–163.

Ji, X., Song, X., Li, J., Bai, Y., Yang, W. and Peng, X. (2007). Size Control of Gold Nanocrystals in Citrate Reduction: The Third Role of Citrate. *Journal of the American Chemical Society*, *129*(45), 13939–13948.

Ji, Z., Jin, X., George, S., Xia, T., Meng, H., Wang, X., … Zink, J. I. (2010). Dispersion and Stability Optimization of TiO 2 Nanoparticles in Cell Culture Media. *Environmental Science & Technology*, *44*(19), 7309–7314.

Jiang, W. H. and Han, S. J. (1998). Study of interaction between polyethylene glycol and chitosan by viscosity method. *Journal of Polymer Science Part B: Polymer Physics*, *36*(8), 1275–1281.

Jiang, X., Dai, H., Leong, K. W., Goh, S.-H., Mao, H.-Q. and Yang, Y.-Y. (2006). Chitosan-g-PEG/DNA complexes deliver gene to the rat liver via intrabiliary and intraportal infusions. *The Journal of Gene Medicine*, *8*(4), 477–487.

Johannes, L. and Popoff, V. (2008). Tracing the Retrograde Route in Protein Trafficking. *Cell*, *135*(7), 1175–1187.

Johnsen, K. B., Bak, M., Kempen, P. J., Melander, F., Burkhart, A., Thomsen, M. S., … Andresen, T. L. (2018). Antibody affinity and valency impact brain uptake of transferrin receptor-targeted gold nanoparticles. *Theranostics*, *8*(12), 3416–3436.

Johnsen, K. B. and Moos, T. (2016). Revisiting nanoparticle technology for blood–brain barrier transport: Unfolding at the endothelial gate improves the fate of transferrin receptor-targeted liposomes. *Journal of Controlled Release*, *222*, 32–46.

Jokerst, J. V, Lobovkina, T., Zare, R. N. and Gambhir, S. S. (2011). Nanoparticle PEGylation for imaging and therapy. *Nanomedicine*, *6*(4), 715–728.

Jones, A. R. and Shusta, E. V. (2007). Blood-brain barrier transport of therapeutics via receptor-mediation. *Pharmaceutical Research*, *24*(9), 1759–1771.

Joshi, C. R., Raghavan, V., Vijayaraghavalu, S., Gao, Y., Saraswathy, M., Labhasetwar, V. and Ghorpade, A. (2018). Reaching for the Stars in the Brain: Polymer-Mediated Gene Delivery to Human Astrocytes. *Molecular Therapy - Nucleic Acids*, *12*, 645–657.

Joshi, S., Singh-Moon, R., Wang, M., Chaudhuri, D. B., Ellis, J. A., Bruce, J. N., … Straubinger, R. M. (2014). Cationic surface charge enhances early regional deposition of liposomes after intracarotid injection. *Journal of Neuro-Oncology*, *120*(3), 489–497.

Kafil, V. and Omidi, Y. (2011). Cytotoxic Impacts of Linear and Branched Polyethylenimine Nanostructures in A431 Cells. *BioImpacts: BI*, *1*(1), 23–30.

Kaksonen, M. and Roux, A. (2018). Mechanisms of clathrin-mediated endocytosis. *Nature Reviews Molecular Cell Biology*, *19*(5), 313–326.

Karakoti, A. S., Das, S., Thevuthasan, S. and Seal, S. (2011). PEGylated Inorganic Nanoparticles. *Angewandte Chemie International Edition*, *50*(9), 1980–1994.

Karjoo, Z., Chen, X. and Hatefi, A. (2016). Progress and problems with the use of suicide genes for targeted cancer therapy. *Advanced Drug Delivery Reviews*, *99*(Pt A), 113–128.

Kasibhatla, S., Amarante-Mendes, G. P., Finucane, D., Brunner, T., Bossy-Wetzel, E. and Green, D. R. (2006). Acridine Orange/Ethidium Bromide (AO/EB) Staining to Detect Apoptosis. *CSH Protocols*, *2006*(3), pdb.prot4493.

Kawabata, H. (2018). Transferrin and transferrin receptors update. Free Radical Biology and Medicine. https://doi.org/10.1016/j.freeradbiomed.2018.06.037

Kawabata, H., Tong, X., Kawanami, T., Wano, Y., Hirose, Y., Sugai, S. and Phillip Koeffler, H. (2004). Analyses for binding of the transferrin family of proteins to the transferrin receptor 2. *British Journal of Haematology*, *127*(4), 464–473.

Kawabata, H., Yang, R., Hirama, T., Vuong, P. T., Kawano, S., Gombart, A. F. and Koeffler, H. P. (1999). Molecular cloning of transferrin receptor 2. A new member of the transferrin receptor-like family. *The Journal of Biological Chemistry*, *274*(30), 20826–20832.

Kawano, T., Yamagata, M., Takahashi, H., Niidome, Y., Yamada, S., Katayama, Y. and Niidome, T. (2006). Stabilizing of plasmid DNA in vivo by PEG-modified cationic gold nanoparticles and the gene expression assisted with electrical pulses. *Journal of Controlled Release*, *111*(3), 382–389.

Khan, A. I., Liu, J. and Dutta, P. (2018). Iron transport kinetics through blood-brain barrier endothelial cells. *Biochimica et Biophysica Acta (BBA) - General Subjects*, *1862*(5), 1168–1179.

Khlebtsov, N. and Dykman, L. (2011). Biodistribution and toxicity of engineered gold nanoparticles: a review of in vitro and in vivo studies. *Chemical Society Reviews*, *40*(3), 1647–1671.

Khosla, D. (2016). Concurrent therapy to enhance radiotherapeutic outcomes in glioblastoma. *Annals of Translational Medicine*, *4*(3), 54–61.

Kim, J. A., Åberg, C., Salvati, A. and Dawson, K. A. (2012a). Role of cell cycle on the cellular uptake and dilution of nanoparticles in a cell population. *Nature Nanotechnology*, *7*(1), 62–68.

Kim, S.-S., Harford, J. B., Pirollo, K. F. and Chang, E. H. (2015). Effective treatment of glioblastoma requires crossing the blood-brain barrier and targeting tumors including cancer stem cells: The promise of nanomedicine. Biochemical and Biophysical Research *Communications*, *468*(3), 485–489.

Kim, T. H., Jo, Y. G., Jiang, H. H., Lim, S. M., Youn, Y. S., Lee, S., … Lee, K. C. (2012b). PEG-transferrin conjugated TRAIL (TNF-related apoptosis-inducing ligand) for therapeutic tumor targeting. *Journal of Controlled Release*, *162*(2), 422–428.

Kindrat, I., Tryndyak, V., de Conti, A., Shpyleva, S., Mudalige, T. K., Kobets, T., … Pogribny, I. P. (2016). MicroRNA-152-mediated dysregulation of hepatic transferrin receptor 1 in liver carcinogenesis. *Oncotarget*, *7*(2), 1276–1287.

Kitching, M., Ramani, M. and Marsili, E. (2015). Fungal biosynthesis of gold nanoparticles: mechanism and scale up. *Microbial Biotechnology*, *8*(6), 904–917.

Kleemann, E., Neu, M., Jekel, N., Fink, L., Schmehl, T., Gessler, T., … Kissel, T. (2005). Nano-carriers for DNA delivery to the lung based upon a TAT-derived peptide covalently coupled to PEG–PEI. *Journal of Controlled Release*, *109*(1–3), 299–316.

Kleihues, P., Barnholtz-Sloan, J. and Ohgaki, H. (2014). Tumours of the nervous system. In B. W. Stewart and C. P. Wild (Eds.), *World Cancer Report 2014* (pp. 511–521). International Agency for Research on Cancer.

Kleven, M. D., Jue, S. and Enns, C. A. (2018). Transferrin Receptors TfR1 and TfR2 Bind Transferrin through Differing Mechanisms. *Biochemistry*, *57*(9), 1552–1559.

Kneuer, C., Mohammad, S., Bakowsky, U., Schiestel, T., Schirra, H., Schmidt, H. and Lehr, C.-M. (2000). A Nonviral DNA Delivery System Based on Surface Modified Silica-Nanoparticles Can Efficiently Transfect Cells in Vitro. *Bioconjugate Chemistry*, *11*(6), 926–932.

Kodiha, M., Wang, Y. M., Hutter, E., Maysinger, D. and Stochaj, U. (2015). Off to the organelles - killing cancer cells with targeted gold nanoparticles. *Theranostics*, *5*(4), 357–370.

Koo, Y.-E. L., Reddy, G. R., Bhojani, M., Schneider, R., Philbert, M. A., Rehemtulla, A., … Kopelman, R. (2006). Brain cancer diagnosis and therapy with nanoplatforms. *Advanced Drug Delivery Reviews*, *58*(14), 1556–1577.

Kotterman, M. A., Chalberg, T. W. and Schaffer, D. V. (2015). Viral Vectors for Gene Therapy: Translational and Clinical Outlook. *Annual Review of Biomedical Engineering*, *17*(1), 63–89.

Kumar, V., Qin, J., Jiang, Y., Duncan, R. G., Brigham, B., Fishman, S., … Kasperkovitz, P. V. (2014). Shielding of Lipid Nanoparticles for siRNA Delivery: Impact on Physicochemical Properties, Cytokine Induction, and Efficacy. *Molecular Therapy - Nucleic Acids*, *3*, e210.

Kunath, K., Merdan, T., Hegener, O., Häberlein, H. and Kissel, T. (2003). Integrin targeting using RGD-PEI conjugates for in vitro gene transfer. *The Journal of Gene Medicine*, *5*(7), 588–599.

Kwiatkowska, A., Nandhu, M. S., Behera, P., Chiocca, E. A. and Viapiano, M. S. (2013). Strategies in gene therapy for glioblastoma. *Cancers*, *5*(4), 1271–1305.

Lai, F., Fadda, A. M. and Sinico, C. (2013). Liposomes for brain delivery. *Expert Opinion on Drug Delivery*, *10*(7), 1003–1022.

Lajoie, J. M. and Shusta, E. V. (2015). Targeting receptor-mediated transport for delivery of biologics across the blood-brain barrier. *Annual Review of Pharmacology and Toxicology*, *55*, 613–31.

Lakadamyali, M., Rust, M. J. and Zhuang, X. (2006). Ligands for clathrin-mediated endocytosis are differentially sorted into distinct populations of early endosomes. *Cell*, *124*(5), 997–1009.

Lambert, L. A. (2012). Molecular evolution of the transferrin family and associated receptors. *Biochimica et Biophysica Acta (BBA) - General Subjects*, *1820*(3), 244–255.

Lambert, L. A., Perri, H. and Meehan, T. J. (2005). Evolution of duplications in the transferrin family of proteins. *Comparative Biochemistry and Physiology Part B: Biochemistry and Molecular Biology*, *140*(1), 11–25.

Lane, D. J. R., Merlot, A. M., Huang, M. L.-H., Bae, D.-H., Jansson, P. J., Sahni, S., … Richardson, D. R. (2015). Cellular iron uptake, trafficking and metabolism: Key molecules and mechanisms and their roles in disease. *Biochimica et Biophysica Acta (BBA) - Molecular Cell Research*, *1853*(5), 1130–1144.

Larin, S. S., Georgiev, G. P. and Kiselev, S. L. (2004). Gene transfer approaches in cancer immunotherapy. *Gene Therapy*, *11*(S1), S18–S25.

Lauko, A., Thapa, B., Venur, V. A. and Ahluwalia, M. S. (2018). Management of Brain Metastases in the New Era of Checkpoint Inhibition. *Current Neurology and Neuroscience Reports*, *18*(10), 70.

Lazarus, G. G., Revaprasadu, N., López-Viota, J. and Singh, M. (2014). The electrokinetic characterization of gold nanoparticles, functionalized with cationic

functional groups, and its' interaction with DNA. *Colloids and Surfaces B: Biointerfaces*, *121*, 425–431.

Lazarus, G. G. and Singh, M. (2016). Cationic modified gold nanoparticles show enhanced gene delivery in vitro. *Nanotechnology Reviews*, *5*(5), 425–434.

Lee, J., Arun Kumar, S., Jhan, Y. Y. and Bishop, C. J. (2018). Engineering DNA vaccines against infectious diseases. *Acta Biomaterialia*, *80*, 31–47.

Lee, J. H., Engler, J. A., Collawn, J. F. and Moore, B. A. (2001). Receptor mediated uptake of peptides that bind the human transferrin receptor. *European Journal of Biochemistry*, *268*(7), 2004–2012.

Lee, K. M., Kim, I. S., Lee, Y. B., Shin, S. C., Lee, K. C. and Oh, I. J. (2005). Evaluation of transferrin-polyethylenimine conjugate for targeted gene delivery. *Archives of Pharmacal Research*, *28*(6), 722–729. Retrieved from

Leitner, D. F. and Connor, J. R. (2012). Functional roles of transferrin in the brain. *Biochimica et Biophysica Acta (BBA) - General Subjects*, *1820*(3), 393–402.

Lentz, T. B., Gray, S. J. and Samulski, R. J. (2012). Viral vectors for gene delivery to the central nervous system. *Neurobiology of Disease*, *48*(2), 179–188.

Lerman, L. S. (1971). A Transition to a Compact Form of DNA in Polymer Solutions. *Proceedings of the National Academy of Sciences of the United States of America*, *68*(8), 1886-1890.

Li, C.-H., Shyu, M.-K., Jhan, C., Cheng, Y.-W., Tsai, C.-H., Liu, C.-W., … Kang, J.-J. (2015). Gold Nanoparticles Increase Endothelial Paracellular Permeability by Altering Components of Endothelial Tight Junctions, and Increase Blood-Brain Barrier Permeability in Mice. *Toxicological Sciences*, *148*(1), 192–203.

Li, F., Zhang, H., Dever, B., Li, X.-F. and Le, X. C. (2013a). Thermal stability of DNA functionalized gold nanoparticles. *Bioconjugate Chemistry*, *24*(11), 1790–1797.

Li, J., Ge, Z. and Liu, S. (2013b). PEG-sheddable polyplex micelles as smart gene carriers based on MMP-cleavable peptide-linked block copolymers. *Chemical Communications*, *49*(62), 6974–6976.

Li, J., Li, Q., Ma, X., Tian, B., Li, T., Yu, J., … Hua, Y. (2016). Biosynthesis of gold nanoparticles by the extreme bacterium Deinococcus radiodurans and an evaluation of their antibacterial properties. *International Journal of Nanomedicine*, *11*, 5931–5944.

Liang, W. and Lam, J. K. W. (2012). Endosomal Escape Pathways for Non-Viral Nucleic Acid Delivery Systems. In B. Ceresa (Ed.), *Molecular Regulation of Endocytosis* (pp. 429–456). InTech.

Link, S. and El-Sayed, M. A. (1999). Spectral Properties and Relaxation Dynamics of Surface Plasmon Electronic Oscillations in Gold and Silver Nanodots and Nanorods. *The Journal of Physical Chemistry B*, *103*(40), 8410–8426.

Liu, H.-L., Hua, M.-Y., Chen, P.-Y., Chu, P.-C., Pan, C.-H., Yang, H.-W., … Wei, K.-C. (2010). Blood-Brain Barrier Disruption with Focused Ultrasound Enhances Delivery of Chemotherapeutic Drugs for Glioblastoma Treatment. *Radiology*, *255*(2), 415–425.

Liu, K., Liu, P., Liu, R. and Wu, X. (2015). Dual AO/EB staining to detect apoptosis in osteosarcoma cells compared with flow cytometry. *Medical Science Monitor Basic Research*, *21*, 15–20.

Liu, X., Huang, N., Li, H., Jin, Q. and Ji, J. (2013). Surface and Size Effects on Cell Interaction of Gold Nanoparticles with Both Phagocytic and Nonphagocytic Cells. *Langmuir*, *29*(29), 9138–9148.

Liu, Y., Miyoshi, H. and Nakamura, M. (2007). Nanomedicine for drug delivery and imaging: A promising avenue for cancer therapy and diagnosis using targeted functional nanoparticles. *International Journal of Cancer*, *120*(12), 2527–2537.

Loh, J. W., Saunders, M. and Lim, L.-Y. (2012). Cytotoxicity of monodispersed chitosan nanoparticles against the Caco-2 cells. *Toxicology and Applied Pharmacology*, *262*(3), 273–282.

Lopez-Chaves, C., Soto-Alvaredo, J., Montes-Bayon, M., Bettmer, J., Llopis, J. and Sanchez-Gonzalez, C. (2018). Gold nanoparticles: Distribution, bioaccumulation and toxicity. In vitro and in vivo studies. *Nanomedicine: Nanotechnology, Biology and Medicine*, *14*(1), 1–12.

Louis, D. N., Perry, A., Reifenberger, G., von Deimling, A., Figarella-Branger, D., Cavenee, W. K., … Ellison, D. W. (2016). The 2016 World Health Organization Classification of Tumors of the Central Nervous System: a summary. *Acta Neuropathologica*, *131*(6), 803–820.

Luck, A. N. and Mason, A. B. (2012). Transferrin-Mediated Cellular Iron Delivery. *Current Topics in Membranes*, *69*, 3–35.

Luo, Q., Gao, H., Peng, L., Liu, G. and Zhang, Z. (2016). Synthesis of PEGylated chitosan copolymers as efficiently antimicrobial coatings for leather. Journal of Applied Polymer *Science*, *133*(22).

Luria-Pérez, R., Helguera, G. and Rodríguez, J. A. (2016). Antibody-mediated targeting of the transferrin receptor in cancer cells. *Boletín Médico Del Hospital Infantil de México*, *73*(6), 372–379.

Luty-Błocho, M., Wojnicki, M. and Fitzner, K. (2017). Gold Nanoparticles Formation via Au(III) Complex Ions Reduction with l -Ascorbic Acid. *International Journal of Chemical Kinetics*, *49*(11), 789–797.

Ma, D. (2014). Enhancing endosomal escape for nanoparticle mediated siRNA delivery. *Nanoscale*, *6*(12), 6415.

Macedo, M. F. and de Sousa, M. (2008). Transferrin and the transferrin receptor: of magic bullets and other concerns. *Inflammation & Allergy Drug Targets*, *7*(1), 41–52.

Malatesta, M., Giagnacovo, M., Costanzo, M., Conti, B., Genta, I., Dorati, R., … Zancanaro, C. (2012). Diaminobenzidine photoconversion is a suitable tool for tracking the intracellular location of fluorescently labelled nanoparticles at transmission electron microscopy. *European Journal of Histochemistry*, *56*(2), 123–128.

Malhotra, M., Toulouse, A., Godinho, B. M. D. C., Mc Carthy, D. J., Cryan, J. F. and O'Driscoll, C. M. (2015). RNAi therapeutics for brain cancer: current advancements in RNAi delivery strategies. *Molecular BioSystems*, *11*(10), 2635–2657.

Managit, C., Kawakami, S., Nishikawa, M., Yamashita, F. and Hashida, M. (2003). Targeted and sustained drug delivery using PEGylated galactosylated liposomes. *International Journal of Pharmaceutics*, *266*(1–2), 77–84.

Manivasagan, P., Bharathiraja, S., Moorthy, M. S., Mondal, S., Nguyen, T. P., Kim, H., … Oh, J. (2018). Biocompatible chitosan oligosaccharide modified gold nanorods as highly effective photothermal agents for ablation of breast cancer cells. *Polymers*, *10*(3), 232-248.

Manson, J., Kumar, D., Meenan, B. J. and Dixon, D. (2011). Polyethylene glycol functionalized gold nanoparticles: The influence of capping density on stability in various media. *Gold Bulletin*, *44*(2), 99–105.

Mao, H. Q., Roy, K., Troung-Le, V. L., Janes, K. A., Lin, K. Y., Wang, Y., … Leong, K. W. (2001). Chitosan-DNA nanoparticles as gene carriers: synthesis, characterization and transfection efficiency. *Journal of Controlled Release*, *70*(3), 399–421.

Martínez-Torres, A. C., Zarate-Triviño, D. G., Lorenzo-Anota, H. Y., Ávila-Ávila, A., Rodríguez-Abrego, C. and Rodríguez-Padilla, C. (2018). Chitosan gold nanoparticles induce cell death in HeLa and MCF-7 cells through reactive oxygen species production. *International Journal of Nanomedicine*, *13*, 3235–3250.

Masserini, M. (2013). Nanoparticles for Brain Drug Delivery. *ISRN Biochemistry*, *2013*, 1–18.

McDonagh, B. H., Volden, S., Lystvet, S. M., Singh, G., Ese, M. H. G., Ryan, J. A., … Glomm, W. R. (2015). Self-assembly and characterization of transferrin-gold nanoconstructs and their interaction with bio-interfaces. *Nanoscale*, *7*(17), 8062–8070.

McErlean, E. M., McCrudden, C. M. and McCarthy, H. O. (2016). Delivery of nucleic acids for cancer gene therapy: overcoming extra- and intra-cellular barriers. *Therapeutic Delivery*, *7*(9), 619–637.

McNeill, K. A. (2016). Epidemiology of Brain Tumors. *Neurologic Clinics*, *34*(4), 981–998.

Mehier-Humbert, S. and Guy, R. H. (2005). Physical methods for gene transfer: Improving the kinetics of gene delivery into cells. *Advanced Drug Delivery Reviews*, *57*(5), 733–753.

Mellott, A. J., Forrest, M. L. and Detamore, M. S. (2013). Physical Non-Viral Gene Delivery Methods for Tissue Engineering. *Annals of Biomedical Engineering*, *41*(3), 446–468.

Mendes, R., Fernandes, A. and Baptista, P. (2017). Gold Nanoparticle Approach to the Selective Delivery of Gene Silencing in Cancer—The Case for Combined Delivery? *Genes*, *8*(3), 94.

Menon, S., Shanmugam, R. and Kumar, V. (2017). A review on biogenic synthesis of gold nanoparticles, characterization, and its applications. *Resource-Efficient Technologies*, *3*(4), 516–527.

Min, S.-H., Park, K. C. and Yeom, Y. Il. (2014). Chitosan-mediated non-viral gene delivery with improved serum stability and reduced cytotoxicity. Biotechnology and *Bioprocess Engineering*, *19*(6), 1077–1082.

Mirkin, C. A., Letsinger, R. L., Mucic, R. C. and Storhoff, J. J. (1996). A DNA-based method for rationally assembling nanoparticles into macroscopic materials. *Nature*, *382*(6592), 607–609.

Mirza, A. Z. and Siddiqui, F. A. (2014). Nanomedicine and drug delivery: a mini review. *International Nano Letters*, *4*(1), 94.

Mishra, S., Webster, P. and Davis, M. E. (2004). PEGylation significantly affects cellular uptake and intracellular trafficking of non-viral gene delivery particles. *European Journal of Cell Biology*, *83*(3), 97–111.

Misra, S. K., Biswas, J., Kondaiah, P. and Bhattacharya, S. (2013). Gene transfection in high serum levels: case studies with new cholesterol based cationic gemini lipids. *PLOS One*, *8*(7), e68305.

Moses, C., Garcia-Bloj, B., Harvey, A. R. and Blancafort, P. (2018). Hallmarks of cancer: The CRISPR generation. *European Journal of Cancer*, *93*, 10–18.

Mpourmpakis, G. and Vlachos, D. G. (2009). Growth Mechanisms of Metal Nanoparticles via First Principles. *Physical Review Letters*, *102*(15), 155505.

Mullard, A. (2018). 2017 FDA drug approvals. *Nature Reviews Drug Discovery*, *17*(2), 81–85.

Nady, S. (2017). Apoptotic Effect of Gold Nanoparticles on Human Colon Cancer Cell Lines Caco-2 But Not on the Normal Epithelial Cell Lines Wish. *World Journal of Pharmaceutical Research*, *6*(7), 127–148.

Naghavi, M., Abajobir, A. A., Abbafati, C., Abbas, K. M., Abd-Allah, F., Abera, S. F., … Murray, C. J. L. (2017). Global, regional, and national age-sex specific mortality for 264 causes of death, 1980–2016: a systematic analysis for the Global Burden of Disease Study 2016. *The Lancet*, *390*(10100), 1151–1210.

Narayanan, R. L. and Sivakumar, M. (2014). Preparation and Characterization of Gold Nanoparticles in Chitosan Suspension by One-Pot Chemical Reduction Method. *Nano Hybrids*, *6*, 47–57.

Natte, K., Friedrich, J. F., Wohlrab, S., Lutzki, J., von Klitzing, R., Österle, W. and Orts-Gil, G. (2013). Impact of polymer shell on the formation and time evolution of nanoparticle–protein corona. *Colloids and Surfaces B: Biointerfaces*, *104*, 213–220.

Nayerossadat, N., Maedeh, T. and Ali, P. A. (2012). Viral and nonviral delivery systems for gene delivery. *Advanced Biomedical Research*, *1*(2), 27–37.

Niidome, T., Akiyama, Y., Yamagata, M., Kawano, T., Mori, T., Niidome, Y. and Katayama, Y. (2009). Poly(ethylene glycol)-Modified Gold Nanorods as a Photothermal Nanodevice for Hyperthermia. *Journal of Biomaterials Science, Polymer Edition*, *20*(9), 1203–1215.

Niidome, T., Yamagata, M., Okamoto, Y., Akiyama, Y., Takahashi, H., Kawano, T., … Niidome, Y. (2006). PEG-modified gold nanorods with a stealth character for in vivo applications. *Journal of Controlled Release*, *114*(3), 343–347.

Niu, J., Chu, Y., Huang, Y.-F., Chong, Y.-S., Jiang, Z.-H., Mao, Z.-W., … Gao, J.-Q. (2017). Transdermal Gene Delivery by Functional Peptide-Conjugated Cationic Gold Nanoparticle Reverses the Progression and Metastasis of Cutaneous Melanoma. *ACS Applied Materials & Interfaces*, *9*(11), 9388–9401.

O'Brien, J. A. and Lummis, S. C. (2011). Nano-biolistics: a method of biolistic transfection of cells and tissues using a gene gun with novel nanometer-sized projectiles. *BMC Biotechnology*, *11*(1), 66–71.

Ogris, M., Brunner, S., Schüller, S., Kircheis, R. and Wagner, E. (1999). PEGylated DNA/transferrin–PEI complexes: reduced interaction with blood components, extended circulation in blood and potential for systemic gene delivery. *Gene Therapy*, *6*(4), 595–605.

Ogris, M., Steinlein, P., Carotta, S., Brunner, S. and Wagner, E. (2001). DNA/polyethylenimine transfection particles: Influence of ligands, polymer size, and PEGylation on internalization and gene expression. *AAPS PharmSci*, *3*(3), 43–53.

Oh, K. S., Kim, R. S., Lee, J., Kim, D., Cho, S. H. and Yuk, S. H. (2008). Gold/Chitosan/Pluronic Composite Nanoparticles for Drug Delivery. *Journal of Applied Polymer Science*, *108*(5), 3239–3244.

Ohtsuki, S. and Terasaki, T. (2007). Contribution of Carrier-Mediated Transport Systems to the Blood–Brain Barrier as a Supporting and Protecting Interface for the Brain; Importance for CNS Drug Discovery and Development. *Pharmaceutical Research*, *24*(9), 1745–1758.

Ojala, D. S., Amara, D. P. and Schaffer, D. V. (2015). Adeno-Associated Virus Vectors and Neurological Gene Therapy. *The Neuroscientist*, *21*(1), 84–98.

Otero, C., Groettrup, M. and Legler, D. F. (2006). Opposite fate of endocytosed CCR7 and its ligands: recycling versus degradation. *The Journal of Immunology*, *177*(4), 2314–2323.

Pabisch, S., Feichtenschlager, B., Kickelbick, G. and Peterlik, H. (2012). Effect of interparticle interactions on size determination of zirconia and silicabased systems – A comparison of SAXS, DLS, BET, XRD and TEM. *Chemical Physics Letters*, *521*(C), 91–97.

Pahle, J. and Walther, W. (2016). Vectors and strategies for nonviral cancer gene therapy. *Expert Opinion on Biological Therapy*, *16*(4), 443–461.

Pan, L., Liu, J. and Shi, J. (2018). Cancer cell nucleus-targeting nanocomposites for advanced tumor therapeutics. *Chemical Society Reviews*, *47*(18), 6930–6946.

Pan, Y., Neuss, S., Leifert, A., Fischler, M., Wen, F., Simon, U., … Jahnen-Dechent, W. (2007). Size-Dependent Cytotoxicity of Gold Nanoparticles. *Small*, *3*(11), 1941–1949.

Pandolfi, S. and Stecca, B. (2015). Luciferase Reporter Assays to Study Transcriptional Activity of Hedgehog Signaling in Normal and Cancer Cells. In N. A. Riobo (Ed.), *Hedgehog Signalling Protocols* (2nd ed., pp. 71–79). Humana Press.

Parab, H. J., Huang, J. H., Lai, T. C., Jan, Y. H., Liu, R. S., Wang, J. L., … Pang, J. H. S. (2011). Biocompatible transferrin-conjugated sodium hexametaphosphate-stabilized gold nanoparticles: Synthesis, characterization, cytotoxicity and cellular uptake. *Nanotechnology*, *22*(39), 395706.

Pardridge, W. M. (2007). Blood-brain barrier delivery. *Drug Discovery Today*, *12*(1–2), 54–61.

Parodi, A., Corbo, C., Cevenini, A., Molinaro, R., Palomba, R., Pandolfi, L., … Tasciotti, E. (2015). Enabling cytoplasmic delivery and organelle targeting by surface modification of nanocarriers. *Nanomedicine*, *10*(12), 1923–1940.

Patravale, V., Dandekar, P. and Jain, R. (2012). Nanotoxicology: evaluating toxicity potential of drug-nanoparticles. In *Nanoparticulate drug delivery: perspectives on the transition from laboratory to market* (1st ed., pp. 123–155). Woodhead Publishing.

Perala, S. R. K. and Kumar, S. (2013). On the Mechanism of Metal Nanoparticle Synthesis in the Brust–Schiffrin Method. *Langmuir*, *29*(31), 9863–9873.

Pernodet, N., Fang, X., Sun, Y., Bakhtina, A., Ramakrishnan, A., Sokolov, J., … Rafailovich, M. (2006). Adverse Effects of Citrate/Gold Nanoparticles on Human Dermal Fibroblasts. *Small*, *2*(6), 766–773.

Perrault, S. D., Walkey, C., Jennings, T., Fischer, H. C. and Chan, W. C. W. (2009). Mediating Tumor Targeting Efficiency of Nanoparticles Through Design. *Nano Letters*, *9*(5), 1909–1915.

Perumal, O. P., Inapagolla, R., Kannan, S. and Kannan, R. M. (2008). The effect of surface functionality on cellular trafficking of dendrimers. *Biomaterials*, *29*(24–25), 3469–3476.

Pinto, M. P., Arce, M., Yameen, B. and Vilos, C. (2017). Targeted brain delivery nanoparticles for malignant gliomas. *Nanomedicine*, *12*(1), 59–72.

Pitek, A. S., O'Connell, D., Mahon, E., Monopoli, M. P., Baldelli Bombelli, F. and Dawson, K. A. (2012). Transferrin Coated Nanoparticles: Study of the Bionano Interface in Human Plasma. *PLOS One*, *7*(7), e40685.

Polte, J. (2015). Fundamental growth principles of colloidal metal nanoparticles – a new perspective. *CrystEngComm*, *17*(36), 6809–6830.

Polte, J., Ahner, T. T., Delissen, F., Sokolov, S., Emmerling, F., Thünemann, A. F. and Kraehnert, R. (2010). Mechanism of Gold Nanoparticle Formation in the Classical Citrate Synthesis Method Derived from Coupled In Situ XANES and SAXS Evaluation. *Journal of the American Chemical Society*, *132*(4), 1296–1301.

Pong, B.-K., Elim, H. I., Chong, J.-X., Ji, W., Bernhardt L. Trout, A. and Lee, J.-Y. (2007). New Insights on the Nanoparticle Growth Mechanism in the Citrate Reduction of Gold(III) Salt: Formation of the Au Nanowire Intermediate and Its Nonlinear Optical Properties. *The Journal of Physical Chemistry*, *111*(17), 6281–6287.

Posadas, I., Monteagudo, S. and Ceña, V. (2016). Nanoparticles for brain-specific drug and genetic material delivery, imaging and diagnosis. *Nanomedicine*, *11*(7), 833–849.

Prades, R., Guerrero, S., Araya, E., Molina, C., Salas, E., Zurita, E., … Giralt, E. (2012). Delivery of gold nanoparticles to the brain by conjugation with a peptide that recognizes the transferrin receptor. *Biomaterials*, *33*(29), 7194–7205.

Qian, Z. M., Li, H., Sun, H. and Ho, K. (2002). Targeted drug delivery via the transferrin receptor-mediated endocytosis pathway. *Pharmacological Reviews*, *54*(4), 561–87.

Queiroz, M. F., Melo, K., Sabry, D., Sassaki, G. and Rocha, H. (2014). Does the Use of Chitosan Contribute to Oxalate Kidney Stone Formation? *Marine Drugs*, *13*(1), 141–158.

Rafael, D., Andrad, F., Arranja, A., Luís, S. and Videira, M. (2015). Lipoplexes and Polyplexes: Gene Delivery Applications. In M. K. Mishra (Ed.), *Encyclopedia of Biomedical Polymers and Polymeric Biomaterials* (1st ed., pp. 4335–4347). Taylor & Francis.

Raghubar, K. P., Mahone, E. M., Yeates, K. O., Cecil, K. M., Makola, M. and Ris, M. D. (2017). Working memory and attention in pediatric brain tumor patients treated with and without radiation therapy. *Child Neuropsychology*, *23*(6), 642–654.

Rahme, K., Chen, L., Hobbs, R. G., Morris, M. A., O'Driscoll, C. and Holmes, J. D. (2013). PEGylated gold nanoparticles: polymer quantification as a function of PEG lengths and nanoparticle dimensions. *RSC Advances*, *3*(17), 6085–6094.

Railsback, J. G., Singh, A., Pearce, R. C., McKnight, T. E., Collazo, R., Sitar, Z., … Melechko, A. V. (2012). Weakly Charged Cationic Nanoparticles Induce DNA Bending and Strand Separation. *Advanced Materials*, *24*(31), 4261–4265.

Ramezani, M. R., Naderi-Manesh, H. and Pour, A. H. R. (2014). Cytotoxicity assessment of a gold nanoparticle-chitosan nanocomposite as an efficient support for cell immobilization: comparison with chitosan hydrogel and chitosan-gelatin. *Biocell*, *38*(1–3), 11–16.

Ramjiawan, R. R., Griffioen, A. W. and Duda, D. G. (2017). Anti-angiogenesis for cancer revisited: Is there a role for combinations with immunotherapy? *Angiogenesis*, *20*(2), 185–204.

Ranganathan, R., Madanmohan, S., Kesavan, A., Baskar, G., Krishnamoorthy, Y. R., Santosham, R., … Venkatraman, G. (2012). Nanomedicine: Towards development of patient-friendly drug-delivery systems for oncological applications. *International Journal of Nanomedicine*, *7*, 1043–1060.

Raub, T. J. and Newton, C. R. (1991). Recycling kinetics and transcytosis of transferrin in primary cultures of bovine brain microvessel endothelial cells. *Journal of Cellular Physiology*, *149*(1), 141–151.

Recht, L., Torres, C. O., Smith, T. W., Raso, V. and Griffin, T. W. (1990). Transferrin receptor in normal and neoplastic brain tissue: implications for brain-tumor immunotherapy. *Journal of Neurosurgery*, *72*(6), 941–945.

Rejman, J., Oberle, V., Zuhorn, I. S. and Hoekstra, D. (2004). Size-dependent internalization of particles via the pathways of clathrin- and caveolae-mediated endocytosis. *The Biochemical Journal*, *377*(Pt 1), 159–169.

Ribble, D., Goldstein, N. B., Norris, D. A. and Shellman, Y. G. (2005). A simple technique for quantifying apoptosis in 96-well plates. *BMC Biotechnology*, *5*(1), 12–18.

Richard, I., Thibault, M., De Crescenzo, G., Buschmann, M. D. and Lavertu, M. (2013). Ionization Behavior of Chitosan and Chitosan–DNA Polyplexes Indicate That Chitosan Has a Similar Capability to Induce a Proton-Sponge Effect as PEI. *Biomacromolecules*, *14*(6), 1732–1740.

Riley II, M. K. and Vermerris, W. (2017). Recent Advances in Nanomaterials for Gene Delivery—A Review. *Nanomaterials*, *7*(5), 94–112.

Ritthidej, G. C. (2011). Nasal Delivery of Peptides and Proteins with Chitosan and Related Mucoadhesive Polymers. In C. Van Der Walle (Ed.), *Peptide and Protein Delivery* (pp. 47–68). Academic Press.

Roberts, R., Fine, R. and Sandra, A. (1993). Receptor-mediated endocytosis of transferrin at the blood-brain barrier. *Journal of Cell Science*, *140*(2), 521–532.

Rodrigues, S., Dionísio, M., López, C. R. and Grenha, A. (2012). Biocompatibility of Chitosan Carriers with Application in Drug Delivery. *Journal of Functional Biomaterials*, *3*(3), 615–641.

Rosager, A. M., Sørensen, M. D., Dahlrot, R. H., Hansen, S., Schonberg, D. L., Rich, J. N., … Kristensen, B. W. (2017). Transferrin receptor-1 and ferritin heavy and light chains in astrocytic brain tumors: Expression and prognostic value. *PLOS One*, *12*(8), e0182954.

Rosenberg, S. A. (1992). Gene therapy for cancer. *JAMA*, *268*(17), 2416–2419.

Sahay, G., Alakhova, D. Y. and Kabanov, A. V. (2010). Endocytosis of nanomedicines. *Journal of Controlled Release*, *145*(3), 182–95.

Sahin, A., Yoyen-ermis, D., Caban-toktas, S., Horzum, U., Couvreur, P., Esendagli, G. and Capan, Y. (2017). Evaluation of brain-targeted chitosan nanoparticles through blood – brain barrier cerebral microvessel endothelial cells. *Journal of Microencapsulation*, *34*(7), 659–666.

Saraiva, C., Praça, C., Ferreira, R., Santos, T., Ferreira, L. and Bernardino, L. (2016). Nanoparticle-mediated brain drug delivery: Overcoming blood–brain barrier to treat neurodegenerative diseases. *Journal of Controlled Release*, *235*, 34–47.

Sato, H., Hattori, S., Kawamoto, S., Kudoh, I., Hayashi, A., Yamamoto, I., … Kanno, H. (2000). In Vivo Gene Gun-Mediated DNA Delivery into Rodent Brain Tissue. *Biochemical and Biophysical Research Communications*, *270*(1), 163–170.

Sato, T., Ishii, T. and Okahata, Y. (2001). In vitro gene delivery mediated by chitosan. Effect of pH, serum, and molecular mass of chitosan on the transfection efficiency. *Biomaterials*, *22*(15), 2075–2080.

Schaffer, D. V, Fidelman, N. A., Dan, N. and Lauffenburger, D. A. (2000). Vector unpacking as a potential barrier for receptor-mediated polyplex gene delivery. *Biotechnology and Bioengineering*, *67*(5), 598–606.

Schonberg, D. L., Miller, T. E., Wu, Q., Flavahan, W. A., Das, N. K., Hale, J. S., … Rich, J. N. (2015). Preferential Iron Trafficking Characterizes Glioblastoma Stem-like Cells. *Cancer Cell*, *28*(4), 441–455.

Sela, H., Cohen, H., Elia, P., Zach, R., Karpas, Z. and Zeiri, Y. (2015). Spontaneous penetration of gold nanoparticles through the blood brain barrier (BBB). Journal of *Nanobiotechnology*, *13*(1), 71–79.

Semple, S. C., Klimuk, S. K., Harasym, T. O., Dos Santos, N., Ansell, S. M., Wong, K. F., … Scherrer, P. (2001). Efficient encapsulation of antisense oligonucleotides in lipid vesicles using ionizable aminolipids: Formation of novel small multilamellar vesicle structures. *Biochimica et Biophysica Acta - Biomembranes*, *1510*(1–2), 152–166.

Shahbazi, R., Asik, E., Kahraman, N., Turk, M., Ozpolat, B. and Ulubayram, K. (2017). Modified gold-based siRNA nanotherapeutics for targeted therapy of triple-negative breast cancer. *Nanomedicine*, *12*(16), 1961–1973.

Shang, L., Nienhaus, K. and Nienhaus, G. U. (2014). Engineered nanoparticles interacting with cells: Size matters. *Journal of Nanobiotechnology*, *12*(1), 5.

Sharma, G., Lakkadwala, S., Modgil, A. and Singh, J. (2016). The Role of Cell-Penetrating Peptide and Transferrin on Enhanced Delivery of Drug to Brain. *International Journal of Molecular Sciences*, *17*(6), 806–823.

Shin, J., Kong, C., Cho, J. S., Lee, J., Koh, C. S., Yoon, M.-S., … Chang, J. W. (2018). Focused ultrasound–mediated noninvasive blood-brain barrier modulation: preclinical examination of efficacy and safety in various sonication parameters. *Neurosurgical Focus*, *44*(2), E15.

Simberg, D., Weisman, S., Talmon, Y., Faerman, A., Shoshani, T. and Barenholz, Y. (2003). The role of organ vascularization and lipoplex-serum initial contact in intravenous murine lipofection. *The Journal of Biological Chemistry*, *278*(41), 39858–39865.

Simpson, I. A., Ponnuru, P., Klinger, M. E., Myers, R. L., Devraj, K., Coe, C. L., … Connor, J. R. (2015). A novel model for brain iron uptake: introducing the concept of regulation. *Journal of Cerebral Blood Flow and Metabolism*, *35*(1), 48–57.

Singh, P., Pandit, S., Mokkapati, V. R. S. S., Garg, A., Ravikumar, V. and Mijakovic, I. (2018). Gold Nanoparticles in Diagnostics and Therapeutics for Human Cancer. *International Journal of Molecular Sciences*, *19*(7), 1979–1994.

Smith, M. W. and Gumbleton, M. (2006). Endocytosis at the blood–brain barrier: From basic understanding to drug delivery strategies. *Journal of Drug Targeting*, *14*(4), 191–214.

Son, K. K., Tkach, D. and Patel, D. H. (2000). Zeta potential of transfection complexes formed in serum-free medium can predict in vitro gene transfer efficiency of transfection reagent. *Biochimica et Biophysica Acta (BBA) - Biomembranes*, *1468*(1–2), 11–14.

Sonavane, G., Tomoda, K. and Makino, K. (2008). Biodistribution of colloidal gold nanoparticles after intravenous administration: Effect of particle size. *Colloids and Surfaces B: Biointerfaces*, *66*(2), 274–280.

Sonawane, N. D., Szoka, F. C. and Verkman, A. S. (2003). Chloride accumulation and swelling in endosomes enhances DNA transfer by polyamine-DNA polyplexes. *The Journal of Biological Chemistry*, *278*(45), 44826–44831.

Song, L., Guo, Y., Roebuck, D., Chen, C., Yang, M., Yang, Z., … Zhou, D. (2015). Terminal PEGylated DNA-Gold Nanoparticle Conjugates Offering High Resistance to Nuclease Degradation and Efficient Intracellular Delivery of DNA Binding Agents. *ACS Applied Materials & Interfaces*, *7*(33), 18707–18716.

Souho, T., Lamboni, L., Xiao, L. and Yang, G. (2018). Cancer hallmarks and malignancy features: Gateway for improved targeted drug delivery. *Biotechnology Advances*, *36*(7), 1928–1945.

Stamatovic, S. M., Johnson, A. M., Keep, R. F. and Andjelkovic, A. V. (2016). Junctional proteins of the blood-brain barrier: New insights into function and dysfunction. *Tissue Barriers*, *4*(1), e1154641.

Steere, A. N., Byrne, S. L., Chasteen, N. D., Smith, V. C., MacGillivray, R. T. A. and Mason, A. B. (2010). Evidence that His349 acts as a pH-inducible switch to accelerate receptor-mediated iron release from the C-lobe of human transferrin. *Journal of Biological Inorganic Chemistry*, *15*(8), 1341–1352.

Steliarova-Foucher, E. and Frazier, A. L. (2014). Childhood cancer. In Bernard W. Stewart and C. P. Wild (Eds.), *World Cancer Report 2014* (pp. 69–76). International Agency for Research on Cancer.

Stetefeld, J., McKenna, S. A. and Patel, T. R. (2016). Dynamic light scattering: a practical guide and applications in biomedical sciences. *Biophysical Reviews*, *8*(4), 409–427.

Storm, G. and Crommelin, D. J. A. (1998). Liposomes: quo vadis? *Pharmaceutical Science & Technology Today*, *1*(1), 19–31.

Suk, J. S., Xu, Q., Kim, N., Hanes, J. and Ensign, L. M. (2016). PEGylation as a strategy for improving nanoparticle-based drug and gene delivery. *Advanced Drug Delivery Reviews*, *99*, 28–51.

Tajes, M., Ramos-Fernandez, E., Weng-Jiang, X., Bosch-Morato, M., Guivernau, B., Eraso-Pichot, A., … Munoz, F. J. (2014). The blood-brain barrier: structure, function and therapeutic approaches to cross it. *Molecular Membrane Biology*, *31*(5), 152–167.

Takeuchi, I., Nobata, S., Oiri, N., Tomoda, K. and Makino, K. (2017). Biodistribution and excretion of colloidal gold nanoparticles after intravenous injection: Effects of particle size. *Bio-Medical Materials and Engineering*, *28*(3), 315–323.

Tam, V. H., Sosa, C., Liu, R., Yao, N. and Priestley, R. D. (2016). Nanomedicine as a non-invasive strategy for drug delivery across the blood brain barrier. *International Journal of Pharmaceutics*, *515*(1–2), 331–342.

Tashima, T. (2018). Effective cancer therapy based on selective drug delivery into cells across their membrane using receptor-mediated endocytosis. *Bioorganic & Medicinal Chemistry Letters*, *28*(18), 3015–3024.

Thuenauer, R., Müller, S. K. and Römer, W. (2017). Pathways of protein and lipid receptor-mediated transcytosis in drug delivery. *Expert Opinion on Drug Delivery*, *14*(3), 341–351.

Tietz, S. and Engelhardt, B. (2015). Brain barriers: Crosstalk between complex tight junctions and adherens junctions. *The Journal of Cell Biology*, *209*(4), 493–506.

Tlotleng, N., Vetten, M. A., Keter, F. K., Skepu, A., Tshikhudo, R. and Gulumian, M. (2016). Cytotoxicity, intracellular localization and exocytosis of citrate capped and PEG functionalized gold nanoparticles in human hepatocyte and kidney cells. *Cell Biology and Toxicology*, *32*(4), 305–321.

Tortorella, S. and Karagiannis, T. C. (2014). Transferrin Receptor-Mediated Endocytosis: A Useful Target for Cancer Therapy. *The Journal of Membrane Biology*, *247*(4), 291–307.

Treat, L. H., McDannold, N., Vykhodtseva, N., Zhang, Y., Tam, K. and Hynynen, K. (2007). Targeted delivery of doxorubicin to the rat brain at therapeutic levels using MRI-guided focused ultrasound. *International Journal of Cancer*, *121*(4), 901–907.

Tsoli, M., Kuhn, H., Brandau, W., Esche, H. and Schmid, G. (2005). Cellular Uptake and Toxicity of Au55 Clusters. *Small*, *1*(8–9), 841–844.

Turkevich, J., Stevenson, P. C. and Hillier, J. (1951). A study of the nucleation and growth processes in the synthesis of colloidal gold. *Discussions of the Faraday Society*, *11*, 55.

Uz, M., Bulmus, V. and Alsoy Altinkaya, S. (2016). Effect of PEG Grafting Density and Hydrodynamic Volume on Gold Nanoparticle–Cell Interactions: An Investigation on Cell Cycle, Apoptosis, and DNA Damage. *Langmuir*, *32*(23), 5997–6009.

van den Bijgaart, R. J. E., Eikelenboom, D. C., Hoogenboom, M., Fütterer, J. J., den Brok, M. H. and Adema, G. J. (2017). Thermal and mechanical high-intensity focused ultrasound: perspectives on tumor ablation, immune effects and combination strategies. *Cancer Immunology, Immunotherapy*, *66*(2), 247–258.

van der Zande, M., Undas, A. K., Kramer, E., Monopoli, M. P., Peters, R. J., Garry, D., … Bouwmeester, H. (2016). Different responses of Caco-2 and MCF-7 cells to silver nanoparticles are based on highly similar mechanisms of action. *Nanotoxicology*, *10*(10), 1431–1441.

van Meerloo, J., Kaspers, G. J. L. and Cloos, J. (2011). Cell Sensitivity Assays: The MTT Assay. In I. Cree (Ed.), *Cancer Cell Culture. Methods in Molecular Biology (Methods and Protocols)* (Vol. 731, pp. 237–245). Humana Press.

van Tellingen, O., Yetkin-Arik, B., de Gooijer, M. C., Wesseling, P., Wurdinger, T. and de Vries, H. E. (2015). Overcoming the blood–brain tumor barrier for effective glioblastoma treatment. *Drug Resistance Updates*, *19*, 1–12.

van Vlerken, L. E., Vyas, T. K. and Amiji, M. M. (2007). Poly(ethylene glycol)-modified Nanocarriers for Tumor-targeted and Intracellular Delivery. *Pharmaceutical Research*, *24*(8), 1405–1414.

Varkouhi, A. K., Scholte, M., Storm, G. and Haisma, H. J. (2011). Endosomal escape pathways for delivery of biologicals. *Journal of Controlled Release*, *151*(3), 220–228.

Verbaan, F. J., Oussoren, C., Snel, C. J., Crommelin, D. J. A., Hennink, W. E. and Storm, G. (2004). Steric stabilization of poly(2-(dimethylamino)ethyl methacrylate)-based polyplexes mediates prolonged circulation and tumor targeting in mice. *Journal of Gene Medicine*, *6*(1), 64–75.

Verma, H. N., Singh, P. and Chavan, R. M. (2014). Gold nanoparticle: synthesis and characterization. *Veterinary World*, *7*(2), 72–77.

Vermeulen, L. M. P., Brans, T., Samal, S. K., Dubruel, P., Demeester, J., De Smedt, S. C., … Braeckmans, K. (2018). Endosomal Size and Membrane Leakiness Influence Proton Sponge-Based Rupture of Endosomal Vesicles. *ACS Nano*, *12*(3), 2332–2345.

Vieira, D. B. and Gamarra, L. F. (2016). Getting into the brain: liposome-based strategies for effective drug delivery across the blood-brain barrier. *International Journal of Nanomedicine*, *11*, 5381–5414.

Wang, K., Kievit, F. M. and Zhang, M. (2016). Nanoparticles for cancer gene therapy: Recent advances, challenges, and strategies. *Pharmacological Research*, *114*, 56–66.

Watkins, S., Robel, S., Kimbrough, I. F., Robert, S. M., Ellis-Davies, G. and Sontheimer, H. (2014). Disruption of astrocyte–vascular coupling and the blood–brain barrier by invading glioma cells. *Nature Communications*, *5*(1), 4196–4225.

Welling, P. A. and Weisz, O. A. (2010). Sorting it out in endosomes: an emerging concept in renal epithelial cell transport regulation. *Physiology*, *25*(5), 280–292.

Wen, P. Y. and Kesari, S. (2008). Malignant Gliomas in Adults. *New England Journal of Medicine*, *359*(5), 492–507.

West, A. P., Bennett, M. J., Sellers, V. M., Andrews, N. C., Enns, C. A. and Bjorkman, P. J. (2000). Comparison of the Interactions of Transferrin Receptor and Transferrin Receptor 2 with Transferrin and the Hereditary Hemochromatosis Protein HFE. *Journal of Biological Chemistry*, *275*(49), 38135–38138.

White, M. K. and Khalili, K. (2016). CRISPR/Cas9 and cancer targets: future possibilities and present challenges. *Oncotarget*, *7*(11), 12305–12317.

Wiley, D. T., Webster, P., Gale, A. and Davis, M. E. (2013). Transcytosis and brain uptake of transferrin-containing nanoparticles by tuning avidity to transferrin receptor. *Proceedings of the National Academy of Sciences of the United States of America*, *110*(21), 8662–8667.

Win, K. Y. and Feng, S.-S. (2005). Effects of particle size and surface coating on cellular uptake of polymeric nanoparticles for oral delivery of anticancer drugs. *Biomaterials*, *26*(15), 2713–2722.

Wirth, T., Parker, N. and Yla-Herttuala, S. (2013). History of gene therapy. *Gene*, *525*(2), 162–169.

Wong, H. L., Wu, X. Y. and Bendayan, R. (2012). Nanotechnological advances for the delivery of CNS therapeutics. *Advanced Drug Delivery Reviews*, *64*(7), 686–700.

Wong, J. K. L., Mohseni, R., Hamidieh, A. A., MacLaren, R. E., Habib, N. and Seifalian, A. M. (2017). Will Nanotechnology Bring New Hope for Gene Delivery? *Trends in Biotechnology*, *35*(5), 434–451.

World Health Organization. (2018). World health statistics 2018: monitoring health for the SDGs, sustainable development goals. Geneva.

Wu, C.-C., Wu, F.-C., Hsu, Y.-T., Hsiao, Y.-C., Yang, Y.-C., Chang, C. A. and Chang, C.-L. (2017). Enhanced anti-tumor therapeutic efficacy of DNA vaccine by fusing the E7 gene to BAFF in treating human papillomavirus-associated cancer. *Oncotarget*, *8*(20), 33024–33036.

Xu, Z. P., Zeng, Q. H., Lu, G. Q. and Yu, A. B. (2006). Inorganic nanoparticles as carriers for efficient cellular delivery. *Chemical Engineering Science*, *61*(3), 1027–1040.

Yallapu, M. M., Chauhan, N., Othman, S. F., Khalilzad-Sharghi, V., Ebeling, M. C., Khan, S., … Chauhan, S. C. (2015). Implications of protein corona on physico-chemical and biological properties of magnetic nanoparticles. *Biomaterials*, *46*, 1–12.

Yang, P. H., Sun, X., Chiu, J. F., Sun, H. and He, Q. Y. (2005). Transferrin-mediated gold nanoparticle cellular uptake. *Bioconjugate Chemistry*, *16*(3), 494–496.

Yarmush, M. L., Golberg, A., Serša, G., Kotnik, T. and Miklavčič, D. (2014). Electroporation-Based Technologies for Medicine: Principles, Applications, and Challenges. *Annual Review of Biomedical Engineering*, *16*(1), 295–320.

Yeh, Y.-C., Creran, B. and Rotello, V. M. (2012). Gold nanoparticles: preparation, properties, and applications in bionanotechnology. *Nanoscale*, *4*(6), 1871–80.

Yin, H., Kanasty, R. L., Eltoukhy, A. A., Vegas, A. J., Dorkin, J. R. and Anderson, D. G. (2014). Non-viral vectors for gene-based therapy. *Nature Reviews Genetics*, *15*, 541–555.

You, W. and Henneberg, M. (2018). Cancer incidence increasing globally: The role of relaxed natural selection. *Evolutionary Applications*, *11*(2), 140–152.

Yu, Y. J., Zhang, Y., Kenrick, M., Hoyte, K., Luk, W., Lu, Y., … Dennis, M. S. (2011). Boosting Brain Uptake of a Therapeutic Antibody by Reducing Its Affinity for a Transcytosis Target. *Science Translational Medicine*, *3*(84), 84ra44.

Yue, J., Feliciano, T. J., Li, W., Lee, A. and Odom, T. W. (2017). Gold Nanoparticle Size and Shape Effects on Cellular Uptake and Intracellular Distribution of siRNA Nanoconstructs. *Bioconjugate Chemistry*, *28*(6), 1791–1800.

Zaki, N. M. and Tirelli, N. (2010). Gateways for the intracellular access of nanocarriers: a review of receptor-mediated endocytosis mechanisms and of strategies in receptor targeting. *Expert Opinion on Drug Delivery*, *7*(8), 895–913.

Zhang, G., Sun, X., Jasinski, J., Patel, D., and Gobin, A. M. (2012). Gold/Chitosan Nanocomposites with Specific Near Infrared Absorption for Photothermal Therapy Applications. *Journal of Nanomaterials*, *2012*, 1–9.

Zhang, S., Tang, C. and Yin, C. (2015). Effects of poly(ethylene glycol) grafting density on the tumor targeting efficacy of nanoparticles with ligand modification. *Drug Delivery*, *22*(2), 182–190.

Zhang, W.-W., Li, L., Li, D., Liu, J., Li, X., Li, W., … Lam, D. M.-K. (2018). The First Approved Gene Therapy Product for Cancer Ad- p53 (Gendicine): 12 Years in the Clinic. *Human Gene Therapy*, *29*(2), 160–179.

Zhang, Y. and Anchordoquy, T. J. (2004). The role of lipid charge density in the serum stability of cationic lipid/DNA complexes. *Biochimica et Biophysica Acta (BBA) - Biomembranes*, *1663*(1–2), 143–157.

Zhang, Y., Li, H., Sun, J., Gao, J., Liu, W., Li, B., … Chen, J. (2010). DC-Chol/DOPE cationic liposomes: A comparative study of the influence factors on plasmid pDNA and siRNA gene delivery. *International Journal of Pharmaceutics*, *390*(2), 198–207.

Zhong, D., Jiao, Y., Zhang, Y., Zhang, W., Li, N., Zuo, Q., … Liu, Z. (2013). Effects of the gene carrier polyethyleneimines on structure and function of blood components. *Biomaterials*, *34*(1), 294–305.

Appendix

Appendix A:
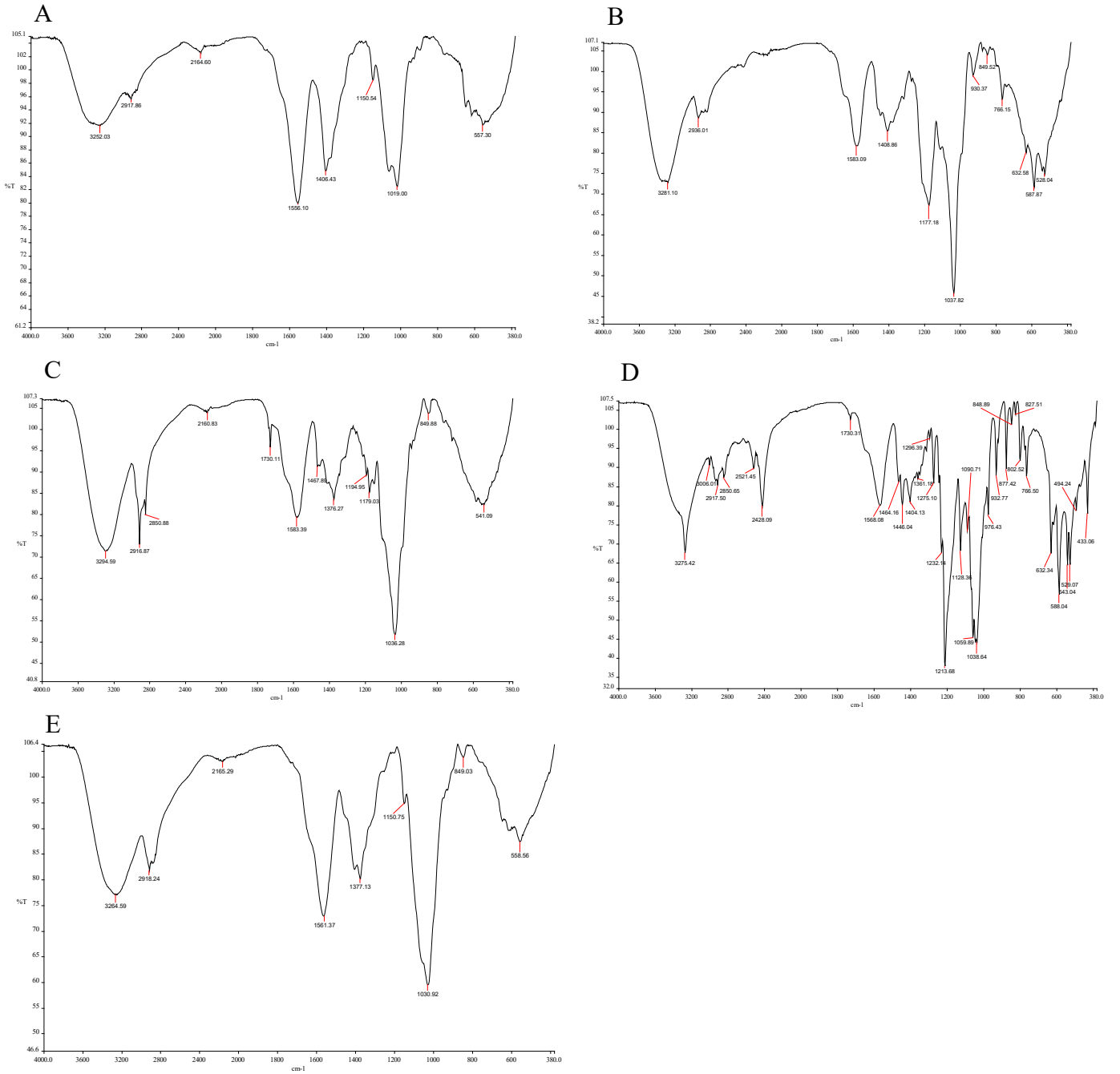
FTIR spectra of A) AuCS, B) AuCSTf, C) AuCS-2% PEG, D) AuCSTf-2% PEG, and E) AuCS-5% PEG